UNIVERSITÀ DEGLI STUDI DI PADOVA

UNIVERSITA' DEGLI STUDI DI PADOVA

DIPARTIMENTO DI INGEGNERIA INDUSTRIALE

CORSO DI LAUREA MAGISTRALE IN CHEMICAL AND PROCESS ENGINEERING

Tesi di Laurea Magistrale in

Chemical and Process Engineering

A comprehensive ionic reaction model for mineral carbonation at cement industry

Relatore: Prof. Fabrizio Bezzo

Correlatore: Ing. S. Zuhair B.Tabrizi

Laureando: Mohsen Sohrabi

ANNO ACCADEMICO 2024/2025

Abstract

This thesis develops a comprehensive ionic reaction model to examine mineral carbonation processes in supplementary cementitious materials, addressing a significant opportunity to reduce carbon dioxide emissions from the cement industry. The work focuses on the complex reaction kinetics and transport phenomena involved when cementitious materials interact with CO_2 in aqueous environments. The research introduces an innovative ionic reaction model that effectively captures physicochemical processes, including calcium leaching from supplementary cementitious materials, CO_2 dissolution and carbonate speciation reactions, solid surface reaction, and calcium carbonate precipitation. Unlike traditional shrinking core or two-film models, this approach explicitly accounts for the evolution of solution chemistry and the dynamic interplay between reaction kinetics and diffusion limitations. Parameter estimation was conducted using various optimization techniques (Genetic Algorithm, Differential Evolution, and a hybrid approach), with the model demonstrating excellent agreement with experimental measurements of calcium hydroxide consumption, pH evolution, and calcium carbonate formation. The analysis revealed three distinct kinetic regimes during carbonation: an initial reaction-limited phase dominated by $Ca(OH)_2$ dissolution, a transition phase with competing mechanisms, and a final diffusion-limited phase controlled by transport through precipitated layers on the particles. The model provides valuable insights into carbonate speciation dynamics, the relative contributions of different calcium sources to carbonation, and the progressive development of diffusion barriers. These findings establish a foundation for optimizing carbonation processes in supplementary cementitious materials, potentially enabling more efficient CO_2 utilization in the cement industry and contributing to decarbonization efforts through carbon mineralization.

Table of Contents

Introduction

Cement production stands as one of the world's most carbon-intensive industries, contributing significantly to global CO_2 emissions while requiring substantial energy inputs. As environmental concerns grow, there is an increasing shift from simply capturing and storing carbon dioxide to finding productive ways to utilize it in various processes. This paradigm shift presents an interesting opportunity when supplementary cementitious materials (SCMs) are naturally rich in calcium compounds. By bringing these two elements together (CO_2 that needs to be managed and calcium-rich materials' construction waste), mineral carbonation emerges as a promising pathway that addresses both waste management and carbon utilization goals simultaneously.

Despite the potential of mineral carbonation processes, current modeling approaches have significant limitations in predicting the complex ionic interactions within these systems. These ionic properties play a crucial role in determining reaction rates, product formation, and overall process efficiency. Without accurate models that capture these dynamics, designing optimal reactors for industrial-scale applications becomes challenging, creating a bottleneck in the practical implementation of these technologies.

To address this gap, an ionic reaction model has been developed that provides more accurate predictions of the kinetic behavior during mineral carbonation. This model considers the complex interplay between various ionic species, pH changes, and reaction pathways that occur when CO_2 reacts with calcium-containing materials. However, as with any mathematical model, proper validation and parameter identification through experimental data is essential. This identifying process forms a critical step in establishing the model's reliability for predicting carbonation behavior under various conditions and ultimately supporting the design of more efficient carbon utilization processes.

Chapter 1 introduces the fundamental concepts of cement and concrete production, their environmental impact, and various decarbonization strategies, with a particular focus on SCMs and their carbonation potential. Chapter 2 delves into mineral carbonation mechanisms and kinetics, examining traditional modeling approaches such as the shrinking core model and two-film theory while highlighting their limitations in capturing the complex reaction networks in cementitious systems. Chapter 3 presents the formulation of a novel ionic model that explicitly accounts for calcium leaching, CO_2 dissolution, carbonate speciation reactions, and precipitation phenomena, incorporating solution chemistry effects that previous models often neglected. Chapter 4 outlines the parameter estimation methodology employed, describing the experimental dataset and optimization techniques (Genetic Algorithm, Differential Evolution,

and hybrid approaches) used to calibrate the model parameters. Chapter 5 provides a comprehensive analysis of model results, revealing the distinct kinetic regimes during carbonation, the evolution of carbonate species, and the progressive development of diffusion barriers while also evaluating parameter sensitivity and identifiability. The findings establish a foundation for understanding and optimizing carbonation processes, offering valuable insights for implementing CO_2 mineralization strategies in the cement industry.

Chapter 1

Decarbonization of the cement industry: the role of CO_2 mineralization

In this chapter, the carbon footprint of cement and concrete production will be addressed. This will be followed by a discussion on carbon capture and storage, exploring its significance and strategies in reducing CO2 emissions.
Then, Supplementary Cementitious Materials (SCMs) and how it would be helpful in reducing CO_2 emissions, along with the role of carbonated supplementary cementitious materials (cSCMs), will be introduced. Finally, emerging technologies aimed at utilizing emitted carbon dioxide will be examined.

1.1 Carbon Dioxide Emission

In recent decades, active measures have begun to be taken to solve global problems due to the increase in the concentration of the greenhouse gas CO_2 in the atmosphere. Now it exceeds 400 ppm. An increase in the concentration of carbon dioxide in the atmosphere (together with water vapor, methane, nitrous oxide) is one of the main reasons for the gradual increase in the global average annual temperature of the surface air layer. According to the studies (Kabir et al., 2023; Preston & Jones, 2006), the average annual temperature increase reaches 0.2 - 0.7 °C, while this indicator was 0.005 - 0.07 °C per year in the past century. Such climate change due to an increase in the CO_2 content in the atmosphere leads to a change in climatic zones, the appearance of drought-prone regions, erosion of the ice cover at both poles of the Earth, and accordingly sea level rise (Yurak & Fedorov, 2024). Subsequently, main types of natural and anthropogenic sources will be considered for carbon dioxide and chemical reactions of CO_2 formation.

1.1.1 Natural emissions and removals of carbon dioxide

The amount of carbon dioxide emissions from natural sources has been reported to vary between 550 to 848 billion ton/year in the period 1990 – 2022. Considering the average values over the years, the share of natural CO_2 emissions will be 94.7 – 97.1% of the total carbon

dioxide emissions into the atmosphere. Many researchers divide natural CO_2 emissions into five large types: (1) respiration of living organisms; (2) respiration of soils; (3) processes in the world ocean; (4) volcanic activity (including earthquakes); and (5) mineral formation (Yurak & Fedorov, 2024).

Based on the data given in the literature from 1990 to 2022, the average values for natural CO_2 emissions in each of the five types are calculated. The obtained values are used to construct a pie chart shown in Figure 1.1, which are processes in oceans and photosynthesis of plants. Figure 1.1 shows that a little less than half (43.0%) of natural carbon dioxide emissions are occupied by processes occurring in oceans. This is primarily due to the large space occupied by oceans (more than 70% of the Earth's area). The remaining share is divided almost equally between the respiration of soils and living organisms (more than 28% for each type). Small portions (less than 0.1%) are occupied by volcanic activity and mineral formation.

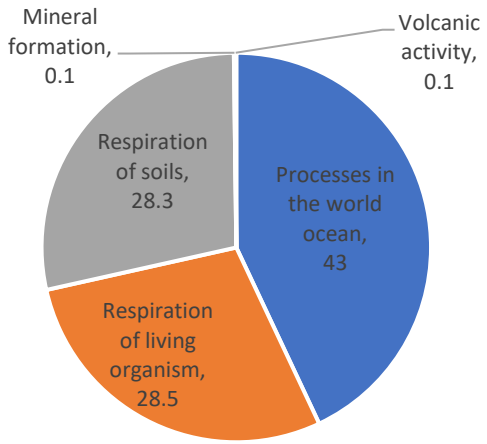

Figure 1.1 Pie chart based on average literature data of the main sources of natural carbon dioxide emissions.

1.1.2 Anthropogenic carbon dioxide emissions

According to various estimates, the average amount of carbon dioxide emissions because of human activity increased from 24.9 to 41 billion tons/year in the period from 1990 to 2022 (Yurak & Fedorov, 2024). Production volumes are growing every year, and the number of vehicles is increasing due to the growth of the world's population.

The most important anthropogenic source of carbon dioxide emissions into the atmosphere is the combustion of fossil fuels. CO_2 emissions from agriculture, deforestation, cement, and concrete production also make a significant contribution. If only the year 2022 is considered, the results will be categorized into three groups (without deforestation): 84.7% combustion of fossil fuels, 9.1% agriculture, and 6.2% cement and concrete production. Figure 1.2 shows that

almost 80% of all anthropogenic emissions are taken up by the combustion of fossil fuels. This is not surprising since nowadays, not only vehicles but almost all production depends on fossil fuels (power plants, mining and metallurgical plants, etc.). The remaining quarter is divided between agriculture (8.7%), cement and concrete production (5.7%), and deforestation (5.2%), each of which makes a significant contribution to anthropogenic CO_2 emissions (Yurak & Fedorov, 2024). Hence, the amount of carbon dioxide emitted by the cement industry is highly significant, making it a crucial area for investigation to optimize processes and reduce energy consumption and carbon dioxide emissions.

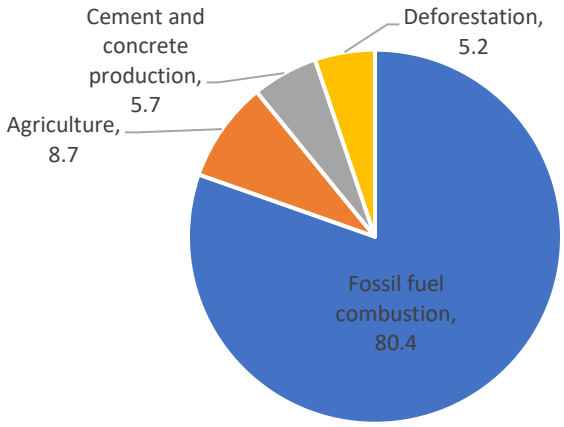

Figure 1.2 *Pie chart based on average literature data of the main sources of anthropogenic carbon dioxide emissions.*

As the objectives of this project are aligned with decarbonization in the cement industry, it is essential to provide a general conceptual understanding of cement and concrete production, as well as the sources of CO_2 emissions within this industry. This background will facilitate a comprehensive analysis of the processes contributing to carbon emissions and the potential strategies for their mitigation.

1.2 Cement and concrete production

Cement and concrete production have emerged as significant contributors to greenhouse gas emissions, necessitating urgent decarbonization efforts. The environmental impact of these industries is driven by the CO_2 released during cement manufacturing, along with energy-intensive processes involved in grinding and transportation. Concrete, which heavily relies on cement, further amplifies these environmental challenges. Thus, decarbonizing cement and concrete production is crucial for sustainable construction practices and mitigating climate change. Decarbonization offers several key benefits. First, it is an essential element of global climate change mitigation strategies, aligning with international goals and targets. By reducing

CO_2 emissions from cement and concrete production, significant progress can be made toward achieving climate objectives. Additionally, decarbonization supports sustainable development in the construction industry, ensuring long-term environmental preservation and resource conservation (Barbhuiya et al., 2024).

1.2.1. Carbon footprint of cement and concrete

Cement production is known for its significant energy consumption. The primary energy source used in cement plants is fossil fuels, such as coal, petroleum coke, and natural gas. These fuels are combusted in kilns (high-temperature furnaces) to provide the high temperatures necessary for clinker formation.

The combustion of fossil fuels results in the release of carbon dioxide into the atmosphere, contributing to climate change. To address these environmental concerns, the cement industry is actively seeking ways to reduce its carbon footprint. Energy efficiency measures, such as optimizing kiln design, improving heat recovery systems, and implementing alternative fuels, can significantly reduce energy consumption and CO_2 emissions. Alternative fuels include biomass, waste-derived fuels, and even non-recyclable plastics, which can be used as a substitute for traditional fossil fuels.

Moreover, the cement industry is exploring innovative technologies like carbon capture and storage (CCS) to capture CO_2 emissions from cement plants. CCS involves capturing the CO_2 emitted during cement production, transporting it, and safely storing it underground or utilizing it in other industrial processes. (Barbhuiya et al., 2024).

Concrete production is a fundamental process in the construction industry, involving the mixing of cement, aggregates, water, and sometimes additives to create versatile and durable construction material. The process of concrete production begins with the selection and preparation of aggregates, which typically include sand, gravel, crushed stone, or recycled materials. Aggregates are carefully graded to achieve the desired strength, workability, and durability of the concrete. At the next step, cement (i.e. Portland cement) as the binding agent, is combined with the graded aggregates. Water is then added to the mix to initiate the chemical reaction called hydration, where the cement particles react with water and form a paste that coats the aggregates (Sari & Pasamehmetoglu, 2005).

The water-cement ratio is crucial as it determines the workability and strength of the concrete. Proper control of water content is essential to achieve a concrete mix that is easy to place, compact, and has the desired strength and durability. In some cases, additives are incorporated into the concrete mix to enhance specific properties (Diamantonis et al., 2010). These additives can include plasticizers, which improve workability; air-entraining agents, which introduce microscopic air bubbles to increase freeze-thaw resistance; or superplasticizers, which enhance flowability without compromising strength.

Once the concrete mix is thoroughly mixed, it is transported to the construction site and placed into formwork. The concrete is then compacted to remove air voids and ensure proper consolidation. Various methods can be used for compaction, including vibration, tamping, or the use of special equipment (Şengün et al., 2019). Finally, concrete undergoes a curing process to allow the hydration reactions to continue and the concrete to gain strength (Barbhuiya et al., 2024).

According to the importance of cement and concrete production, the extraction of raw materials, energy consumption during manufacturing, and transportation of materials contribute to carbon emissions and resource depletion. To address these concerns, efforts are being made to incorporate sustainable practices, such as using recycled aggregates, optimizing mix designs to reduce cement content, and embracing alternative cementitious materials with lower carbon footprints.

1.2.2 CO_2 emissions in cement and concrete industry

CO_2 emissions in the cement industry are a significant environmental concern. While concrete itself does not directly emit carbon dioxide during its curing and hardening process, the production of concrete involves the use of cement, which is a major source of CO_2 emissions. The process of cement production involves the transformation of raw materials, such as limestone and clay, into clinker, which is a powdered form of cement. This transformation is achieved through a process called calcination. During calcination, limestone, which contains a significant amount of calcium carbonate, is subjected to high temperatures in a kiln. As a result, the limestone undergoes chemical decomposition, releasing carbon dioxide into the atmosphere.

$$CaCO_3 \xrightarrow{\Delta} CaO + CO_2 \tag{1.1}$$

This process of calcination is one of the major contributors to carbon emissions in the cement industry. On average, for every ton of clinker produced, approximately 0.5 – 0.7 tons of CO_2 are emitted solely from the calcination process. In addition to calcination, the combustion of fossil fuels represents another significant source of carbon emission in the cement industry.
Fossil fuels, including coal, petroleum coke, and natural gas, are commonly used as fuel sources to generate the high temperatures required in cement kilns. When these fuels are burned, they release carbon dioxide into the atmosphere, contributing to the overall carbon footprint of cement production. The amount of CO_2 emissions from fossil fuel combustion in the cement industry depends on several factors, including the type of fuel used, the efficiency of the combustion process, and the implementation of emission control measures (Barbhuiya et al., 2024).

1.3 Strategies for decarbonizing cement and concrete production

Strategies for decarbonizing cement production involve a range of approaches aimed at reducing carbon emissions and promoting sustainability. One strategy is the use of alternative cementitious materials, such as fly ash, slag, and pozzolans, which can partially replace traditional clinker and reduce carbon intensity. Carbon capture and storage (CCS) technology is another important strategy, capturing CO_2 emissions from cement plants and storing them underground. Improving energy efficiency in cement manufacturing through process optimization, waste heat recovery, and energy-efficient technologies is also critical. The development of low-carbon cement, including blended cement and novel binders, offer greener alternatives. Circular economy approaches, such as recycling concrete waste and utilizing alternative fuels, further contribute to decarbonization efforts in the cement industry (Barbhuiya et al., 2024).

1.3.1 Using alternative clinker technologies

Alternative clinker technologies are innovative approaches aimed at reducing the carbon footprint of cement production. These technologies seek to replace or minimize the use of traditional clinkers, which is a major source of CO_2 emissions. By exploring and adopting alternative clinker technologies, the cement industry can contribute to global efforts in mitigating climate change and achieving sustainability goals. One example of an alternative clinker technology is calcined clay-based cement, such as LC3 (Limestone Calcined Clay Cement) (Sharma et al., 2021). These cements utilize calcined clay as a partial substitute for clinkers, resulting in reduced energy consumption and CO_2 emission.

Calcined clay is a by-product of various industrial processes and can be readily available, making it an attractive option for sustainable cement production. The incorporation of calcined clay also enhances the properties of the cement, such as improved durability and strength (L. Wang et al., 2021). Ongoing research and development efforts are focused on optimizing the blend ratios and production techniques to maximize the benefits of calcined clay-based cement.

Another approach in alternative clinker technologies is the use of belite-based cements. Belite is a low-temperature phase in cement production that requires less energy during the kiln process compared to traditional clinker. By reducing the clinker content and increasing the proportion of belite, these cements offer a more sustainable alternative to Portland cement. Belite-based cements have shown promising results in terms of reducing CO_2 emissions and conserving energy (Antunes et al., 2022). However, further research is needed to optimize the composition and properties of belite-based cements to ensure their commercial viability.

1.3.2 Carbon capture, storage, and utilization (CCSU) in cement, and concrete plants

Carbon Capture and Storage (CCS) is a promising technology for reducing carbon emissions in cement plants. CCS aims to capture the CO_2 produced in cement production and prevent it from being released, thus mitigating climate change. In the context of cement plants, CCS can be implemented through various methods to reduce carbon emissions. Two common approaches are post-combustion and pre-combustion capture. Additionally, carbon capture and utilization (CCU) offer innovative solutions to reduce the carbon impact of concrete production and enhance its sustainability. One approach in concrete production involves the production of alternative binders or aggregates using captured CO_2 through chemical reactions. Subsequently, each mentioned approach will be addressed.

1.3.2.1 carbon capture methods

Post-combustion capture involves capturing CO_2 from the flue gases generated during cement production (Laribi et al., 2019). This process typically employs chemical solvents or sorbents that selectively capture CO_2 from the flue gas stream. The flue gases are passed through an absorber where the CO_2 reacts with the solvent, forming a solution of CO_2-rich solvent. The solvent is then regenerated by heating, releasing the captured CO_2, which can be further purified and compressed for transport and storage.

Another method is pre-combustion capture, where CO_2 is captured from the fuel before it is combusted. In cement plants, this can be achieved by reforming fuel, such as coal or natural gas, to produce a hydrogen-rich gas stream. The fuel reacts with steam in a process called steam methane reforming or coal gasification, resulting in the production of a gas stream containing hydrogen and CO_2. CO2 is then separated from this gas stream using processes like pressure swing adsorption or membranes, producing a concentrated CO_2 stream that can be transported and stored (Park et al., 2013).

Both post- and pre-combustion capture methods have their advantages and challenges. Post-combustion capture can be retrofitted to existing cement plants, allowing for the reduction of carbon emissions without significant modifications to the existing infrastructure. However, it requires a large amount of energy for the capture and regeneration processes, which can impact the overall energy efficiency of the plant. Pre-combustion capture, on the other hand, offers the advantage of higher CO_2 capture efficiency and potential co-production of hydrogen, which has its industrial applications. However, it requires additional processing units and may necessitate changes in the fuel supply and combustion systems (Barbhuiya et al., 2024). Table 1.1 shows the summary of pre–combustion and post-combustion characteristics.

Table 1.1 *Comparison between post-combustion and pre-combustion c*arbon capture methods.

	Advantageous	**Disadvantageous**	**Technology**
Post-combustion	Retrofitting Compatible with various fuel types	High energy consumption High operational costs Large space requirements	Chemical Absorption Oxyfuel Combustion Membrane Separation
Pre-combustion	Easier to capture Lower energy requirements Potential for hydrogen use	Non- Retrofitting Complex technology High initial investment	Gasification Shift Reaction, and CO_2 removal

1.3.2.2 Carbon storage

Once carbon dioxide is captured from cement plants, it must be transported to suitable storage sites. The transportation method depends on factors such as the distance to the storage site and the volume of CO_2 to be transported. The most common transportation options are pipelines, ships, and trucks. Pipelines are often preferred for long-distance transport of large volumes of CO_2. Dedicated pipelines can be constructed to connect the capture facility to the storage site, ensuring a continuous and efficient flow of CO_2. Pipelines offer a secure and cost-effective means of transportation and they are widely used in existing CO_2 capture and storage projects. For shorter distances or when pipeline infrastructure is not available, ships and trucks can be used for CO_2 transportation. CO_2 can be transported in specially designed containers on ships or in pressurized tanks on trucks. This mode of transportation is more flexible and suitable for smaller volumes of CO_2 or when the storage site is located near a waterway or roadway (Svensson et al., 2004).

The storage sites for CO_2 are typically deep underground geological formations. These formations provide secure and permanent storage for the captured CO_2, preventing it from entering the atmosphere and contributing to climate change. The most common storage sites include depleted oil and gas reservoirs and saline aquifers. Depleted oil and gas reservoirs are considered ideal storage sites due to their geological characteristics. These reservoirs have been previously used to extract oil and gas and once they are depleted, they can be repurposed for CO_2 storage. The existing infrastructure, such as wells and infrastructure for oil and gas extraction, can be utilized for CO_2 injection. Saline aquifers are porous rock formations that contain salty water. They have large storage capacities and can potentially store significant amounts of CO_2. CO2 is injected into the saline aquifers, where it is trapped in the pore spaces of the rock formation (Ajayi et al., 2019).

1.3.2.3 Carbon capture and utilization

Carbon utilization offers innovative solutions to reduce the carbon impact of concrete production and enhance its sustainability. One approach to CCU in concrete production is the capture and utilization of CO_2 emissions from industrial sources. By capturing CO_2 from power plants, cement factories, or other emission-intensive processes, the greenhouse gas is diverted from the atmosphere and prevented from contributing to climate change. This captured CO_2 can then be utilized in the incorporation of captured CO_2 into the concrete mix itself. This can be achieved by chemically converting CO_2 into mineralized carbonates, which can act as a SCMs. These carbonates can be used as a mineral admixture in concrete, partially replacing traditional cement. Utilizing CO_2 using this approach, carbonation content is enhanced, leading to increased carbon sequestration within the concrete and reducing the overall carbon footprint of the material (Ghiat & Al-Ansari, 2021).

Another CCU approach in concrete production involves the production of alternative binders or aggregates using captured CO_2. Through chemical reactions, CO_2 can be bound with certain materials to produce cementitious products with reduced carbon footprints. These alternative binders can be used as substitutes for traditional cement in concrete production, further reducing CO_2 emissions associated with the manufacturing process. CCU technologies in concrete production not only help to mitigate CO_2 emissions but also contribute to the circular economy by transforming waste CO_2 into a valuable resource. The slow nature of natural carbonation requires extended periods for significant carbon sequestration. Accelerated carbonation techniques must be optimized to ensure consistent and efficient carbonation throughout the concrete matrix (Zajac et al., 2021).

1.3.3 Improved energy efficiency in cement manufacturing

A key strategy for improving energy efficiency in cement production is the optimization of kiln operations. This can be achieved through the deployment of advanced control systems that continuously monitor and adjust critical kiln parameters, such as temperature, airflow, and fuel-to-air ratios. Fine-tuning these variables ensures optimization of operations, thereby minimizing energy consumption and carbon emissions. Additionally, the integration of heat recovery systems allows for the capture and reuse of waste heat generated during cement manufacturing, further contributing to overall energy efficiency.

Another crucial approach is the utilization of alternative fuels and raw materials. Replacing traditional fossil fuels with renewable or low-carbon alternatives, such as biomass, waste-derived fuels, or non-recyclable plastics, significantly reduces reliance on conventional energy sources and helps lower carbon emissions. Moreover, incorporating industrial by-products like slag or fly ash in cement production not only makes use of waste materials but also enhances

process efficiency. This leads to lower energy demands and a reduced environmental footprint, making cement manufacturing more sustainable (Barbhuiya et al., 2024).

1.3.4 Circular economy approaches in cement production

The adoption of circular economy principles in cement manufacturing is gaining traction as a sustainable alternative to the conventional linear model of production, consumption, and disposal. Instead of treating resources as disposable, the circular approach focuses on minimizing waste and maximizing resource efficiency, thereby reducing the environmental impact of cement production.

One of the core strategies in circular cement production is the use of alternative raw materials. Traditionally, cement relies on virgin materials such as limestone and clay, but integrating recycled materials and industrial by-products into the production process can significantly decrease the demand for new resource extraction. By utilizing slag from steel production or fly ash from coal-fired power plants as supplementary cementitious materials (SCMs), manufacturers can reduce both environmental impact and raw material dependency while promoting more efficient resource use.

Another important aspect of circularity is industrial symbiosis, where cement plants collaborate with other industries—such as steel, glass, or chemical manufacturing—to exchange by-products, materials, and energy. This synergy allows industries to repurpose waste heat, secondary raw materials, or alternative fuels, thus optimizing resource use and reducing waste generation. For example, waste heat from cement kilns can be used to support nearby industrial operations, reducing the need for additional energy inputs, while cement plants can, in turn, utilize industrial residues as raw materials or alternative fuels.

Additionally, concrete recycling and reuse are integral to circular economy efforts in cement production. Demolished concrete structures and construction waste can be crushed, processed, and repurposed as aggregates in new concrete production. This practice conserves natural resources, reduces landfill waste, and lowers the carbon footprint of the cement industry. Furthermore, incorporating recycled concrete aggregates into new concrete formulations enhances sustainability while maintaining structural performance.

By adopting these circular economy approaches, the cement industry can transition toward a more sustainable, low-waste production system, ultimately contributing to resource conservation and reduced environmental impact (Barbhuiya et al., 2024).

1.3.5 Use of supplementary cementitious materials

The use of Supplementary Cementitious Materials (SCMs) is a crucial strategy in the construction industry's efforts to decarbonize concrete production and reduce its environmental impact. A key focus lies in the substitution within the binder, which includes cement and its

constituents. SCMs, such as fly ash, slag cement, silica fume, and natural pozzolans, have the potential to partially replace Portland cement in concrete mixtures, thereby lowering the carbon footprint associated with cement production. Beyond their environmental benefits, SCMs enhance the performance of concrete, reducing the reliance on cement while simultaneously improving durability and overall material efficiency. This dual advantage supports the sustainability of the construction sector by minimizing resource consumption and mitigating environmental degradation.

Targeting the substitution of cement constituents within the binder is particularly significant for reducing the environmental footprint of cement and concrete production. Since clinker production is the most carbon-intensive process in cement manufacturing, incorporating SCMs presents a viable pathway to decreasing emissions. Additionally, this approach promotes resource efficiency by integrating industrial by-products into the binder matrix, thereby reducing waste. Although achieving large-scale substitution of cement with non-cementitious materials poses challenges, prioritizing the replacement of cement constituents within the binder provides a practical and effective means of advancing sustainability without compromising essential construction properties.

SCMs offer numerous benefits, including improved durability, reduced cracking, increased resistance to chemical attacks (degradation caused by exposure to aggressive chemical substance, i.e. sulfate attack, acid attack, and carbonation), and enhanced permeability properties. However, challenges such as regional availability and material variability must be addressed to ensure consistent quality and performance. Rigorous testing, quality control measures, and region-specific implementation strategies are essential for the successful integration of SCMs. Furthermore, widespread adoption requires supportive policies, updated industry standards, and proactive government interventions to encourage the use of low-carbon materials. Collaboration between researchers, industry stakeholders, and policymakers is vital for optimizing SCM performance, exploring new sources, and accelerating their implementation, ultimately ensuring a more sustainable future for concrete production (Pamenter & Myers, 2021; van Deventer et al., 2021).

1.4 SCMs and carbonated SCMs

It was common during most of the early and mid-twentieth century to use paving mixtures that employed Portland cement as the sole binder. From the early 1980s onward, there was an increase in the use of SCMs, such as fly ash and slag cement, and today SCMs are used routinely in concrete paving mixtures to provide improvement in workability, long-term strength, durability, and sustainability to the economy.

Studies have shown that for typical concrete, roughly 85% of energy and 90% of the GHG emissions associated with concrete production are results of the manufacturing of Portland

cement. Some reduction of GHG emissions can be achieved through improved plant efficiency, but roughly half of the CO_2 emitted is from the decomposition of raw materials, thus limiting the potential improvement through this route alone. Therefore, one of the most effective strategies to reduce the GHG emissions (mentioned in section 1.3) associated with concrete without negatively affecting concrete performance is to reduce the amount of Portland cement clinker used as a binder in concrete. On a larger scale, the amount of clinker used as binder can be reduced significantly by replacing Portland cement with SCMs, either by adding SCMs to the concrete mixture at the concrete plant or using blended cement.

1.4.1 Types of Supplementary Cementitious Materials

SCMs are materials that by being blended with Portland cement contribute to the properties of concrete through hydraulic activity, pozzolanic activity, or both. Hydraulic activity occurs when phases in SCM chemically react with water, forming cementitious hydration products similar to those formed through the hydration of Portland cement. This contrasts with pozzolanic activity, which is characterized by the reaction between siliceous or aluminosiliceous material in the SCM with calcium hydroxide (a reaction product from the hydration of Portland cement), forming calcium silicate hydrate and other cementitious compounds. Calcium silicate hydrate is a more desirable hydration product and thus the pozzolanic reaction is considered to have a positive impact on the long-term properties of the hardened concrete (Van Dom, 2013).

1.4.1.1 Fly ashes

Fly ash is an industrial by-product material produced at coal-fired power plants. As the pulverized coal combusts, mineral impurities are carried away in the flue gases, solidifying into spherical glass particles. These particles, being roughly the same size as cement grains, are collected by electrostatic precipitators or bag filters. As industrial by-product material, the composition, reactivity, and properties of fly ash are highly variable. This variability can be extreme for different classes of fly ash, for the same class of fly ash from different sources, and even for fly ash produced at the same electrical plant given that coal sources, burning techniques, and environmental technologies are changing rapidly. These differences and variability must be recognized in design and construction and rigorous testing of fly ash must be conducted frequently to ensure its continued suitability for use in concrete (Van Dom, 2013).

1.4.1.2 Slag cement

Slag cement is an industrial by-product of the iron blast furnace in which pig iron is extracted from iron ore and the remaining molten material (slag) is directed into a granulator, in which water quenches the material to form glassy, sand-like particles of amorphous oxides of calcium, aluminum, magnesium, and iron. These particles are then ground to a similar size as, or slightly

finer than, Portland cement. Slag cement is reactive, either slowly in the presence of water alone or more vigorously when activated in water in the presence of sodium hydroxide or calcium hydroxide. The latter is the condition present in the pore solution of hydrating Portland cement and, thus, the two react in a complementary manner. As an industrial by-product material, slag cement will vary from source to source, but variability for a given source is usually very low. Often the properties of the slag cement are altered slightly as a result of the fineness of the grind, with more finely-ground slag cement being more reactive (Van Dom, 2013).

1.4.1.3 Recycled Concrete Aggregate (RCA)

Concrete waste can be generated from various activities such as construction, demolition, and renovation. Instead of simply discarding this waste, it can be processed and utilized beneficially. One commonly used method for recycling concrete waste is through the process of crushing and screening. The waste concrete is broken down into smaller pieces and sorted based on their size. The resulting material, known as recycled concrete aggregate (RCA), can be used as a substitute for natural aggregates in the production of new concrete. RCA retains the structural properties of conventional aggregates while significantly reducing the need for virgin materials and minimizing the extraction of new aggregates. The simplified flow of the concrete recycling process is depicted in Figure 1.4 (Barbhuiya et al., 2024).

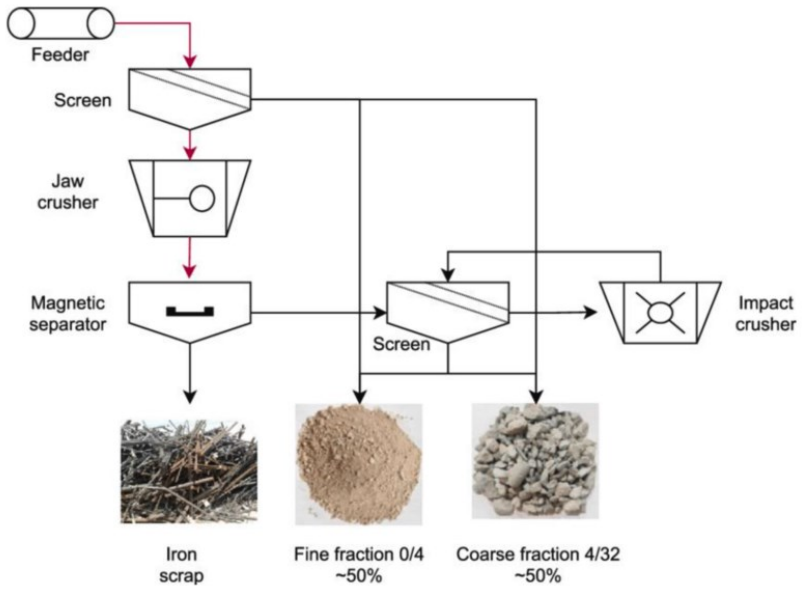

Figure 1.3 Simplified flow of the concrete recycling process (Barbhuiya et al., 2024).

Recycled concrete can also serve as a sustainable base material for constructing roads, pavements, and foundations. By using recycled concrete as a substitute for traditional granular materials, the consumption of natural resources can be reduced, leading to a decrease in the carbon footprint associated with the transportation of construction materials. Furthermore, recycled concrete can be processed into smaller particles called recycled concrete fines (RCF).

These particles can be employed as a replacement for sand in specific applications, such as road sub-base layers and pipe bedding.

1.4.2 Application of carbonated SCMs

The integration of carbonated materials as Supplementary Cementitious Materials in composite cement presents a promising strategy for enhancing sustainability in the cement industry. This approach involves the carbonation of materials rich in calcium, such as RCP, steel slag, and other industrial by-products, which are then utilized to partially replace clinker in cement formulations. By doing so, the overall carbon footprint of cement production can be significantly reduced.

One notable application is the use of carbonated recycled concrete paste (cRCP), which enhances the pozzolanic reactivity. Through carbonation, the calcium hydroxide present in recycled concrete reacts with CO_2 to form stable calcium carbonate. This process not only sequesters CO_2 but also enhances the material's pozzolanic properties, making it a viable SCM (Zajac et al., 2020).

SCMs contribute to the formation of C-S-H with a higher calcium-to-silica (Ca/Si) ratio initially, which decreases over time as the pozzolanic reaction progresses. In contrast, cRCP, contains an amorphous alumina-silica gel that reacts rapidly with $Ca(OH)_2$. This results in a faster consumption of portlandite and the formation of a low-calcium C-S-H phase at early ages. This rapid reaction contributes to early strength development, which is different from the slower reaction of non-carbonated SCMs.

In a similar way, compressive strength of cement blends with SCMs typically increases gradually over time as the pozzolanic reaction progresses. While Cement blends with carbonated materials exhibit higher early compressive strength due to the rapid reaction of the alumina-silica gel.

Incorporating cRCP into composite cements has been shown to improve hydration characteristics and mechanical performance, while also contributing to waste reduction and resource efficiency. Similarly, the carbonation of steelmaking slags results in the formation of calcium carbonate, which densifies the slag's microstructure. This densification increases the slag's hydration activity and reduces pore size, leading to improved durability and strength in the resulting composite cement (Zajac et al., 2020).

The adoption of carbonated materials as SCMs aligns with circular economy principles by repurposing industrial waste and by-products, thereby minimizing environmental impact. However, challenges such as the variability in the composition of recycled materials and the need for standardized processing methods must be addressed to ensure consistent performance in cement applications.

In conclusion, the application of carbonated materials as SCMs in composite cement offers a multifaceted solution to reduce CO_2 emissions, enhance material performance, and promote

resource efficiency in the cement industry. Ongoing research and development are essential to optimize these processes and facilitate their widespread implementation.

1.5 Kinetic modeling of SCMs to cSCMs

Kinetic modeling of supplementary cementitious materials (SCMs) undergoing carbonation is essential for optimizing their performance and durability in concrete applications.

Carbonation kinetics focuses on the reaction of CO_2 with alkaline phases (e.g., portlandite, C-S-H, and calcium silicates) in SCMs to form stable carbonates. Understanding the reaction rates and mechanisms of carbonation enables accurate predictions of the long-term behavior of SCMs in composite cements.

A robust kinetic model allows researchers to predict reaction rates by assessing the influence of variables like CO_2 concentration, temperature, humidity, particle size, and solution chemistry, while also optimizing reactor design by determining ideal parameters such as gas flow rate, pressure, and contact time to maximize CO_2 uptake with minimal energy consumption. Additionally, kinetic models enable the scale-up of carbonation processes from laboratory to industrial applications by simulating the impact of system size and operational conditions. Various modeling approaches, including the shrinking core model, which predicts carbonation based on diffusion-controlled or reaction-controlled mechanisms, and ionic reaction models, which focus on ion transport and precipitation kinetics, are used to simplify complex interactions and enhance computational efficiency.

Ionic reaction modeling mimics the physical real-world complex chemical interactions by focusing on the ionic species and their reactions, reducing simplifying assumptions and making it more feasible to identify systems with lower model uncertainties. This approach can capture the essential features of carbonation kinetics, such as ion diffusion and precipitation reactions, which are critical for predicting the reaction progress in aqueous conditions.

1.6 Motivation and objectives of the Thesis

The cement industry is responsible for approximately 8% of global CO_2 emissions, with clinker production being the most carbon-intensive component. To address this environmental challenge, SCMs present a valuable opportunity. Rather than simply capturing and storing CO_2, we can utilize it to carbonate SCMs, creating materials that can partially replace traditional clinkers in cement production. These carbonated cSCMs not only reduce the carbon footprint of cement but can also enhance its performance properties. To effectively implement this solution on an industrial scale, we need accurate models that capture the complex reaction kinetics and transport phenomena, enabling optimal reactor design for the carbonation process.

Current modeling approaches like the shrinking core model, surface coverage model, and two-film theory fall short when applied to these complex cementitious systems. These models typically focus on molecular-level reactions and surface diffusion mechanisms while assuming single-phase material reactions. This simplified approach fails to capture the heterogeneous nature of cement materials, which contain multiple reactive phases including calcium hydroxide, calcium silicate hydrates, and various anhydrous components interacting simultaneously.

Existing models also struggle to account for the critical role of ionic interactions and transport phenomena. They cannot adequately predict pH evolution during carbonation or the concentrations of intermediate ionic species that govern reaction pathways. This creates a substantial disconnect between theoretical predictions and experimental observations, hampering our ability to design efficient reactors for SCM carbonation.

This thesis aims to develop a comprehensive ionic reaction model for mineral carbonation that overcomes these limitations. Rather than focusing solely on solid-state transformations, our approach incorporates the complex interplay of ionic interactions and transport phenomena, integrating multiple reaction pathways including calcium leaching from different sources, CO_2 dissolution and speciation, and calcium carbonate precipitation. By accounting for the dynamic evolution of solution chemistry, particularly pH changes and carbonate speciation, we can better represent the actual physicochemical processes.

Through parameter estimation with experimental data, we seek to identify the dominant reaction mechanisms and rate-limiting steps throughout the carbonation process. This understanding will enable more targeted optimization strategies and establish a foundation for improved reactor design for producing carbonated SCMs. The ionic model provides more comprehensive insights by explicitly accounting for aqueous-phase reactions, allowing prediction of crucial parameters like pH, ionic strength, and activity coefficients that significantly influence carbonation kinetics.

By bridging the gap between theoretical modeling and experimental observations, this work aims to advance our understanding of mineral carbonation and contribute to more efficient CO_2 utilization technologies. Ultimately, our goal is to support sustainable construction practices through the development of carbonated SCMs, helping to reduce the environmental impact of the cement industry while creating value from what would otherwise be wasted CO_2.

Chapter 2

Mineral carbonation: Mechanisms and kinetics

The increasing concentration of atmospheric carbon dioxide (CO_2) and its role in climate change has driven a critical need for effective carbon capture, utilization, and storage (CCUS) technologies. Mineral carbonation, a process where CO_2 reacts with metal oxides to form stable carbonates, presents a promising avenue for permanent CO_2 storage (Zajac et al., 2023a). This chapter explores the state of the art in mineral carbonation, focusing on various modeling approaches, including the shrinking core model, the two-film theory, and a general rate equation. Finally, the potential of ionic modeling to improve current models is considered.

2.1 Mineral Carbonation: Fundamental Overview

Mineral carbonation involves the reaction of alkaline earth metal oxides, primarily calcium (Ca) and magnesium (Mg), with CO_2 to form stable carbonates. These reactions are thermodynamically favorable under ambient conditions, making mineral carbonation a viable approach for CO_2 sequestration. The process can be represented by the following general equation, where M is typically Ca or Mg:

$$MO + CO_2 \rightarrow MCO_3 \tag{2.1}$$

This reaction is exothermic (releasing heat), and the resulting carbonates are stable and nearly insoluble under normal atmospheric conditions (Zajac et al., 2023). CO_2 mineralization technologies can be divided into below-ground (in-situ) mineralization and above-ground (ex-situ) mineralization. The in-situ process involves the injection of CO_2 into a geological formation, such as a decommissioned offshore oil well, where, with time, it will form carbonates by reaction with ultramafic and mafic geological formations. The ex-situ technology covers above-ground processes that require processing of the suitable precursor before their conversion into carbonates and other products (Sanna et al., 2014). Ex-situ CO_2 mineralization is applied to valorize cementitious materials in engineered processes. These processes can be divided into four categories: (*i*) direct carbonation, (*ii*) indirect carbonation, (*iii*) carbonation

curing, and (*iv*) carbonation mixing. Regardless of the Feedstock (Discussed in section 1.4), the carbonation process consists of two main reactions with optional additional steps. In the dissolution step, the reactive metal compounds (calcium or magnesium) are removed from the mineral matrix as ions, primary oxides, or hydroxides. Those intermediates are carbonated in a second step, i.e., they react with CO_2 to form calcium carbonate ($CaCO_3$) or magnesium carbonate ($MgCO_3$). Figure 2.1 briefly overviews several mineral carbonation technologies that apply those carbonation reactions.

Direct and indirect carbonation methods can be characterized as manufacturing processes of carbonate products that can be further used in various applications. In contrast, carbonation curing and mixing are optional processes in concrete production. Figure 2.2 shows direct carbonation as a one-stage process where CO_2 is directly mineralized into calcium carbonate and other products. This method can be carried out under dry, semi-dry, or wet conditions, depending on the specific requirements of the material and the desired outcome. On the other hand, indirect carbonation involves a multi-stage process. Initially, an extraction agent is used to extract CO_2, which is then mineralized to produce calcium carbonate and other products. These products may be separated depending on the application. Both methods aim to enhance the properties of cementitious materials by incorporating CO_2, thereby contributing to carbon capture and utilization efforts in the construction industry (Zajac et al., 2023).

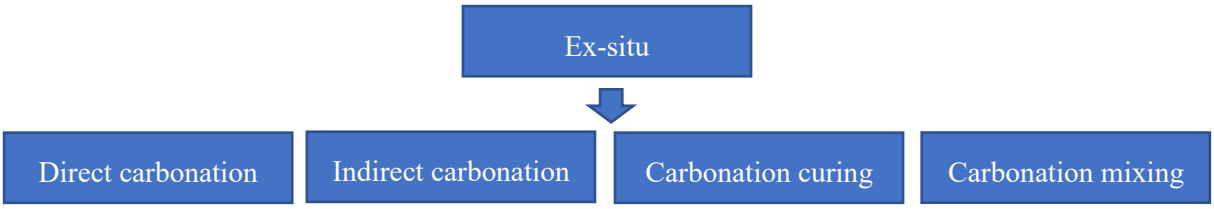

Figure 2.1 *Classification of ex-situ carbonation technologies.*

2.1.1 Direct Carbonation

Direct carbonation refers to the case when metal dissolution and carbonation happen simultaneously in one reactor. In direct gas-solid carbonation, gaseous CO_2 is fed into a reactor, where it reacts directly with a ground feedstock.

The optimum maximum conversion rates for a single-step gas-solid direct carbonation is reported to require energy-intensive reaction conditions (340 bar, 500°C, 2 h) and a reactor type that enables strong particle interactions between the two phases, such as a fluidized bed reactor (Olajire, 2013). Although this direct carbonation route represents the simplest carbonation process, it has relatively lower reaction rates than other procedures. That is why research on this technology has mostly stopped.

So far, the most investigated route is direct aqueous carbonation. In this process, CO_2-containing or pure CO_2 gas is injected into a single reactor with ground feedstock dissolved in a slurry or wet solution. CO_2 is dissolved in water and reacts with hydrogen ions and hydrogen

carbonate. Due to the emerging hydrogen ions, the pH drops slightly, promoting the release of metal ions from the feedstock. Those metal ions react with the hydrogen carbonate, which leads to the precipitation of carbonates as the final reaction product (Olajire, 2013). In Figure 2.3, the schematic of different mineralization processes is shown.

The dissolution step is the rate-limiting step of the whole route. It can be enhanced by additives and variations of temperature, pressure, CO_2 concentration, and particle size of the minerals. Direct aqueous carbonation routes are commonly conducted in continuously stirred tank reactors or, in the case of steel slag, in rotating packed bed reactors, which is referred to as high gravity carbonation as well.

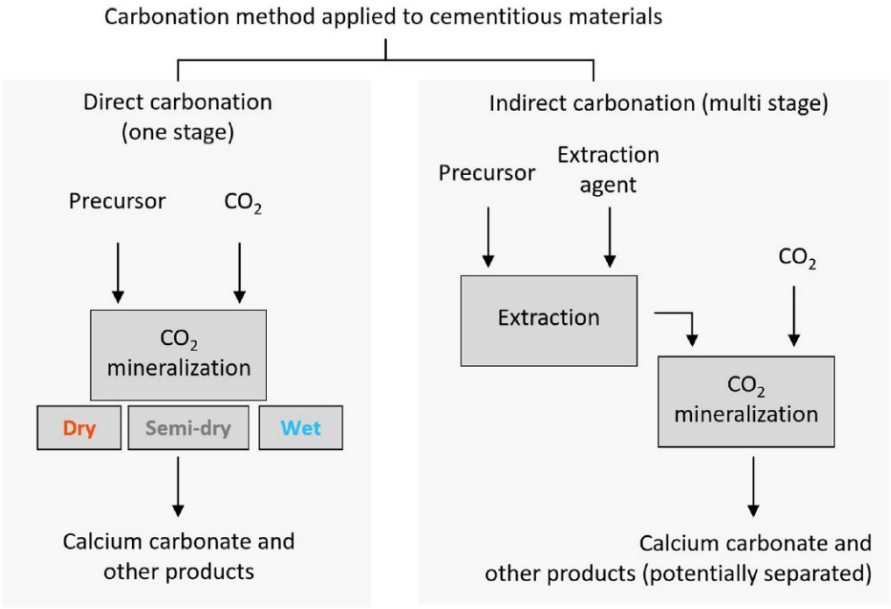

Figure 2.2 *Direct mineral carbonation is accomplished in one step, while indirect mineral carbonation is conducted in two or more steps (Zajac et al., 2023).*

2.1.2 Indirect carbonation

Indirect carbonation methods involve at least two steps, where metal dissolution and carbonation reactions occur separately under distinct conditions in different reactors. These methods can be classified into gas-solid and aqueous processes. In indirect gas-solid carbonation, metal extraction can be performed either through a solid/solid reaction at elevated temperatures of up to 600°C and pressures reaching 100 bar or by dissolving metals using acidic solutions. The final stage typically involves a dry carbonation reaction, often conducted in a pressurized fluidized bed reactor (Chakraborty & Jo, 2018).

One notable gas-solid carbonation method is the ÅA-route, developed by the Finnish Åbo Akademi (ÅA). This multi-stage process begins with the extraction of magnesium from serpentine using ammonium sulfate at temperatures ranging between 400 and 440°C, leading to the formation of solid magnesium sulfate. In the next stage, magnesium hydroxide is

precipitated by introducing aqueous ammonia while the additives are recovered for reuse. Finally, magnesium hydroxide undergoes carbonation in a fluidized bed reactor at temperatures

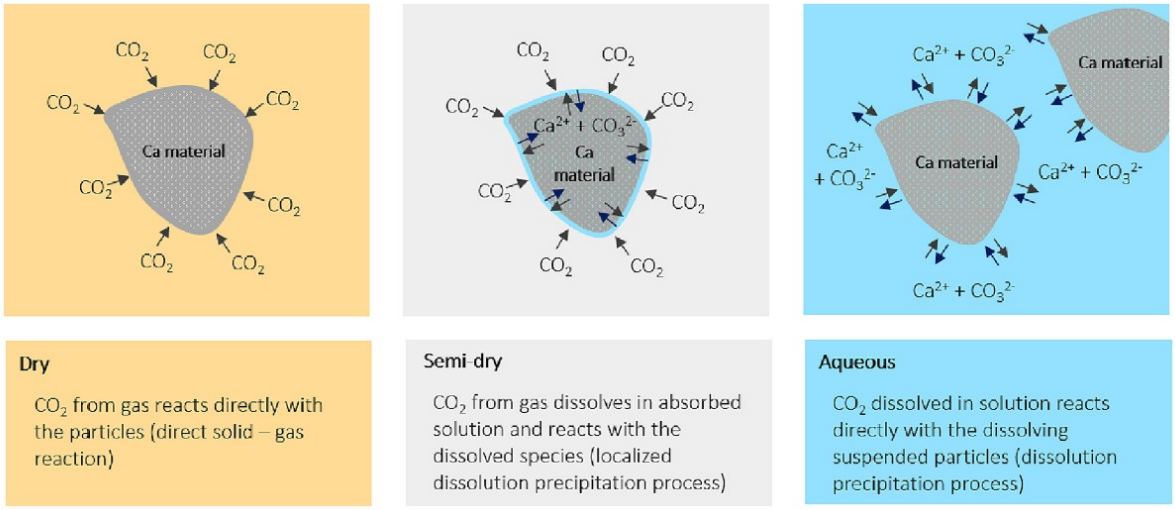

Figure 2.3 *Differences between direct gas-solid (dry), semi- and aqueous (wet) mineralization processes, adopted from (Zajac et al., 2023).*

between 450 and 500°C and a pressure of 20 bar, resulting in the formation of $MgCO_3$ (Zevenhoven & Fagerlund, 2010). However, recovering these additives is often challenging due to the high energy demands associated with the process. In acidic environments, the dissolution of reactive metal ions is enhanced, while the carbonation reaction proceeds more efficiently under basic conditions. This contrast in optimal conditions has led to the development of the pH-swing process, where acids are used to dissolve minerals, followed by the introduction of a base to facilitate carbonation (Chakraborty & Jo, 2018; Olajire, 2013).

A significant advantage of indirect carbonation over direct methods is the improved control over the morphology and particle size of the carbonation products, as well as their enhanced purity. This makes indirect carbonation particularly suitable for producing high-value materials that can be used in industries such as paper and plastic manufacturing.

2.1.3 Carbonation curing

Carbonation curing of cementitious materials, initially proposed in the 1970s, involves the early-age curing of cement-based products in a sealed chamber with pressurized, high-purity CO_2. Carbonation curing offers an alternative to the more traditional, energy-intensive steam curing process. In calcium-based cement systems, such as ordinary Portland cement (OPC), CO_2 reacts with calcium silicates to form a hybrid binder structure composed of calcium-silicate-hydrate and $CaCO_3$. This reaction enhances the strength of cement or concrete products by increasing their density. Additionally, recent studies have explored the incorporation of alkaline solid wastes, such as steel slag or fly ash, as supplementary cementitious materials in

cement and concrete products. These SCMs form a binary binder with cement during carbonation curing. By utilizing SCMs, which are waste products, the carbon footprint of construction materials can be significantly reduced (Olajire, 2013).

2.1.4 Carbonation mixing

Carbonation mixing, or CO_2 mixing, is another application in concrete production. This process involves injecting high-purity CO_2 into the mixture of cement, coarse and fine aggregates, water, and admixtures. The CO_2 reacts with the calcium silicate clinker in OPC to form $CaCO_3$ nanoparticles. This reaction can enhance the compressive strength of the concrete or allow for a reduction in binder usage without compromising strength, leading to indirect CO_2 emission savings. However, the potential CO_2 uptake in carbonation mixing is considerably lower compared to carbonation curing (Olajire, 2013).

2.2 Carbonation potential and degree

The carbonation potential of a material is defined as the ultimate amount of carbon dioxide that can be sequestered, whereas the degree (α) is the ratio of the actual bound CO_2 content compared to the maximum carbonation potential:

$$\alpha = \frac{\mathrm{CO_2^{measure}}}{CO_2^{theory}} \ , \tag{2.2}$$

In the field of cementitious materials, CO_2 is bound mainly to calcium and magnesium. Hence, the maximum CO_2 sequestration potential of a material is usually calculated based on its calcium and magnesium content. For this purpose, the so-called Steinour formula is used (Zajac et al., 2023b):

$$CO_2^{theor} = 0.785 \times (CaO - 0.56CaCO_3 - 0.7SO_3) + 1.091 \times (MgO - 0.479MgCO_3) \tag{2.3}$$

where CO_2^{theor} is the maximum theoretically achievable CO_2 sequestration related to the initial material mass and CaO, $CaCO_3$, SO_3, MgO, and $MgCO_3$ are weight fractions of the corresponding oxides and phases in the carbonated samples. According to this formula, the carbonation potential of the recycled concrete paste can be >400 kg CO_2/t(RCP), whereas the carbonation potential of steel slags varies between 200 and 400 kg CO_2/t(slag) depending on the chemical composition. However, the carbonation potential of the material does not only depend on the chemical composition. Particularly, in the case of steel slags and fly ashes, a significant amount of CaO and MgO can be bound in crystalline phases, which are hard or even not possible to carbonate at industrially feasible conditions. The carbonation potential of

amorphous CaO-MgO-Al_2O_3- SiO_2 glasses is not well recognized, despite these materials being components of steel slags, fly ashes, and recycled concrete pastes. The recycled concrete pastes contain a fraction of sand and aggregates that do not react with CO_2. All these features reduce the carbonation potential based on the chemical composition. Therefore, the actual carbonation potential and degree depend on the mineralogical composition of the given material, the reactivity of the phases constituting the material, and the carbonation method that is applied. The carbonation degree varies between 10% and close to 90%, depending on the material used and the carbonation conditions (Zajac et al., 2023). Consequently, the result of the carbonation and the potential of the CO_2 sequestration must be evaluated by experimental methods to properly assess the valorization approaches and not only calculate theoretical values based on the Steinour equation or similar formulas. The applicable techniques are similar to those used for a typical hydration study including X-ray diffraction complemented by Rietveld refinements or thermogravimetry methods.

2.2 Modeling approach for mineral carbonation

Effective modeling is essential to understanding and optimizing mineral carbonation processes. Various models have been developed to capture the complex interplay of physical and chemical phenomena, including mass transfer, reaction kinetics, and phase transformations. In the following, different mathematical models, such as the shrinking core model and two-film liquid theory, are presented along with their equations, limitations, and weaknesses to provide a clearer conceptual understanding of the phenomena occurring in the system.

2.2.1 Shrinking core model

The shrinking core model is a widely used approach to describe the kinetics of particle-fluid reactions, particularly in the context of carbonation. It's a powerful tool for understanding how materials react and transform, and how we can use that knowledge to optimize processes like CO_2 sequestration. This model simplifies the complex reality of chemical reactions into a more manageable framework, allowing us to predict and control the outcomes of these reactions.

At its core, the shrinking core model visualizes a solid reactant particle as having a core of unreacted material that shrinks over time as the reaction progresses (Li, 2020). The reaction is assumed to take place at the outer surface of this core, and the product of the reaction forms a layer around it. As the reaction proceeds, this product layer grows thicker, and the core shrinks (Figure 2.4).

Here's how the shrinking core model is applied to gas-solid reactions, like carbonation:

- **Initial Stage**: Initially, the gas reactant contacts the outer surface of the solid reactant. The reaction proceeds rapidly at the surface.

• **Product Layer Formation**: As the reaction continues, a layer of solid product forms around the unreacted core.

• **Diffusion through Product Layer**: For the reaction to continue, the gas reactant has to diffuse through the product layer to reach the unreacted core. This diffusion process can be slower than the initial surface reaction, and it can become the rate-limiting step.

• **Shrinking Core**: As the reaction progresses, the unreacted core shrinks, and the product layer becomes thicker.

The shrinking core model can be applied to different shapes of solid reactants, including spheres, cylinders, and slabs, each with its specific mathematical representation. The model considers several key factors that influence the reaction rate, including (Li, 2020; Wei et al., 2021):

- The rate of the chemical reaction at the surface.
- The rate of diffusion of the gas reactant through the product layer.
- The physical shape and size of the reactant particles.

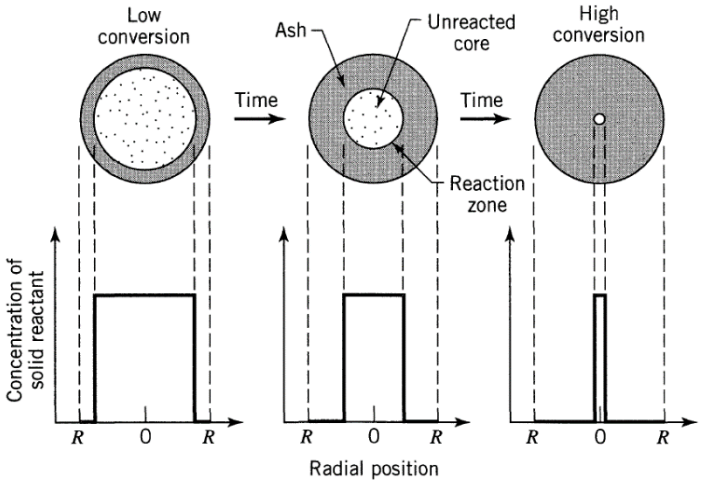

Figure 2.4 *According to the shrinking-core model, the reaction proceeds at a narrow front which moves into the solid particle. The reactant is completely converted as the front passes by (Octave Levenspiel).*

In this section, the carbonation reaction by the shrinking core model will be described, which could be considered as a fluid-solid reaction of the following equation:

$$CO_{2(\text{fluid})} + CaO_{(solid)} \rightarrow CaCO_{3(\text{solid})} \tag{2.4}$$

The carbonation reaction rate can be expressed as equations (2.5, 2.6) (Wei et al., 2021) :

$$v = -\frac{\mathrm{d}n}{\mathrm{d}t} = \frac{4\pi R_0^2 \cdot k' D_e R}{D_e R + k(R_0 R - R_0^2)} \ , \tag{2.5}$$

$$v_A = -4\pi R_0^2 \rho_s \frac{\mathrm{d}R}{\mathrm{d}t} \ , \tag{2.6}$$

Where v $(mol.s^{-1})$ is the gas diffusion flow rate through the solid phase product layer, v_A is solid mass rate variation, R (cm) is the radius of the solid, R_0 (cm) is the radius of the reactant inside the sphere, k' (s^{-1}) is the first-order rate constant for the surface reaction, D_e $(cm^2\ s^{-1})$ is the effective diffusion coefficient, ρ_s (mol cm^{-3}) is the molar density of the solid, and t (s) is the reaction time.

Based on the following assumptions, the final equation is shown as time (t) and carbonation conversion % (X_B) (Miao, Du, Wang, et al., 2023; Wei et al., 2021) :

1) The reaction occurs on the solid exterior at the beginning, then proceeds at a narrow front, last moves into the solid, and leaves behind a completely reacted product, which is referred to as the "ash" layer.
2) The density of the solid reactant and its product are similar.
3) The reaction process satisfies the quasi-steady-state approximation ($v = v_A$).
4) CO_2 is excessive and the external diffusion resistance is neglected.
5) CO_2 undergoes mass transfer in the form of molecular diffusion, and chemical reactions occur only at the active interface of the plate.
6) If the effective diffusion coefficients are considered to be the rate-limiting step, which meant $k' \gg D_e$, the relationship between reaction time and carbonation conversion is shown as:

$$\frac{2D_eC}{R^2\rho_s}t = 1 - \frac{2}{3}X_B - (1 - X_B)^{2/3} \ , \tag{2.7}$$

$$t = \frac{\rho_s R^2}{6D_eC}\left[1 - 3(1 - X_B)^{2/3} + 2(1 - X_B)\right] = \tau\left[1 - 3(1 - X_B)^{2/3} + 2(1 - X_B)\right] \ , \tag{2.8}$$

7) If considering the chemical reaction between reactants is the rate-limiting step, which meant $k' \ll D_e$, the relationship between reaction time and carbonation conversion is shown as:

$$\frac{k'C}{\rho R}t = 1 - (1 - X_B)^{1/3} \ , \tag{2.9}$$

$$t = \frac{\rho_s R}{k'C}\left[1 - (1 - X_B)^{1/3}\right] = \tau\left[1 - (1 - X_B)^{1/3}\right] \ , \tag{2.10}$$

where the C $(mol\ cm^{-3})$ is the aqueous concentration of CO_2, and based on assumption 4 the value is computed by Henry's law.

The traditional shrinking core model assumes a uniform and continuous product layer enveloping the unreacted core of a solid particle, with the reaction interface advancing inward over time. However, this model does not account for the variability in diffusion coefficients throughout the reaction, nor does it consider the formation of non-uniform product structures. Recent observations indicate that solid products often develop as three-dimensional, island-like formations on the reactant surface, leading to the development of improved models such as the

modified shrinking core model and the surface coverage model. In the following sections, we will explore each of these models, discussing their limitations and applications.

2.2.1.1 Modified shrinking core model

Modified shrinking core models based on **diffusion-controlled** mechanisms were proposed to evaluate the carbonation process. The theoretical framework assumes a contracting interface mechanism where active CaO reacts with CO_2 to form a product layer. The effective diffusion coefficient of CO_2 through the product layer decreases over time, giving deficient carbonation efficiency.

One key additional assumption to the previously mentioned points is (Miao, Du, Wang, et al., 2023):

- The effective diffusion coefficient is a function of time.

According to the assumption, the effective diffusion coefficient of the product layer is a function of time. Thus, one may assume that:

$$D_e = D_0 e^{-\eta t}, \tag{2.11}$$

where D_0 is the initial effective diffusion coefficient of the product layer ($m^2\ s^{-1}$) and η is a coefficient reflecting the decay rate of D_0.

By considering Assumption 3, which states that the process operates in a quasi-steady-state, the following equation governing carbon dioxide flux holds valid:

$$J_1 = J_2 = J_3, \tag{2.12}$$

J_1 is the amount of CO_2 diffused through the liquid film near the surface, J_2 is the amount of CO_2 diffused through the product layer and J_3 is the amount of CO_2 consumed at the active interface of the surface. Hence, the final modified shrinking core model for spherical particles is obtained as (Miao, Du, Wang, et al., 2023):

$$k''t = -\frac{1}{\theta}\ln\left[1-\theta\left(1-\frac{2}{3}X_B-(1-X_B)^{\frac{2}{3}}\right)\right], \tag{2.13}$$

Where:

$$k'' = \frac{2M_{CaO}CD_0}{\rho_s f_{CaO} R_0^2}, \tag{2.14}$$

$$X_{B,max}(t=\infty) = \frac{1}{\sqrt{\theta}}, \tag{2.15}$$

M_{CaO} is Molar mass of CaO ($g\ mol^{-1}$) and f_{CaO} is mass fraction of CaO in particles (wt.%).

Therefore, the apparent rate constant of the carbonation reaction is determined to be k''. The reciprocal of θ is proportional to the square of the $X_{B,max}$, indicating that the maximum conversion efficiency is simply controlled by the accumulation mechanism of the product and independent of the initial reaction rate. A higher θ value results in a higher density and lower

porosity of the product layer. Equation (2.13) can be used to perform a nonlinear fit to the experimental value of carbonation efficiency to determine $k''$and D_0.

2.2.1.2 General rate equation theory

In the shrinking-core model, the formation of a uniform solid product layer covering the entire solid surface with a sharp interface between the solid reactant and the product is assumed. However, theories involving a uniform solid product layer cannot predict the kinetic transition behavior that occurs in some gas-solid reactions.

This work (Li, 2020) proposes that the growth of solid product islands occurs instead of the progressive formation of a uniform solid product layer in traditional shrinking-core models and establishes a general rate equation theory to model the kinetics of gas-solid reactions for solid reactants of various shapes. The growth of the product islands is calculated using the rate equation theory and is integrated into the shrinking-core model, in which the microstructure of the solid reactant is also considered.

Elemental steps of chemical reaction, surface diffusion, and product layer diffusion are included in the general rate equation theory. The initial step involves the adsorption of gas onto the grain surface, followed by a reaction between the adsorbed gas and the solid. The solid products formed by this surface reaction are monomers. These product monomers can diffuse across the grain surface and collide with one another, leading to the formation and growth of solid product islands, as illustrated in Figure 2.5. These islands can grow by consuming the product monomers, further reducing the surface coverage. As a result, multiple solid product islands form on the grain surface, as depicted in Figure 2.5(b). As the reaction progresses, the number of product islands increases, and they gradually cover the grain surface, as shown in Figure 2.5(c). Eventually, the grain surface becomes fully covered by product islands, as seen in Figure 2.5(d). At this stage, a layer of solid product separates the reaction surface of the solid from the gas phase molecules, preventing direct contact between the gas phase molecules and the unreacted grain surface.

Consequently, for the reaction to continue, solid ions or gas molecules must diffuse through the solid product layer. At this point, the chemical reaction enters the stage controlled by product layer diffusion. During this stage, the chemical reaction occurs at the interface between the solid product and the gas phase or the interface between the solid reactant and solid product (via gas diffusion through the product layer), and the unreacted core shrinks, as shown in Figure 2.5(e) (Li, 2020).

After detailed derivation (Li, 2020), the final model expressions for solid reactants of different

shapes can be found in the equations (2.16-2.17), where the former equation represents the fraction of the unoccupied reactant surface, and the latter describes the fraction of solid conversion.

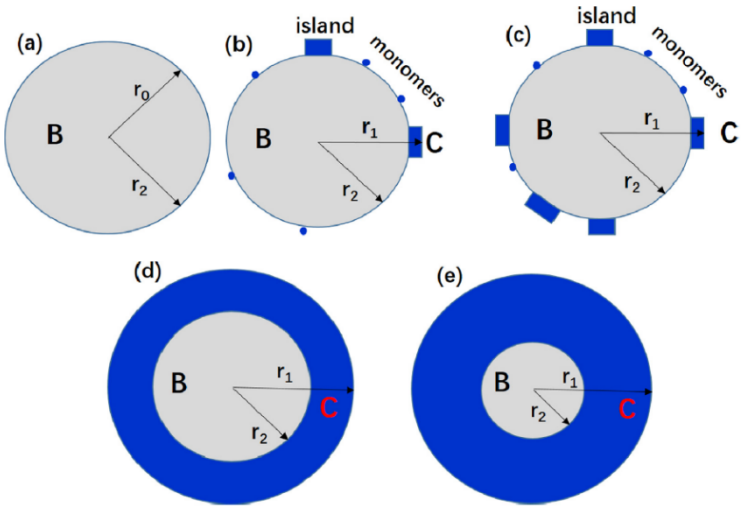

Figure 2.5 *Formation and growth of solid products on the grain surface in the shrinking-core model. The figure is adopted from (Li, 2020).*

$$\frac{\mathrm{d}\delta}{\mathrm{d}t} = -\frac{k_s Z}{\xi_c}\frac{C - C_e}{1 + K_s(C - C_e)}\delta \ , \tag{2.16}$$

$$\frac{\mathrm{d}X}{\mathrm{d}t} = \frac{k_s S_0}{1 - \varepsilon_0}\kappa_s(X)(C - C_e) \times \left[\frac{\delta}{1 + K_s(C - C_e)} + \frac{1 - \delta}{g_D(X) + \beta \cdot (C - C_e)p_D(\delta, X)}\right], \tag{2.17}$$

δ is the product island growth model, k_s is the chemical reaction rate constant ($m^4\ mol^{-1}\ s^{-1}$), Z is the ratio of the molar volume of the solid product to that of the solid reactant, ξ_c is the critical thickness of the product layer (m), C is the concentration of gas inside the particle ($mol\ m^{-3}$), C_e is the equilibrium concentration of the gas ($mol\ m^{-3}$), K_s is the ratio of the chemical reaction rate to the surface diffusion rate, S_0 initial surface area of solid reactant per unit volume of the solid
particle ($m^2\ m^{-3}$), ε_0 is initial porosity, $\kappa_s(X)$, $g_D(X)$ and $p_D(\delta, X)$ are geometric model functions, and β is a model parameter (Li, 2020).

As seen in equation (2.17), the developed rate equation theory unifies the kinetically controlled regime and the diffusion-controlled regime into a single general model by introducing the parameter δ.

As a conclusion, when surface diffusion is very slow (small diffusion coefficient), the reactant surface is rapidly covered by many small product islands, and the reaction becomes controlled by the diffusion of reactants through the product layer. When surface diffusion is very fast (large diffusion coefficient), the product islands are large, and the reactant surface is not fully

covered. The reaction is controlled by chemical reaction kinetics. At intermediate diffusion coefficient values, it follows a two-stage kinetic behavior. The first stage is fast and driven by the chemical reaction. The second stage is slower and controlled by product layer diffusion. This behavior can be described by a general rate equation in a single expression (Miao, Du, Wang, et al., 2023).

2.2.2 Two-Film theory model

The two-film theory is a model used to describe mass transfer processes, particularly in systems involving a gas and a liquid phase, and it applies to the study of **direct aqueous mineral carbonation**. It provides a framework for understanding how reactants move from one phase to another and how reaction rates are influenced by the resistances encountered during this transfer. The theory is based on the idea that a thin film exists at the interface of two phases, across which mass transfer occurs.

To understand how the two-film theory describes mineral carbonation, we first examine the process itself. In mineral carbonation, CO_2 gas dissolves into a liquid phase before reacting with a solid reactant, such as calcium hydroxide, to form a solid product, calcium carbonate. The two-film theory provides a framework for analyzing the mass transfer of CO_2 from the gas phase into the liquid phase, where the solid reactant is suspended. Similar to the shrinking-core model, we can define a boundary and categorize the ongoing phenomena into two distinct stages (Miao, Du, Zheng, et al., 2023) :

Gas-Liquid Mass Transfer: In this stage, CO_2 transfers from the bulk gas phase to the bulk liquid phase. The two-film theory suggests the presence of thin boundary layers—one in the gas phase and another in the liquid phase—at the interface where gas bubbles meet the liquid. CO_2 molecules must diffuse through these layers to dissolve into the liquid phase before further reactions can occur. The efficiency of this transfer depends on factors such as temperature, pressure, and the concentration gradient of CO_2 across the interface.

Solid-Liquid Mass Transfer and Reaction: Once dissolved in the liquid, CO_2 reacts with the solid reactant. This stage involves the transfer of dissolved CO_2 and reactive ions from the bulk liquid phase to the surface of solid particles, where carbonation reactions occur, leading to the precipitation of calcium carbonate or other carbonate minerals. The reaction rate in this stage is influenced by factors such as the surface area of the solid, the diffusion rate of reactants through boundary layers, and the presence of any inhibitors or catalysts.

As analyzing the stages for the following reaction (2.18) (Miao et al., 2022),

$$Ca(OH)_{2(aq)} + CO_{2(aq)} \rightarrow CaCO_{3(s)} \quad (2.18)$$

Two stages are likely to be encountered during the direct aqueous mineral carbonation process as shown in Figure 2.6. At Stage I, the mass transfer of $Ca(OH)_2$ dissolution is better than that of CO_2 absorption. At the initial stage of the reaction, the dissolution rate of $Ca(OH)_2$ is

relatively fast compared to the absorption rate of CO_2. Under steady-state conditions, the concentration of $Ca(OH)_2$ in the bulk liquid remains constant. The reaction plane of CO_2 and $Ca(OH)_2$ is located in the liquid film near the gas-liquid interface. The mass transfer of CO_2 from the gas phase to the liquid phase is the rate-controlling step, Figure 2.6(a).

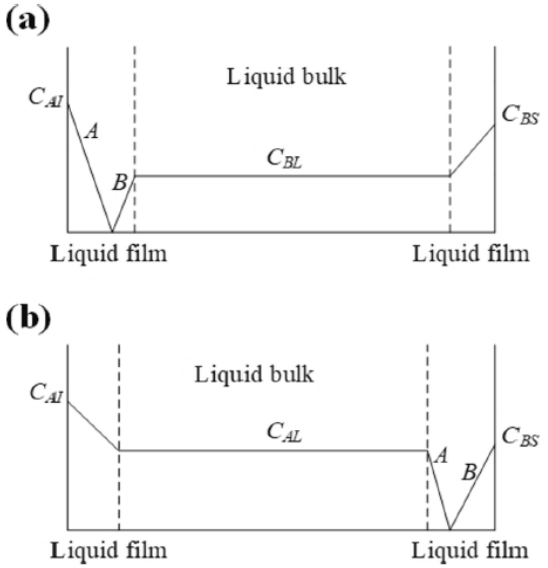

Figure 2.6 *Schematic diagram of (a) carbonation stage I and (b) carbonation stage II (Miao et al., 2022)*.

In stage II, Figure 2.6(b) the mass transfer of CO_2 absorption is higher than that of $Ca(OH)_2$ dissolution. As the reaction proceeds, the increased carbonation efficiency of $Ca(OH)_2$ reduces the effective solid-liquid contact area and dissolution rate. The dissolved $Ca(OH)_2$ in the bulk liquid is consumed and the mass transfer of $Ca(OH)_2$ becomes the rate-controlling step. Thus, the reaction front shifts to the liquid film near the solid-liquid interface. If the CO_2 absorption rate is much faster than that of $Ca(OH)_2$ dissolution, the product $CaCO_3$ will be deposited on the $Ca(OH)_2$ surface to inhibit further dissolution, thereby reducing the carbonation efficiency of mineral particles.

Before deriving the equation for the mentioned model, the following assumptions are necessary to simplify the mathematical framework and make it more manageable. Based on the literature (Miao, Du, Zheng, et al., 2023; Miao et al., 2022), assumptions are:

1. CO_2 is an ideal gas, and the change of superficial gas velocity caused by solvent evaporation is neglected.
2. The ionization of CO_2 and $Ca(OH)_2$ is neglected, and the mass transfer is in the form of molecules.
3. The mass transfer resistance is concentrated within the film, and the reactants have no concentration gradient in the bulk liquid.

4. The liquid-side film resistance of low-solubility CO_2 near the gas-liquid interface is much greater than the gas-side film resistance, so the gas-side film resistance is neglected.
5. The reaction in the liquid phase is irreversible and instantaneous. The mass transfer rate in the liquid film is enhanced by the chemical reaction between the absorbed CO_2 and the dissolved $Ca(OH)_2$.
6. The particle size of the solid is relatively large compared to the thickness of the liquid film.
7. The solid particles are isotropic rigid bodies, which are uniformly suspended in the liquid bulk under stirring. The mass transfer of the particles to the liquid is controlled only by the turbulence in the surrounding fluid.
8. The effective solid-liquid contact area decreases over time owing to the shrinkage of particles and the covering of products.
9. There is no temperature gradient in the reaction system.
10. The carbonation process satisfies the quasi-steady-state approximation.

For Stage I, the rate of CO_2 into the liquid phase and rate of $Ca(OH)_2$ dissolution is given by (Miao et al., 2022):

$$R_A = k_L a C_{AI} \left[1 + \frac{D_B C_{BL}}{D_A C_{AI}}\right] , \tag{2.19}$$

$$R_B = k_s A_p (C_{BS} - C_{BL}) , \tag{2.20}$$

Where:
R_A is the rate of CO_2 absorption ($mol\ m^{-3}\ s^{-1}$),
k_L is the liquid-film mass transfer coefficient of CO_2 ($m\ s^{-1}$),
a is the gas–liquid interfacial area ($m^2\ m^{-3}$),
C_{AI} is the concentration of CO_2 at the gas–liquid interface ($mol\ m^{-3}$),
C_{BL} is the concentration of $Ca(OH)_2$ in the bulk liquid ($mol\ m^{-3}$),
D_A and D_B are the diffusivities of CO_2 and $Ca(OH)_2$ in water ($m^2\ s^{-1}$),
$[1 + D_B C_{BL}/D_A C_{AI}]$ is the enhancement factor of CO_2 absorption,
R_B is the rate of $Ca(OH)_2$ dissolution ($mol\ m^{-3}\ s^{-1}$),
k_s is the liquid-film mass transfer coefficient of $Ca(OH)_2$ ($m\ s^{-1}$),
A_p is effective solid–liquid contact area ($m^2\ m^{-3}$),
C_{BS} is the solubility of $Ca(OH)_2$ ($mol\ m^{-3}$).
For Stage II, we have:

$$R_A = k_L a (C_{AI} - C_{AL}) , \tag{2.21}$$

$$R_B = k_s A_p C_{BS} \left[1 + \frac{D_A C_{AL}}{D_B C_{BS}}\right] , \tag{2.22}$$

where $[1 + D_A C_{AL}/D_B C_{BS}]$ is the enhancement factors of $Ca(OH)_2$ dissolution, and C_{AL} is the concentration of CO_2 in the bulk liquid ($mol\ m^{-3}$).

According to assumption 8:

$$A_p = A_0 e^{-\theta t} , \tag{2.23}$$

where A_0 is the initial effective solid-liquid contact area ($m^2\ m^{-3}$). θ is a coefficient reflecting the decay rate of A_0.

Also considering quasi-steady-state, assumption 10, we have: $R_A = R_B$. After mathematical calculation and integration, the final equation to compute carbonation efficiency X_B is obtained.

$$X_B = \frac{1}{\alpha}\left[t + \frac{1}{\theta}\ln\left(1 + \frac{\beta}{\alpha}\right) - \frac{1}{\theta} ln\left(1 + \frac{\beta}{\alpha} e^{\theta t}\right)\right] , \tag{2.24}$$

$$\frac{\mathrm{d}X_B}{\mathrm{d}t} = \frac{1}{a + \beta e^{\theta t}} , \tag{2.25}$$

Parameter α and β are:

$$\alpha = \frac{\mathrm{m}_0}{k_L a M_B V (C_{BS} D_B / D_A + C_{AI})} , \beta = \frac{\mathrm{m}_0}{k_s A_0 M_B V (C_{AI} D_A / D_B + C_{BS})} , \tag{2.26}$$

Where m_0 is the initial mass of $Ca(OH)_2$(g). M_B is molar mass of $Ca(OH)_2$ ($g\ mol^{-1}$) and V is the slurry volume (m^3).

Also, θ could be expressed as a function of maximum carbonation efficiency, α and β :

$$\theta = \frac{1}{\alpha X_{B,max}} \ln\left(1 + \frac{\alpha}{\beta}\right) , \tag{2.27}$$

Equation (2.24) can be utilized to perform a non-linear fit to the experimental carbonation efficiency values to determine $k_L a$ and θ. Equations (2.26) indicate that α and βe^a correspond to the gas-liquid and solid-liquid mass transfer resistance, respectively. When gas-liquid mass transfer acts as the rate-controlling step (i.e., $\alpha \gg \beta e^{\theta t}$), the carbonation rate dX_B/dt remains constant at $1/\alpha$, resulting in a linear dependence of carbonation efficiency on time. As the reaction time progresses, the value of $\beta e^{\theta t}$ increases and eventually exceeds α, leading to a decrease in carbonation rate and a nonlinear relationship between carbonation efficiency and time.

2.3 Ionic modeling and future direction

While the models discussed provide significant insights into the carbonation process, they often do not explicitly account for ionic interactions and transport within the liquid phase. The behavior of ions such as Ca^{2+}, CO_3^{2-}, OH^-, and other species plays a critical role in the

dissolution, transport, leaching, and precipitation processes. Moreover, the pH of the system can be calculated throughout the reaction, which is a key advantage of the ionic model over other models. This capability is particularly beneficial in reactor design, as pH monitoring plays a crucial role in optimizing process conditions.

An advanced ionic model should consider:

- **Ionic activity**: The true concentration of ions in a solution is not the same as their analytical concentration, particularly at high ionic strength.
- **Electrochemical effects**: The diffusion and transport of ions are influenced by electrochemical gradients.
- **Complexation**: The ions may interact with each other to form complex ions.
- **Precipitation and dissolution**: The formation of solid phases like $CaCO_3$ depends on solution saturation which is affected by ionic concentration.

Incorporating ionic transport into carbonation models can lead to more accurate predictions of reaction kinetics, particularly in systems with complex solution chemistry such as in cementitious materials. For example, the presence of sulfate ions in the solution could affect the carbonation reaction by increasing the gypsum formation, which limits the carbonation potential of recycled concrete. Alkali concentration increases the solubility of CO_2 in the solution, thus accelerating the reaction, and also counteracts gypsum formation, which will increase the leaching of sulfate ions from the cement paste to the solution.

Chapter 3

Model formulation

The role of supplementary cementitious materials in decarbonizing the cement industry was discussed. Additionally, two primary classes of models that have been used to calculate the carbonation efficiency of these materials were highlighted. Moving forward, this chapter will focus on the implementation of our kinetic model for wet carbonation of cementitious materials. We will discuss key aspects such as calcium leaching from calcium hydroxide (CH) and calcium silicate hydrate (CSH) phases, the dissolution of carbon dioxide in the aqueous medium, reactions occurring within the system, and the precipitation of calcium carbonate. These elements are critical to understanding the mechanisms and efficiency of carbonation processes in cementitious systems.

3.1 Carbonation Reaction Mechanisms and Model Development

Wet carbonation of cementitious materials is a complex process involving multiple simultaneous reactions across different phases. At ambient conditions, the carbonation reaction proceeds via the gas-liquid-solid pathway, where anhydrous cement particles, hydrates, and CO_2 interact through various mechanisms. Based on experimental observations and theoretical considerations, we can divide the carbonation process into two distinct kinetic steps (Zajac et al., 2020).

3.1.1 Two-Phase Reaction Model

The evolution of the solution concentrations and phase assemblage during the aqueous carbonation of cement paste suggests that the reaction kinetics can be described by two main kinetic steps:

Phase 1: Initial Rapid Carbonation (CH Dissolution Limited)
In the first kinetic step, the carbonation is limited mainly by the amount of CO_2 available for the reaction and the dissolution rate of calcium hydroxide (CH). The carbonation experiment is initiated by adding the precursor to the carbonation solution, which increases the pH as a result of the rapid dissolution of hydrates and cement phases. During this stage, the saturation indices

of the dissolving phases increase, whereas the CO_2 concentration in the solution is low (Zajac et al., 2023).

Furthermore, the kinetics for calcium carbonate nucleation and precipitation plays an important role in this first stage. The hindrances of calcium carbonate nucleation may result in a local minimum in the pH evolution, which is related to a reduction of the rate of precipitation of carbonation products and accumulation of CO_2 in the solution. During this stage of carbonation, several reactions occur, which transform the hydrates into calcium carbonate and an alumina-silica gel or result in decalcification of the C-(A)-S-H phase.

During this reaction period, calcium dissolves in the carbonation solution and precipitates afterwards as calcium carbonate. Once the rapidly dissolving and reacting hydrates are depleted, the second kinetic step is initiated, as seen by the first decrease in pH (Zajac et al., 2020).

Phase 2: Extended Carbonation (Diffusion Limited)

In the second kinetic step, the dissolution kinetics of the hydrates control the progress of carbonation. The reaction kinetics are dominated by the dissolution of hydrates and the transport of calcium to the surface of the paste grains. At this stage, the solution properties become dominated by a high CO_2 concentration that builds up in the solution due to limited amounts of calcium availability. The saturation indices of the dissolving phases decrease significantly when the CO_2 concentration in the solution is high, and the pH starts to decrease to reach its lower limit (Zajac et al., 2023).

During this carbonation stage, where the carbonation reaction is well advanced, only larger cement-paste grains continue to react since small particles have already fully reacted. Under such conditions, diffusion of calcium outward from uncarbonated centers of the grains is a slow process that competes with penetration of CO_2 into the grains. This results in the precipitation of calcium carbonate within the cement-paste grains, leading to increased diffusion resistance over time.

In the case of portlandite carbonation, the main part of the reaction is accomplished after the sharp decrease in pH. During the carbonation of cement paste, and particularly of C-(A)-S-H phases, this stage with a steady-state low pH level represents the stage where the final decalcification and decomposition of the C-(A)-S-H phase takes place. Moreover, all alumina-bearing hydrates are decomposed with the exception of hydrotalcite (Zajac et al., 2023).

3.1.2 Model Assumptions

To develop a mathematical model of the wet carbonation process, we make the following key assumptions:

1. Carbonation system is well-mixed, with a uniform concentration of dissolved species in the bulk solution, with gradient in surface and bulk.
2. Cementitious particles are assumed to be spherical with a uniform size distribution.

3. Dissolution of $Ca(OH)_2$ follows a first-order kinetic model with respect to available $Ca(OH)_2$.
4. Dissolution of CSH phases is influenced by a time-dependent diffusion coefficient that decreases as carbonation progresses, according to the variations in mineral porosity.
5. CO_2 mass transfer from gas to liquid follows established gas-liquid transfer principles, and mass transfer in gas phase is negligible.
6. The reactions of dissolved CO_2 with hydroxide ions and subsequent carbonate speciation reach equilibrium rapidly relative to dissolution processes.
7. $CaCO_3$ precipitation occurs instantaneously once saturation is reached.
8. Activity coefficients for ionic species are calculated using the extended Debye-Hückel equation.
9. Carbonation system is isothermal, with negligible heat effects from reactions.
10. Effects of other ions (e.g., sulfates, alkalis) on the carbonation process are negligible compared to the main calcium and carbonate interactions.
11. Inter-particle calcium concentration gradient along radius is neglected.
12. The only source of calcium that moves into the solvent bulk comes from CH phase.

Two significant phenomena must be carefully considered: **inter-particle phenomena** and **extra-particle phenomena**. These processes play a crucial role in determining the overall behavior and reactivity of calcium within the system.
In the following sections, we will delve into each phenomenon in detail, examining their underlying mechanisms, and their influence on the system's physicochemical properties. Understanding these processes is essential for accurately modeling and optimizing the reaction environment (Meijssen & Mazzotti, 2022).

3.2 Inter-particle phenomena

Inter-particle phenomena focus on the chemical reactions at the surface of the solid particles, where calcium atoms are transferred into the solution through dissolution processes. In a simplified view, the main calcium-containing phases of cement or supplementary cementitious material are calcium silicate hydrate (CSH) and calcium hydroxide (CH), which form during the curing of cement, i.e., during the reactions of clinker with water (Meijssen et al., 2023).
The first step involves dissolving calcium from a leachable calcium-rich mineral phase such as Calcium Hydroxide (CH) and Calcium Silicate Hydrate (CSH) into the solution. This step depends on the availability of acid, the mineral structure and temperature. During the curing of supplementary cementitious materials, the alite and belite phases react with water according to the following reactions:

$$nCaO.SiO_2 + (2n+1)H_2O \leftrightarrow xCaO.SiO_2.yH_2O + (2n-3)Ca(OH)_2 \quad (3.1)$$

Where:

- n = 2 for belite (contributes to long-term strength and reacts slower but ensures durability).
- n = 3 for alite (contributes to early strength and has a fast reaction with water).

For both reactions, the first product is calcium silicate hydrate (CSH) and the second product is calcium hydroxide (CH). In reality, CSH is not a single specific molecular structure but a group of similar molecular structures that can be written as $xCaO.SiO_2.yH_2O$, with *x* being the ratio between CaO and SiO_2, also referred to as the C/S ratio.

3.2.1 $Ca(OH)_2$ Dissolution Kinetics

The chemical reaction at the surface of the solid, where calcium atoms are transferred into the solution. During dissolution of CH into an **aqueous** solution, whereby the following dissociation reaction takes place:

$$Ca(OH)_2(s) \leftrightarrow Ca^{2+} + OH^- \tag{3.2}$$

Therefore, by considering the assumptions (2, 3, 11, and 12), the reactive diffusion model can be transformed from a partial differential equation (PDE) (3.3) into an ordinary differential equation (ODE) (3.4), simplifying the mathematical representation and analysis of the system.

$$\varepsilon \frac{\partial C_{Ca}^S}{\partial t} + (1-\varepsilon)\left(\frac{\partial n_1}{\partial t} + \frac{\partial n_2}{\partial t}\right) = \varepsilon D\left(\frac{\partial^2 C_{Ca}^S}{\partial r^2} + \frac{2}{r}\frac{\partial C_{Ca}^S}{\partial r}\right), \tag{3.3}$$

$$\varepsilon \frac{\partial C_{Ca}^S}{\partial t} + (1-\varepsilon)\left(\frac{\partial n_1}{\partial t}\right) = 0\ , \tag{3.4}$$

C_{Ca}^S is apparent liquid concentration of Calcium component (mol/kg). n_1 is solid concentration of CH (mol/kg). n_2 is solid concentration of CSH (mol/kg). ε is porosity of rich-calcium particles. D is apparent diffusion coefficient (s^{-1}). Due to assumption 12, the only source of calcium in the bulk comes from CH phase, and CSH phase does not dissolve into the solution.

and:

$$\frac{\mathrm{d}n_1}{\mathrm{d}t} = -k_{\mathrm{L}}(1-S_1)n_1 \quad \text{for } S_1 \leq 1, \tag{3.5}$$

$$S_1 = \frac{(calcium\ \ cation\ activity).(hydroxide\ anion\ acvtivity)^2}{Equilibrium\ solubility\ product\ of\ CH}$$

$$= \frac{[Ca^{2+}].[OH^{-}]^2}{K_{sp.CH}}, \tag{3.6}$$

S_1 is saturation index of Calcium hydroxide.

For $S_1 < 1$, dissolution occurs, while for $S_1 > 1$, precipitation would theoretically occur, although in this model, the kinetics of calcium carbonate precipitation is also based on saturation index.

CH dissolution follows the reaction 3.2; the rate of calcium concentration changes in the solid-liquid interface is given by the product of the concentration itself with a rate constant k_{L} (s^{-1}), and the driving force for dissolution ($1 - S_1$) (Meijssen et al., 2023).

The solubility of $Ca(OH)_2$ in water, S_{CH} (g/kg of solution), is negatively correlated with the temperature, as denoted in the following equation:

$$S_{CH} = -0.0108T + 1.7465, \tag{3.7}$$

Where T is the solution temperature ($°C$).

According to the empirically derived and reported equation of calcium hydroxide (CH) solubility in water (3.7), the solubility product constant ($K_{sp.CH}$) can be determined for various temperatures. This allows for a more precise understanding of CH dissolution behavior under different thermal conditions:

$$K_{sp.CH} = 4\left(\frac{S_{CH}}{Mw_{CH}}\right)^3 , \tag{3.8}$$

Mw_{CH} is molecular weight of CH (g/mol).

3.2.2 CSH Decalcification Kinetics

The dissolution and decalcification of calcium silicate hydrate (CSH) phases is represented by (Meijssen et al., 2023):

$$xCaO.SiO_2.yH_2O(s) \rightarrow (x-\delta)CaO.SiO_2.(y-\delta)H_2O(s) + \delta Ca^{2+} + +2\delta OH^{-} \tag{3.9}$$

The rate of CSH decalcification is more complex than that of $Ca(OH)_2$ because it is influenced by:

1. The diffusion of calcium ions through this layer
2. The precipitation of calcium carbonate on and within this layer

To account for these effects, we predict a model for CSH reaction rate using a time-dependent diffusion coefficient and a product layer resistance factor:

$$\frac{\mathrm{d}C_{CSH}}{\mathrm{d}t} = -k_{\mathrm{CSH}} \cdot C_{CSH} \cdot D_t \cdot \frac{\mathrm{CO}_{2(\mathrm{aq})}}{\alpha_{\mathrm{diff}} \cdot PL_G + 1} , \tag{3.10}$$

where:

k_{CSH} is the reaction rate constant for CSH (s^{-1}),

C_{CSH} is CSH Concentration ($mol.lit^{-1}$)

D_t is the time-dependent diffusion coefficient ($m^2.s^{-1}$),

$CO_{2(aq)}$ is the concentration of dissolved CO_2 ($mol.lit^{-1}$),

α_{diff} is the diffusion resistance parameter due to $CaCO_3$ precipitation (dimensionless),

PL_G is ratio of produced $CaCO_3$ to available CH and CSH phases.

The time-dependent diffusion coefficient decreases exponentially with time:

$$D_t = D_0 \cdot e^{-\alpha \cdot t}, \tag{3.11}$$

where:

D_0 is the initial diffusion coefficient ($m^2.s^{-1}$),

α is the decay parameter (s^{-1}),

t is the reaction time (s).

This formulation accounts for the progressive densification of the product layer and the associated decrease in diffusion rates over time.

3.3 Extra-Particle Phenomena

Extra-particle phenomena describe the transport processes occurring outside the particles, in the bulk solution, and the gas-liquid interface. These processes are crucial for understanding the overall carbonation kinetics and the distribution of reactants and products within the system.

3.3.1 Convective Mass Transfer

The change in bulk liquid calcium concentration due to convection from the particle surface to the liquid bulk is described by the following equation. One of our key assumptions, which is justified by the agitation in the system, is that the system remains well-mixed. This implies that the convective transport rate is significantly higher than the diffusive transport rate. As a result, the diffusive flux can be considered negligible. Under this assumption, we can express the convective flux in terms of the concentration gradient as the driving force, simplifying the mathematical formulation of mass transfer between the particle surface and the bulk liquid phase.

$$\frac{\mathrm{d}C_{Ca}^{B}}{\mathrm{d}t} = k_O \cdot (C_{Ca}^{S} - C_{Ca}^{B}) \ , \tag{3.12}$$

C_{Ca}^{B} is apparent Calcium concentration in the bulk solution ($mol.lit^{-1}$). Similarly, for hydroxide ions:

$$\frac{\mathrm{d}C_{OH}^{B}}{\mathrm{d}t} = k_{O-OH} \cdot (C_{OH}^{S} - C_{OH}^{B}) \,, \tag{3.13}$$

where:

C_{OH}^{B} is the OH^- concentration in the bulk solution ($mol.lit^{-1}$),

C_{OH}^{S} is the OH^- concentration at the particle surface ($mol.lit^{-1}$),

k_O is the convective mass transfer coefficient for Ca^{2+} (s^{-1}),

k_{O-OH} is the convective mass transfer coefficient for OH^- (s^{-1}).

Within the equations presented in this and previous sections, we can determine the calcium concentration at both the particle surface and in the liquid bulk. These calculations are essential for understanding mass transfer dynamics and the overall reaction kinetics in the system. By analyzing the interactions between the solid and liquid phases, we can gain insights into how calcium species are transported and redistributed under the given process conditions.

Building upon this foundation, the next section will focus on evaluating the concentration of carbon dioxide in the liquid phase. As we investigate the mechanisms governing CO_2 dissolution, its equilibrium reactions with water, and the potential chemical interactions that may take place in the system.

3.3.2 CO_2 Mass Transfer

The solubility of CO_2 in pure water is fundamentally governed by Henry's Law, which states that the concentration of a gas dissolved in a liquid is directly proportional to the partial pressure of that gas above the liquid at a constant temperature. This relationship is expressed mathematically as (Miao et al., 2022):

$$C_{CO_2}^{*} = k_H . p_{CO2}, \tag{3.14}$$

$$k_H = 2.82 \times 10^6 e^{-2044/T}, \tag{3.15}$$

Where $C_{CO_2}^{*}$ is the concentration of dissolved CO_2 ($mol.m^{-3}$). k_H is Henry's Law constant ($Pa\ m^3\ mol^{-1}$). p_{CO2} is the partial pressure of CO_2 above the liquid or in the injected bubbles (Pa).

Henry's Law constant, k_H, is temperature dependent. As temperature increases, k_H generally decreases, indicating reduced CO_2 solubility at higher temperatures (Pohoreckl & Moniuk, 1988). This is because the increased kinetic energy of water molecules weakens the

intermolecular forces between CO_2 and water, making it easier for CO_2 to escape the liquid phase.
Numerous studies have determined experimental values of k_H for CO_2 in water across a range of temperatures (Pohoreckl & Moniuk, 1988). These values are crucial for predicting CO_2 solubility in various applications, from carbon capture to ocean acidification studies.
However, it's important to note that Henry's Law is only strictly valid for dilute solutions where the gas concentration is low and interactions between dissolved gas molecules are negligible. At higher pressures or concentrations, deviations from Henry's Law become apparent, necessitating more complex models to accurately describe CO_2 solubility (Kucka et al., 2002).

The rate of CO_2 dissolution is described by (Velts et al., 2011):

$$\frac{\mathrm{d}[CO_2(aq)]}{\mathrm{d}t} = kLa \cdot \left(C^*_{CO_2} - \left[CO_{2(\mathrm{aq})}\right]\right) , \tag{3.16}$$

Where $CO_{2(\mathrm{aq})}$is the actual concentration of dissolved CO_2 ($mol.lit^{-1}$), and kLa is the volumetric mass transfer coefficient (s^{-1}).

3.3.2.1 CO_2 Solubility in Electrolyte Solutions

The presence of electrolytes significantly alters the solubility of CO_2 in water. Electrolytes, which dissociate into ions in solution, affect the solubility through several mechanisms:

- **Ionic strength effects:** Ionic strength, a measure of the total concentration of ions in solution, significantly influences the activity coefficients of the reacting species. This, in turn, affects the reaction rate and thus the overall CO_2solubility.

Increased ionic strength generally reduces the activity coefficients of ions, slowing down the reaction rate and potentially decreasing the overall solubility (Pohoreckl & Moniuk, 1988). However, the exact effect depends on the specific ions present and their interactions with CO_2 and water molecules (Kucka et al., 2002).

- **Salting-out effect:** The addition of salt to water often reduces the solubility of non-polar gases like CO_2. This "salting-out" effect is attributed to the preferential solution of ions by water molecules, leaving fewer water molecules available to interact with and dissolve CO_2. The magnitude of the salting-out effect depends on the nature and concentration of the salt, as well as the temperature (Pohoreckl & Moniuk, 1988). Different ions exhibit different salting-out strengths; some ions may even exhibit a slight salting-in effect at low concentrations, while others always salt out.

When the studied system implies absorption due to a chemical reaction of carbon dioxide into the electrolyte solution, it is necessary to consider the effect of this reaction on the solubility

value. The value of gas solubility could be calculated using the equation 3.14 developed by Setschenow and modified by van Krevelen and Hoftijzer (Gómez-Díaz et al., 2006):

$$\log\left(\frac{C_{CO2}^{*,solution}}{C_{CO2}^{*,water}}\right) = -K_s \cdot I\,, \tag{3.17}$$

where $C_{CO2}^{*,solution}$ is the equilibrium solubility of CO_2 in electrolyte solution, $C_{CO2}^{*,water}$ is the equilibrium solubility of CO_2 in pure water, $K_s$is the salting-out parameter, and I is the ionic strength (will be discussed in section 3.5). The enhancement parameter is defined as the sum of the contributions of all ions present in the solution and the carbon dioxide absorbed in the liquid phase(Gómez-Díaz et al., 2006):

$$K_s = i^+ + i^- + i^g, \tag{3.18}$$

The values corresponding to the i parameter have been obtained from literature (Gómez-Díaz et al., 2006) and the values for the Ca^{2+}, OH^- ions, and carbon dioxide (as high concentrated components in the system) are −0.0547, 0.3875, and 0.2277, respectively.

3.4 Reaction Kinetics and Carbonate Speciation

The overall reaction for CO_2 capture using $Ca(OH)_2$ aqueous solution is expressed as 2.2:

$$Ca(OH)_2(s) + CO_2(g) \leftrightarrow CaCO_3(s) + H_2O(l)\ , \Delta H_{298K}^{\circ} = -109\ kJ/mol\ , \tag{2.2}$$

The reaction is thermodynamically favorable in the temperature range from ambient to 750 °C, and the reaction rate is very fast in aqueous solution. Produced $CaCO_3$ can be reclaimed to a limited extent or regenerated to $Ca(OH)_2$ by calcination and hydration (or slaking).

3.4.1 Individual Reactions during CO_2 Absorption.

Reaction 2.2 includes many individual reactions, such as $Ca(OH)_2$ dissolution and HCO_3^- production. Some individual reactions proceed irrespective of the pH, while others are restricted to a specific pH range (Han et al., 2011). These reactions are classified and discussed in this section.

The carbonic acid ion primarily exists in the form of CO_3^{2-} and HCO_3^- in the pH ranges of pH > 10.5 and 6.5 < pH < 10.5, respectively. At pH < 6.5, H_2CO_3 is the main constituent. Therefore, $CaCO_3$ is not precipitated at pH under 10 because of the absence of CO_3^{2-}. Meanwhile, produced $CaCO_3$ is slightly dissolved in acidic condition at pH under 6.5 (Han et al., 2011).

- **Individual reactions proceed across the pH range**

These are listed as 3.19-3.22:

$$CO_2(g) \leftrightarrow CO_2(aq) \tag{3.19}$$

$$CO_2(aq) + H_2O(l) \leftrightarrow H_2CO_3(aq) \tag{3.20}$$

$$H_2CO_3(aq) \leftrightarrow HCO_3^-(aq) + H^+(aq) \tag{3.21}$$

$$HCO_3^-(aq) \leftrightarrow CO_3^{2-}(aq) + H^+(aq) \tag{3.22}$$

Reactions 3.19 and 3.21 are very fast. Reaction 3.20 can be rate-controlling because its rate is relatively slow, except at high pH. Reaction 3.22 is faster than reaction 3.20 and slower than reaction 3.21 (Han et al., 2011).

Hence, in our model, since Reaction 3.19 proceeds rapidly, we assume an instantaneous equilibrium between gaseous and aqueous carbon dioxide. Furthermore, as Reaction 3.20 is significantly faster than Reaction 3.21, we can assume that all produced H_2CO_3 is immediately converted into bicarbonate and hydrogen ions. Therefore, Reactions 3.20 and 3.21 can be expressed as:

$$CO_2(aq) + H_2O(l) \leftrightarrow HCO_3^-(aq) + H^+(aq) \tag{3.23}$$

- **Individual reactions proceed in 10 < pH < initial value (high)**

Reactions 3.24-3.26 are reported in this range:

$$CO_2(aq) + OH^-(aq) \leftrightarrow HCO_3^-(aq) \tag{3.24}$$

$$HCO_3^-(aq) + OH^-(aq) \leftrightarrow CO_3^{2-}(aq) + H2O(l) \tag{3.25}$$

$$Ca^{2+}(aq) + CO_3^{2-}(aq) \leftrightarrow CaCO_3(s) \tag{3.26}$$

The rate of reaction 3.25 is even faster than that of reaction 3.24, and reaction 3.26 is known to be instantaneous. Therefore, reaction 3.24 can be the rate-controlling step in this range. $CaCO_3$ is produced according to reaction 3.26, in which the nucleation of $CaCO_3$ at pH over 12.5 is followed consecutively by precipitation and growth until pH 10 (Han et al., 2011).

- **Individual reactions proceed in 6.5 < pH < 10**

Two reactions, 3.24 and 3.25, are also reported in this range. However, reaction 3.24 is faster than reaction 3.25, which leads to an even higher concentration of HCO_3^- than CO_3^{2-} in solution. Therefore, $CaCO_3$ is rarely produced in this range (Han et al., 2011).

- **Water ionization**

One of the other reactions to consider is the ionization of water:

$$H^+(aq) + OH^-(aq) \leftrightarrow H_2O(l) \tag{3.27}$$

The degree of ionization is influenced by factors such as temperature, pressure, and the presence of dissolved substances. In practical applications, water ionization plays a crucial role in acid-base chemistry and pH regulation.

3.4.2 Precipitation Kinetics

The precipitation of calcium carbonate occurs when the ion activity product (IAP) of calcium and carbonate ions exceeds the solubility product of $CaCO_3$:

$$Ca^{2+}(aq) + CO_3^{2-}(aq) \leftrightarrow CaCO_3(s) \tag{3.28}$$

The precipitation rate is given by (Velts et al., 2011):

$$\frac{\mathrm{d}[\mathrm{CaCO_3}]}{\mathrm{d}t} = k_p \cdot \left(\frac{[\mathrm{Ca^{2+}}] \cdot [\mathrm{CO_3^{2-}}]}{K_{sp,CaCO_3}} - 1 \right) , \tag{3.29}$$

Where k_p is the precipitation rate constant (s^{-1})., and $K_{sp,CaCO_3}$ is solubility product constant of $CaCO_3$ ($mol^2.lit^{-2}$).

The total $CaCO_3$ formation consists of contributions from both CH carbonation and CSH carbonation:

$$[\mathrm{CaCO_3}]_{\mathrm{total}} = [\mathrm{CaCO_3}]_{CH} + [\mathrm{CaCO_3}]_{CSH}, \tag{3.30}$$

Where $[\mathrm{CaCO_3}]_{CSH}$ is directly linked to the CSH conversion rate:

$$\frac{d[\mathrm{CaCO_3}]_{CSH}}{dt} = -\frac{d[\mathrm{CSH}]}{dt}, \tag{3.31}$$

The nucleation of $CaCO_3$ at pH over 12.5 is followed consecutively by precipitation and growth until pH 10. In the pH range 7-10, $CaCO_3$ is rarely produced from CH phase because HCO_3^- becomes the dominant carbonate species rather than CO_3^{2-}. If CO_2 is continuously supplied to the solution at pH < 7, some $CaCO_3$ dissolution may occur, with $CaCO_3$ converted to $Ca(HCO_3)_2$, which is more soluble (Han et al., 2011).

3.5 Ionic Strength and Activity Coefficients

3.5.1 Ionic Strength Calculation

The ionic strength (I) of the solution significantly affects the activity of ions and, consequently, the reaction rates and equilibrium positions. Ionic strength is calculated as (Kaufmann & Dreybrodt, 2007):

$$I = \frac{1}{2} \sum_i z_i^2 \cdot [X_i] , \tag{3.32}$$

where z_i is the ionic charge, and $[X_i]$ is concentration of a dissolved species X_i. For the ternary system $CaCO_3$–H_2O–CO_2 the ionic strength then reads:

$$I = \frac{1}{2}(4[Ca^{2+}] + [H^+] + [OH^-] + [HCO_3^-] + 4[CO_3^{2-}]) \ , \tag{3.33}$$

The ionic strength profile during carbonation typically follows a distinctive pattern with an initial spike due to $Ca(OH)_2$ dissolution, followed by a decrease as $CaCO_3$ precipitates, and then a gradual increase as CO_2 dissolution leads to the accumulation of H^+ and HCO_3^- ions at lower pH values (Kaufmann & Dreybrodt, 2007).

3.5.2 Activity Coefficient Calculation

The activity coefficient (γ_i) relates the activity of an ion (X_i) to its concentration $[X_i]$ (Kaufmann & Dreybrodt, 2007):

$$\gamma_i = \frac{(X_i)}{[X_i]}, \tag{3.34}$$

To calculate the chemical activity coefficients, several models are available. However, well-known models such as Debye - Huckel or Davies are not adapted to the specific case of cementitious materials, which bear a highly charged pore solution. A modification of Davies' relationship was found to yield good results (Samson et al.,1999):

$$\ln\gamma_i = -\frac{Az_i\sqrt{I}}{1 + a_iB\sqrt{I}} + \frac{(0.2 - 4.17 \times 10^{-5}I)Az_iI}{\sqrt{1000}}, \tag{3.35}$$

The parameters A and B are temperature-dependent:

$$\mathrm{A} = \frac{\sqrt{2}F^2e_0}{8\pi(\epsilon RT)^{\frac{3}{2}}} \ , \tag{3.36}$$

$$B = \sqrt{\frac{2F^2}{\epsilon RT}} \ , \tag{3.37}$$

Where:

a_i is radium of species ion (m),
e_0 is electrical charge of one electron ($1.602\times 10^{-19}\ C$),
F is Faraday constant (9.64846×10^4 C/mol),
$\epsilon\ is$ the permittivity of the medium, given by the dielectric constant times the permittivity of the vacuum.

For uncharged species like CO_2(aq), the activity coefficient is given by (Kaufmann & Dreybrodt, 2007):

$$\gamma_i = 10^{-0.1I}\,, \tag{3.38}$$

This accounts for the "salting-out" effect where the solubility of non-polar molecules decreases with increasing ionic strength.

The ionic size parameters (a_i) for key species in the carbonation system are:

- Ca^{2+}: 1.0×10^{-13} m
- OH^-: 3.0×10^{-10} m
- H^+: 9.0×10^{-11} m
- HCO_3^-: 4.0×10^{-10} m
- CO_3^{2-}: 4.0×10^{-10} m

These activity coefficients significantly impact reaction kinetics and equilibria, particularly in the concentrated solutions that can develop during carbonation processes. For instance, in high ionic strength solutions, the effective concentrations of ions can be substantially lower than their analytical concentrations, affecting reaction rates and equilibrium positions (Kucka et al., 2002).

3.6 Complete System of Differential-Algebraic Equations

The mathematical model for the wet carbonation of cementitious materials consists of a system of ordinary differential equations (ODEs) that describes the temporal evolution of all relevant species and phases. As discussed in Section 3.4, we explored the possible mechanisms governing our system and identified the most influential and effective reactions with considering some other literatures(Velts et al., 2011; William Zappa Pilot-Scale Experimental Work on the Production of Precipitated Calcium Carbonate (PCC) from Steel Slag for CO 2 Fixation, 2014). These reactions form the core of our model and serve as the foundation for further analysis. By focusing on these key reactions, we can develop a comprehensive understanding of the system's behavior and accurately elaborate on its dynamics.

3.6.1 Surface Reactions and Dissolution

For calcium hydroxide dissolution:

$$\frac{\mathrm{d}n_1}{\mathrm{d}t} = -k_{\mathrm{L}}(1 - S_1)n_1 \quad \text{for } S_1 \leq 1, \tag{3.5}$$

$$\frac{\mathrm{d}C_{Ca}^{S}}{\mathrm{d}t} = -\frac{dn}{dt} - K_O \cdot (C_{Ca}^{S} - C_{Ca}^{B}), \tag{3.39}$$

$$\frac{\mathrm{d}C_{OH}^{S}}{\mathrm{d}t} = 2 \cdot \left(-\frac{\mathrm{d}n}{\mathrm{d}t}\right) - K_{O-OH} \cdot (C_{OH}^{S} - C_{OH}^{B}), \tag{3.40}$$

For CSH decalcification:

$$\frac{\mathrm{d}C_{CSH}}{\mathrm{d}t} = -k_{\mathrm{CSH}} \cdot C_{CSH} \cdot D_t \cdot \frac{CO_{2(aq)}}{\alpha_{diff} \cdot PL_G + 1} \ , \tag{3.10}$$

$$\frac{\mathrm{d}[\mathrm{CaCO_3}]_{CSH}}{\mathrm{d}t} = -\frac{\mathrm{d}C_{CSH}}{\mathrm{d}t} \ , \tag{3.41}$$

3.6.2 Bulk Solution Reactions

For calcium and hydroxide ions in the bulk solution:

$$\frac{\mathrm{d}C_{Ca}^{B}}{\mathrm{d}t} = K_O \cdot (C_{Ca}^{S} - C_{Ca}^{B}) - r_p \ , \tag{3.42}$$

$$\frac{\mathrm{d}C_{OH}^{B}}{\mathrm{d}t} = K_{O-OH} \cdot (C_{OH}^{S} - C_{OH}^{B}) - r_5 - r_3 - r_4 \ , \tag{3.43}$$

where r_p is the rate of calcium carbonate precipitation, and r_3 , r_4, and r_5 are the rates of the reactions 3.24, 3.25, and 3.27.

For carbon dioxide and carbonate species:

$$\frac{\mathrm{d}[\mathrm{CO_2(aq)}]}{\mathrm{d}t} = kLa \cdot \left(C_{CO_2}^{*} - [\mathrm{CO_2(aq)}]\right) - r_1 - r_3 + \frac{dC_{CSH}}{dt} \ , \tag{3.44}$$

$$\frac{\mathrm{d}[\mathrm{HCO_3^-}]}{\mathrm{d}t} = r_1 - r_2 + r_3 - r_4 \ , \tag{3.45}$$

$$\frac{\mathrm{d}[\mathrm{CO_3^{2-}}]}{\mathrm{d}t} = r_2 - r_p + r_4 \ , \tag{3.46}$$

$$\frac{\mathrm{d}[\mathrm{H^+}]}{\mathrm{d}t} = r_1 + r_2 - r_5 \ , \tag{3.47}$$

For calcium carbonate precipitation from $Ca(OH)_2$:

$$\frac{\mathrm{d}[\mathrm{CaCO_3}]_{CH}}{\mathrm{d}t} = r_p \ , \tag{3.48}$$

where the rates of the individual reactions are:

$$r_1 = k_1 \cdot [\mathrm{CO_2(aq)}] - \frac{k_1}{K_{\mathrm{eq1}}} \cdot [\mathrm{H^+}] \cdot [\mathrm{HCO_3^-}] \ , \tag{3.49}$$

$$r_2 = k_2 \cdot [\mathrm{HCO_3^-}] - \frac{k_2}{K_{eq2}} \cdot [\mathrm{H^+}] \cdot [\mathrm{CO_3^{2-}}] \ , \tag{3.50}$$

$$r_3 = k_3 \cdot [CO_2(aq)] \cdot [OH^-] - \frac{k_3}{K_{eq3}} \cdot [HCO_3^-] \ , \tag{3.51}$$

$$r_4 = k_4 \cdot [HCO_3^-] \cdot [OH^-] - \frac{k_4}{K_{eq4}} \cdot \left[CO_3^{2-}\right] \ , \tag{3.52}$$

$$r_5 = k_w \cdot \left[H^+\right] \cdot [OH^-] - \frac{k_w}{K_w} \ , \tag{3.53}$$

$$r_p = k_p \cdot \left(\frac{\left[Ca^{2+}\right] \cdot \left[CO_3^{2-}\right]}{K_{sp,CaCO_3}} - 1 \right) \ , \tag{3.54}$$

In these equations, the activity coefficients should be included to account for non-ideal behavior, particularly in high ionic strength solutions. This would modify the reaction rates as follows:

$$r_1 = k_1 \cdot [CO_2(aq)] \cdot \gamma_{CO_2} - \frac{k_1}{K_{eq1}} \cdot \left[H^+\right] \cdot [HCO_3^-] \cdot \gamma_{H^+} \cdot \gamma_{HCO_3^-} \ , \tag{3.55}$$

And similarly for the other reaction rates.

3.6.2.1 Equilibrium and kinetic constant

The thermodynamic equilibrium constant as well as the heat of reaction at 25°C for most of the reactions have been listed alongside.

Table 5.1 *Equilibrium constant and heat reaction of the reactions in the system.*

Reaction	Parameter	$\log K_{eq}(25℃)$	$\Delta H_r^{25}(kJ/mol)$
3.23	k_1, k_1^-	-6.357	9.7
3.22	k_2, k_2^-	7.642	-46.1
3.24	k_3, k_3^-	3.664	-41.1
3.25	k_4, k_4^-	8.307	11.7
3.27	K_w	-13.998	-55.8

3.6.3 System Integration

This system of ODEs is solved numerically to simulate the evolution of the carbonation process over time. The numerical solution provides concentrations of all species as functions of time, which can then be compared with experimental measurements for model validation and parameter estimation.

By solving this system with appropriate initial conditions and parameter values, we can predict the carbonation behavior of cementitious materials under various conditions, providing valuable insights for process optimization and material design.

For numerical solution of this system, we employ a stiff ODE solver, such as MATLAB's ode15s, which is well-suited for systems with widely varying time scales of processes. The stiffness of the system arises from the rapid equilibration of some reactions (e.g., water ionization) compared to the slower processes of dissolution and diffusion.

Chapter 4

Parameter Estimation Methodology

The methods used to determine the optimal parameters for the mathematical model of mineral carbonation processes are presented in this chapter. Parameter estimation is essential for developing models that accurately reflect real-world observations and can reliably predict outcomes under different conditions. The modeling of mineral carbonation involves complex chemical reactions and transport phenomena that occur simultaneously at different rates. Finding the right values for parameters such as reaction rates, diffusion coefficients, and equilibrium constants is challenged by the complicated interactions of these processes, which are difficult to measure directly.

The chapter begins with a description of the experimental dataset, including the setup for wet carbonation of recycled cement paste powder and the key measurements collected: calcium hydroxide consumption, calcium carbonate formation, and pH changes over time. These measurements are used for evaluating how well the model represents the actual carbonation process. The challenges in parameter estimation are then examined, including model complexity, parameter interdependencies, and data limitations. The mathematical approach is subsequently presented, with the model parameters, objective function, and necessary constraints being defined to ensure physically meaningful results.

Three optimization techniques that were used to find the best parameter values are detailed: Genetic Algorithm (GA), Differential Evolution (DE), and a hybrid GA-DE approach. How these methods work, their implementation details, and performance measurement criteria are explained. Finally, sensitivity analysis and parameter identifiability are discussed, which help determine which parameters significantly influence the model outcomes and whether these parameters can be uniquely determined from the available experimental data.

4.1 Dataset

4.1.1 Experimental Setup and Methodology

The wet carbonation process of recycled concrete powder (RCP) was conducted under carefully controlled conditions to assess the carbonation efficiency and product development. To

evaluate our developed model from the previous chapter, experimental data are needed, which are reported in the literature (Zajac et al., 2020).

The experiments were performed at a moderate temperature of 25°C with a steady CO_2 flow rate of 3 L/min (equivalent to 0.06 L/min/g CPP). For each experimental run, 50 grams of CPP was introduced into 500 mL of deionized water, establishing a solid-to-liquid ratio of 1:10. To ensure uniform distribution and efficient mass transfer, the mixture was continuously stirred at 400 rpm using a heating magnetic stirrer. The carbonation process was examined at multiple time intervals (5, 10, 30, and 60 minutes) to track the evolution of carbonation products and reaction kinetics. In the following sections, relevant data extraction, based on the literature will be described.

4.1.2 Calcium Hydroxide Consumption Dynamics

The transformation of calcium hydroxide (CH) during carbonation provides crucial insights into the reaction progress. The initial CPP sample contained a substantial amount of CH (32.34%), which serves as the primary reactive component with CO_2. Upon exposure to the CO_2-enriched aqueous environment, CH underwent rapid dissolution and carbonation. After merely 5 minutes of carbonation, the CH content declined dramatically to approximately 22.5%, indicating that almost one-third of the available CH had already participated in the carbonation reaction. By the 10-minute mark, the CH content had further diminished to approximately 3.5%, revealing that over 89% of the original CH had been consumed. This rapid consumption of CH continues until it becomes virtually undetectable at the 30-minute and 60-minute intervals. This pattern demonstrates the high reactivity of CH with dissolved CO_2 in the aqueous medium and suggests that the early stages of carbonation are predominantly governed by CH conversion, which occurs at a remarkably fast rate compared to other processes in cementitious systems.

$$CH(\%) = \left(\frac{CH_w \times \left(\frac{74}{18}\right)}{M_{900°C}} \right) \times 100\%\,, \tag{4.1}$$

CH_w is water loss content at $900°C$, and $M_{900°C}$the residual mass at $900°C$, $Zajacetal.$,2020.. The concentration of CH in the system is shown in Table 4.1.

4.1.3 Formation and Evolution of Calcium Carbonate

Naturally, a small amount of $CaCO_3$ exists in the RCF. However, no exact value is reported in the literature, so we assume it is negligible.

As calcium hydroxide is consumed during carbonation, calcium carbonate ($CaCO_3$) concurrently forms as the principal carbonation product. Throughout the carbonation process, a steady increase in $CaCO_3$ content was observed, reaching approximately 21.0% after 5

minutes, 35.0% after 10 minutes, 52.0% after 30 minutes, and 59.0% after 60 minutes. The rate of $CaCO_3$ formation was particularly pronounced during the first 30 minutes, after which it began to decelerate. This deceleration is attributable to the exhaustion of readily available CH and the subsequent dependency on the slower decalcification of calcium silicate hydrate (C-S-H) gel and anhydrous phases. The crystallite size of calcite, the most stable polymorph of $CaCO_3$, increased from 50.2 nm at 30 minutes to 60.0 nm at 60 minutes, indicating ongoing crystal growth even as the overall rate of $CaCO_3$ formation slowed (Zajac et al., 2020).
Subsequently, equation 4.2 is utilized to convert experimental data to be usable in our model.

$$Cc(\%) = \left(\frac{C_{CO_2} \times \left(\frac{100}{44}\right)}{M_{900^\circ C}} \right) \times 100\%, \tag{4.2}$$

$Cc(\%)$ is $CaCO_3$ percentage in the system, and C_{CO_2} is the CO_2 loss content.

The concentration of $CaCO_3$ in the system is shown in Table 4.1.

4.1.4 pH Fluctuations and Their Implications

The pH evolution during carbonation provides valuable information about the changing chemical environment and competing reactions. Initially, the deionized water exhibited a neutral pH (approximately 7.0), but upon addition of CPP, the pH rapidly increased to approximately 11.6 and after 5 minutes reaches to 9.7 due to the dissolution of alkaline components, and CO_2 dissolution, respectively. However, as CH was depleted and carbonation progressed, the pH began to decrease significantly, dropping to approximately 9.2 after 30 minutes and further declining to approximately 6.2 after 60 minutes. This pH reduction reflects the increasing dominance of CO dissolution and carbonic acid formation over the diminishing alkaline contribution from the cementitious phases. The transition from an alkaline to a slightly acidic environment also signals a shift in the carbonation mechanism, from predominantly CH carbonation to the decalcification and carbonation of C-S-H gel and remaining anhydrous phases. The pH decline after 10 minutes corresponds closely with the depletion of CH, confirming the critical role of CH in maintaining the alkaline conditions necessary for optimal early-stage carbonation.

Table 4.1 *Extracted data for CH, $CaCO_3$, and pH for different sampling times.*

Property	**Time(min)**											
	0	**5**	**10**	**15**	**20**	**25**	**30**	**35**	**40**	**45**	**50**	**60**
CH (mol/lit)	0.43	0.29	0.046	-	-	-	0	-	-	-	-	-
$CaCO_3$ (mol/lit)	0	0.20	0.35	-	-	-	0.53	-	-	-	-	0.59
pH	11.53	11.16	11.17	10.63	10.24	9.75	9.4	9.1	8.41	7.29	6.33	6.23

4.2 Parameter estimation

The accurate prediction of mineral carbonation processes requires mathematical models that can reliably capture the complex interplay of chemical reactions, mass transfer mechanisms, and kinetic phenomena. However, these models are only as good as the parameters they employ. Parameter estimation, therefore, plays an important role in bridging theoretical constructions with real-world observations, allowing us to fine-tune models for improved predictive capability.

In the context of our mineral carbonation model, which integrates multiple reaction pathways and transport mechanisms, parameter estimation enables us to quantitatively characterize processes that might be difficult to measure directly. The kinetic rate constants, mass transfer coefficients, and diffusion parameters all influence how calcium from supplementary cementitious materials reacts with carbon dioxide to form stable carbonates.

4.2.1 Challenges in parameter estimation

Despite its importance, parameter estimation in mineral carbonation models faces several significant challenges:

1. **Model Complexity**: The inherent complexity of mineral carbonation processes, involving numerous simultaneous reactions and transport phenomena, results in models with multiple interacting parameters.
2. **Parameter Interdependencies**: Many parameters exhibit strong interdependence, making it difficult to isolate their individual effects. For example, the rate constant for calcium leaching and the diffusion coefficient through the product layer both affect the overall carbonation rate, but in ways that are sometimes difficult to distinguish experimentally.
3. **Data Limitations**: Experimental measurements often provide indirect indicators of system behavior, such as pH changes or total carbonation degree, rather than direct measurements of individual reaction rates or intermediate species concentrations.
4. **Nonlinearity**: The highly nonlinear nature of the governing equations makes traditional gradient-based optimization (i.e., local optimization) approaches less effective, necessitating optimization techniques that work globally.
5. **Multiple Time Scales**: Reactions occur across widely differing time scales, from near-instantaneous acid-base equilibria to slow diffusion-limited processes, creating mathematical stiffness that complicates both simulation and parameter estimation.

These challenges lead to an optimization approach that can effectively explore the parametric space for identifying parameter sets that best reproduce experimental observations.

4.2.2 Mathematical formulation

Our mineral carbonation model incorporates multiple reactions and transport phenomena, each dominated by specific parameters. The key parameters requiring estimation are reported as follows.

4.2.2.1 Definition of model parameters

The parameters are divided into three categories, represented in Table 4.2. The first category, Dissolution Parameters, describes the kinetics governing calcium hydroxide dissolution and ions' convective transport in solution. The second category, CSH Reaction Parameters, focuses on the reaction dynamics of calcium silicate hydrate (CSH), including diffusion through the product layer. The last category, Mass Transfer and Reaction Kinetics, covers how CO_2 and carbonate species move and react in solution, including important equilibrium reactions in the carbonation process.

Table 4.2 *Definition of model parameters in three different categories of Dissolution, CSH reaction, and mass transfer and reaction kinetics.*

Category	Parameter	Description
Dissolution Parameters	k_L	Rate constant for dissolution of $Ca(OH)_2$ (s^{-1})
	k_O	Rate constant for convection of Ca^{2+} to bulk solution (s^{-1})
	k_{O-OH}	Rate constant for convection of OH^- to bulk solution (s^{-1})
CSH Reaction Parameters	k_{CSH}	Rate constant for fast-reacting CSH fraction (s^{-1})
	D_0	Initial diffusion coefficient through product layer ($m^2 \cdot s^{-1}$)
	α	Decay parameter for diffusion coefficient (s^{-1})
	α_{diff}	Diffusion resistance parameter for $CaCO_3$ layer (dimensionless)
Mass Transfer and Reaction Kinetics	kLa	Volumetric mass transfer coefficient for CO_2 (s^{-1})
	k_1	Rate constant for $CO_{2\,(aq)} + H_2O \rightleftharpoons HCO_3^- + H^+$ (s^{-1})
	k_2	Rate constant for $HCO_3^- \rightleftharpoons CO_3^{2-} + H^+$ (s^{-1})
	k_3	Rate constant for $CO_2 + OH^- \rightleftharpoons HCO_3^-$ (lit. mol^{-1} s^{-1})
	k_4	Rate constant for $HCO_3^- + OH^- \rightleftharpoons CO_3^{2-} + H_2O$ (lit. mol^{-1} s^{-1})
	k_P	Rate constant for $Ca^{2+} + CO_3^{2-} \rightleftharpoons CaCO_3$ (lit. mol^{-1} s^{-1})

4.2.2.2 Objective function

The objective function (4.3) is a weighted sum of squared errors between model predictions and experimental measurements for three key variables: $Ca(OH)_2$ concentration, pH, and $CaCO_3$ formation. This type of objective function is a standard approach in parameter estimation for complex chemical systems.

Each term in the objective function represents the normalized squared error for a specific measurement type. Normalization by the standard deviation (σ_n, σ_{pH}, and σ_{CaCO3}) is essential to ensure that variables with different magnitudes contribute appropriately to the overall objective. Without this normalization, variables with larger absolute values would dominate the optimization process, potentially leading to poor fits for variables with smaller magnitudes.

The weighting factor w_{pH} is included because pH measurements typically have more data points than the other measurements. This weighting helps balance the influence of pH data against $Ca(OH)_2$ and $CaCO_3$ measurements, preventing the optimization from being biased toward fitting pH at the expense of other important variables.

$$J(\theta) = \sum_{i=1}^{N_{CH}} \left(\frac{n_{model,i}(\theta) - n_{exp,i}}{\sigma_n} \right)^2 + w_{pH} \sum_{j=1}^{N_{pH}} \left(\frac{pH_{model,j}(\theta) - pH_{exp,j}}{\sigma_{pH}} \right)^2 + \sum_{k=1}^{N_{CaCO3}} \left(\frac{CaCO3_{model,k}(\theta) - CaCO3_{exp,k}}{\sigma_{CaCO3}} \right)^2, \quad (4.3)$$

Where (Storn & Price, 1997):

- θ is the vector of parameters to be estimated.
- $n_{model,i}$ and $n_{exp,i}$ are the model-predicted and experimentally measured $Ca(OH)_2$ concentrations.
- $pH_{model,j}$ and $pH_{exp,j}$ are the model-predicted and experimentally measured pH values.
- $CaCO3_{model,k}$ and $CaCO3_{exp,k}$ are the model-predicted and experimentally measured $CaCO_3$ concentrations.
- σ_n, σ_{pH}, and σ_{CaCO3} are the standard deviations of the respective experimental measurements.
- w_{pH} is a weighting factor to balance the influence of pH measurements against other measurements.
- N_{CH}, N_{pH}, and N_{CaCO3} are the number of experimental data points for each measurement type.

Normalization by standard deviations ensures that measurement types with different magnitudes contribute comparably to the objective function. The weighting factor $w_{pH}$is introduced because pH measurements typically have more data points, and without proper weighting, they might dominate the optimization process.

4.2.2.3 Constraints and boundaries

Physical and chemical principles impose natural constraints on the parameter values. For instance, rate constants and diffusion coefficients must be positive. Additionally, based on literature and physical understanding, we established lower and upper bounds for each parameter to ensure physically meaningful results and to constrain the search space.
For numerical stability, the optimization performed in logarithmic space, and the bounds defined as:

$$\log_{10}(lb_i) \leq \log_{10}(\theta_i) \leq \log_{10}(ub_i)\,, \tag{4.4}$$

4.3 Optimization Techniques Employed

Given the non-convexity of the parameter estimation problem, gradient-based optimization methods are prone to getting trapped in local minima. Therefore, two population-based global optimization techniques are employed: GA and DE. Additionally, a hybrid approach combining GA and DE is used to leverage the strengths of both methods.

4.3.1 Genetic Algorithm

A GA is an optimization and search technique inspired by the process of natural selection. GA operates on a population of potential solutions (individuals), evolving them over successive generations through processes that mimic natural selection and genetics. They are used to solve complex problems by evolving solutions over generations. GA operates through a population of potential solutions, applying genetic operators such as selection, crossover, and mutation to improve their quality iteratively. The fittest individuals, determined by an objective function, are selected to create the next generation, ensuring that better solutions emerge over time. This approach is widely used in various fields, including engineering, artificial intelligence, and economics, for solving problems where traditional methods may be inefficient or infeasible (Stubberud, 2023). Subsequently, the key components of a GA include:

1. **Population Initialization**: A set of potential solutions (parameter vectors) is randomly generated within the defined parameter bounds.
2. **Fitness Evaluation**: Each individual is evaluated using the objective function to determine its "fitness" - how well it solves the problem.

3. **Selection**: Individuals are selected for reproduction with probability proportional to their fitness.
4. **Crossover**: Pairs of selected individuals "mate" to produce offspring by exchanging portions of their parameter vectors.
5. **Mutation**: Random alterations are introduced to some of their offspring to maintain genetic diversity and explore new regions of parameter space.
6. **Replacement**: A new generation is formed by replacing some or all of the current population with the offspring.
7. **Convergence criteria**: GA stops when a termination condition is met, such as: a maximum number of generations, no improvement in fitness for a set number of generations, or the solution reaching a predefined threshold.

The iterative application of these operations—selection, crossover, and mutation—gradually refines the population, guiding it toward increasingly optimal solutions. Selection ensures that individuals with higher fitness are more likely to pass their genetic material to the next generation, preserving beneficial traits. Crossover combines information from two parent solutions, promoting diversity and enabling the exploration of new regions in the solution space. Mutation introduces random variations, preventing premature convergence and maintaining genetic diversity. Over successive generations, these processes collectively drive the population toward solutions with higher fitness. The algorithm continues this evolutionary cycle until a predefined convergence criterion is met, such as reaching a maximum number of generations, achieving a solution that satisfies an optimal threshold, or detecting minimal improvement in fitness over multiple iterations. Through this iterative refinement, GA effectively navigates complex search spaces and finds near optimal or optimal solutions in a wide range of optimization problems.

4.3.2 Differential Evolution Methods

Differential Evolution (DE) is a powerful, population-based optimization algorithm that is particularly effective for solving complex problems in continuous parameter spaces. Unlike GA, which often represents solutions as binary strings or discrete encodings, DE works directly with real-valued parameter vectors. This direct manipulation of real numbers makes DE well-suited for numerical optimization tasks, where precision and smooth exploration of the search space are crucial.

The core principle of DE is based on the evolutionary process of mutation, crossover, and selection, similar to GAs, but with a distinct approach. Instead of applying traditional crossover and mutation techniques, DE generates new candidate solutions by perturbing existing ones using scaled differences between randomly selected individuals from the population. This

mechanism allows DE to efficiently explore the search space and adaptively refine solutions for generations (Storn & Price, 1997).

One of the key advantages of DE is its ability to balance exploration and exploitation. The mutation step ensures diversity by introducing novel candidate solutions, while the selection process ensures that only better-performing individuals survive, leading to a gradual convergence toward optimal or near-optimal solutions. Additionally, DE requires fewer hyperparameters compared to GAs, typically only needing control over mutation factor, crossover rate, and population size, making it relatively easy to implement and tune.

Due to its robustness and efficiency, DE has been successfully applied to a wide range of optimization problems, including engineering design, machine learning hyperparameter tuning, signal processing, and financial modeling. Its simplicity, combined with its strong performance in handling high-dimensional and multimodal functions, makes it a preferred choice for many real-world optimization challenges.

Here is a comparative Table 4.3 highlighting the strengths of GA and DE across key metrics.

Table 4.3 *Comparison between GA model and DE model for model optimization procedure*

Metric	Genetic Algorithm (GA)	Differential Evolution (DE)
Final Objective (Fitness)	May find a good solution, but can get stuck in local optima	Often finds better solutions due to effective mutation and exploration
Convergence Rate	Slower due to random genetic operations	Faster convergence with directed mutation strategies
Computational Efficiency	Higher computational cost due to selection, crossover, and mutation	More efficient due to direct real-number operations
Parameter Consistency	Requires careful tuning of crossover rate, mutation probability, and selection strategy	Fewer hyperparameters, making it easier to tune
Stability under initial conditions	Can struggle with poor initial populations, but maintains diversity	More robust, as mutation relies on population differences rather than initial values

4.3.3 Hybrid approach (GA-DE)

The hybrid optimization approach combines GA and DE to improve the accuracy and reliability of parameter estimation. The process begins with GA, which explores the search space by applying selection, crossover, and mutation operations. This step provides an initial set of candidate solutions that are less likely to be trapped in local minima.

Once GA identifies a promising solution, its predicted values are used to define the initial search bounds for DE. The lower and upper bound for DE is defined as coefficients of the x_{GA}, where

represents the solution obtained from GA. This approach ensures that DE starts from an informed region while maintaining sufficient flexibility for refinement. By combining the exploratory search of GA with the fine-tuning capability of DE, the method reduces the risk of premature convergence and improves the overall optimization process.

4.4 Implementation Details

Implementation details of three optimization techniques applied to carbonation modeling – GA, DE, and a Hybrid GA-DE approach – are described here. The focus is specifically on the algorithmic implementation aspects rather than the theoretical foundations or the application domain. All the hyperparameters (e.g., crossover fraction) used in the system are reported in the next chapter 5.

4.4.1 Common Implementation Features

All three optimization methods share several implementation characteristics to ensure fair comparison. Parameter transformation is applied to all parameters, which are converted to a logarithmic scale before optimization to handle the wide range of magnitudes (from 1e-7 to 1e11). This transformation improves search efficiency by creating a more uniform parameter space. A common fitness function (objFuncGA) evaluates how well the model fits experimental data by running the carbonation model with candidate parameters, interpolating model results at experimental time points, calculating normalized errors for $Ca(OH)_2$ concentration, pH, and $CaCO_3$ formation, applying appropriate weighting to balance the influence of different measurements, and returning the sum of squared errors as the fitness value. Lower and upper bounds constrain all parameters within physically meaningful ranges, and the log-space transformation helps prevent violation of these constraints during optimization. The implementation also checks for invalid solutions that produce NaN or Inf values, assigning them high fitness values (1e6) to guide the search away from unstable parameter combinations.

4.4.2 Genetic Algorithm Implementation

The GA implementation uses MATLAB's built-in "ga" function with customized settings. Population initialization creates individuals, with each individual representing a set of parameters in log space. The initial population is randomly generated within the defined bounds. The genetic operators include a crossover fraction of N_{cf}, meaning N_{cf}% of the new population comes from crossover. Mutation uses an adaptive feasible approach that adjusts based on the success of previous generations, while selection employs tournament selection, which is the default in MATLAB's implementation. Regarding stopping criteria, the algorithm runs for a maximum of N_s generations and stops when changes in fitness are below the function tolerance threshold of 1e-6. Parallel processing is enabled to speed up evaluation across

multiple CPU cores, taking advantage of the fact that each individual's fitness evaluation is independent, making this highly parallelizable. The implementation also includes real-time plotting of the best fitness value to visualize progress as optimization proceeds.

4.4.3 Differential Evolution Implementation

algorithm is implemented from scratch rather than using built-in functions. Population initialization creates individuals with random values within log-transformed bounds and performs fitness evaluation for each initial individual. The evolution strategy can be selected through "best/1/bin" or "rand/1/bin", where "best" or "random" means how the mutant vector should be created. In the best mode, the mutant vector is created using the current best individual, while in the rand mode, the mutant vector is created by selecting a random individual from the population. The "1" refers to using one different vector for mutation. Additionally, both strategies involve a "bin" (i.e., binomial) crossover, where the offspring is generated by combining components of the mutant vector and the target vector based on a predefined crossover rate.

The mutation process uses a mutation factor (F) to control the amplification of differential variation. For each individual i in the population, two random individuals r_1 and r_2 (different from i and the best) are selected, and a mutant vector is created as $\overrightarrow{x_{\text{best}}} + F \cdot \left(\overrightarrow{x_{r_1}} - \overrightarrow{x_{r_2}}\right)$, with boundaries enforced to ensure the mutant remains within the defined parameter ranges.

In the "rand" mode, rather than using the best individual as the base vector, a random individual r_0 is selected from the population, and the mutant vector is created as $\overrightarrow{x_{r0}} + F \cdot \left(\overrightarrow{x_{r_1}} - \overrightarrow{x_{r_2}}\right)$. This approach helps maintain diversity in the population and can be particularly effective for multimodal problems where avoiding premature convergence to local optima is crucial. The crossover process employs a crossover probability (CR), which determines for each parameter whether the original value is kept with probability (1-CR), though at least one parameter is always taken from the mutant vector to ensure diversity. This can be represented as:

$$u_{i,j} = \begin{cases} u_{i,j} = v_{i,j} & \text{if } \text{rand}_j(0,1) \le CR \text{ or } j = j_{\text{rand}} \\ u_{i,j} = x_{i,j} & \text{otherwise} \end{cases}, \tag{4.5}$$

where $u_{i,j}$ is the trial vector component, $v_{i,j}$ is the mutant vector component, and j_{rand} is a randomly chosen index.

In the selection process, each trial vector competes with its parent individual, and the one with better fitness survives to the next generation, expressible as:

$$\overrightarrow{x_i^{G+1}} = \begin{cases} \overrightarrow{x_i^{G+1}} = \overrightarrow{u_i^G} & \text{if } f\left(\overrightarrow{u_i^G}\right) \le f\left(\overrightarrow{x_i^G}\right) \\ \overrightarrow{x_i^{G+1}} = \overrightarrow{x_i^G} & \text{otherwise} \end{cases}, \tag{4.6}$$

The DE implementation uses a fixed number of iterations with progress reporting after each generation.

4.4.4 Hybrid GA-DE Implementation

The hybrid approach combines the global exploration capability of GA with the local exploitation strength of DE through sequential execution. The algorithm first runs GA to explore the global parameter space, then uses GA results to define a narrower search space for DE and finally runs DE within this refined space.

The boundary definition for the second phase sets lower bounds at α times the GA optimal values and upper bounds at β times the GA optimal values, creating parameter-specific bounds centered around GA's solution:

$$lower\_bound_i = \alpha \cdot GA\_optimal_i$$
$$upper\_bound_i = \beta \cdot GA\_optimal_i \quad , \tag{4.7}$$

where α and β are scaling factors, and $GA\_optimal_i$ represents the optimal value for parameter i found by GA.

The DE configuration in the hybrid approach uses a population size of N_P, maximum iterations of G_{max}, mutation factor (F), and crossover rate (CR). It employs the "best/1/bin" strategy, where the mutant vector is created as:

$$\overrightarrow{v_i} = \overrightarrow{x_{\text{best}}} + F \cdot \left(\overrightarrow{x_{r_1}} - \overrightarrow{x_{r_2}}\right) \quad , \tag{4.8}$$

This implementation strategy aims to reduce the number of function evaluations needed by having GA provide a good starting point in the global sense, after which DE refines the solution with its effective local search capabilities. The treatment of parameters in this approach assumes GA has found the approximate region of the global optimum, so all parameters receive the same boundary scaling treatment in the second phase.

4.4.4 Performance Measurement Implementation

The implementation includes several metrics to compare the performance of each algorithm. Fitness tracking records the best fitness value at each generation or iteration and compares the final fitness values across methods. Computation time is measured as wall-clock time for each optimization method, providing a practical assessment of computational efficiency.

Error metrics include Root Mean Square Error (RMSE) calculated for each output variable and the coefficient of determination (R^2) to measure goodness of fit, with these metrics calculated in the original (non-log) space. The RMSE is defined as (Z. Wang et al., 2023):

$$\text{RMSE} = \sqrt{\frac{1}{n}\sum_{i=1}^{n}(y_i - \hat{y}_i)^2}, \tag{4.9}$$

Where n is the number of data points, $\hat{y}_i$ is the observed value, and $\hat{y}_i$ is the predicted value.

The coefficient of determination (R^2) is defined as:

$$R^2 = 1 - \frac{\sum_{i=1}^{n}(y_i - \hat{y}_i)^2}{\sum_{i=1}^{n}(y_i - \bar{y})^2}, \tag{4.10}$$

Where $\hat{y}_i$ is the mean of the observed values.

For convergence analysis, fitness history is plotted on a semi-logarithmic scale to allow visual comparison of convergence rates among the different methods.

4.4.5 Implementation Challenges and Solutions

Several challenges were addressed in the implementation. The parameter scale variation challenge, where parameters span many orders of magnitude, was solved through log-space transformation to create a more uniform search space. The problem of simulation failures, where some parameter combinations cause model integration failures, was addressed through error handling that assigns high fitness values to invalid solutions. The computational expense of model integration was mitigated through parallel processing for GA and efficient DE implementation. The challenge of balancing multiple objectives when fitting multiple experimental datasets with different scales was handled through normalization and weighting in the objective function.

4.5 Sensitivity Analysis

Sensitivity analysis determines how changes in model parameters affect output variables. This approach is essential when working with complex models containing many parameters, particularly when experimental determination of all parameters is impractical. Sensitivity analysis serves multiple purposes in model development and validation.

First, sensitivity analysis identifies which parameters most strongly influence model behavior. In chemical reaction systems, some parameters may dominate system dynamics while others have minimal impact. Identifying high-sensitivity parameters helps prioritize experimental efforts to estimate these parameters accurately. Second, sensitivity analysis reveals parameter correlations and redundancies. When multiple parameters affect model outputs similarly, they may be difficult to estimate independently. Understanding these correlations helps simplify models by fixing certain parameter ratios or eliminating redundant parameters. Third, sensitivity analysis guides optimization strategies by focusing computational resources on parameters that matter most. This targeted approach reduces the dimensionality of the parameter estimation problem and improves convergence.

The sensitivity analysis methodology employs several complementary approaches. Parameter scaling examines how model outputs change relative to parameter perturbations. This involves systematically varying each parameter while holding others constant and quantifying output

changes. The sensitivity coefficient for parameter p with respect to output y is typically calculated as (Saltelli et al., 2002):

$$S(p, y) = \frac{\partial y}{\partial p} \times \frac{p}{y}, \tag{4.11}$$

This normalized form expresses sensitivity as the relative change in output per relative change in parameter. Alternative sensitivity metrics include variance-based methods that decompose output variance into contributions from individual parameters and their interactions. Parameter variance analysis compares parameter values across different optimization runs or samples. Parameters with consistent values across methods are typically well-constrained by data, while those showing large variation may have less influence or exhibit correlations with other parameters. Convergence analysis examines how quickly parameters reach stable values during optimization. Early convergence indicates well-defined parameters, while parameters continuing to vary throughout optimization may be less sensitive or correlated with others.

Chapter 5

Mineral Wet Carbonation Ionic Model Identification and Interpretation

This chapter presents the results obtained from the parameter estimation and model validation for the carbonation process model developed in previous chapters. The model was designed to simulate the complex interactions involved in the carbonation of cementitious materials, with particular focus on calcium leaching, CO_2 dissolution, and calcium carbonate formation. By evaluating the estimated parameter values and analyzing the model's predictive capabilities, we gain valuable insights into the underlying reaction mechanisms and transport phenomena governing the mineral carbonation process.

We employed multiple optimization techniques for parameter estimation, including Genetic Algorithm (GA), Differential Evolution (DE), and a hybrid GA-DE approach. While each method has its theoretical strengths, their performance in practice varies significantly for this specific modeling challenge.

The chapter addresses the following key questions:

1. How do different optimization methods (GA, DE, and hybrid) compare in estimating parameters for the carbonation model?
2. Which parameters most significantly influence carbonation behavior?
3. What are the dominant reaction mechanisms and rate-limiting steps at different stages of the process?
4. How can model insights be applied to optimize carbonation processes for CO_2 sequestration in cement-based materials?

Through detailed analysis of simulation results, we develop a fundamental understanding of the physicochemical processes involved in mineral carbonation and establish a foundation for future modeling efforts in this field.

5.1 Differential Evolution Parameter Optimization

Before proceeding with detailed analysis of the GA, DE, and GA-DE models results, it is worth examining the factors that influenced the DE optimization performance. A systematic

investigation was conducted to determine the optimal DE algorithm parameters for this specific problem.

5.1.1 Effect of DE Configuration Parameters

Three key control parameters were varied to assess their impact on DE performance:

1. **Population Size**: Values of 20, 30, and 50 were tested.
2. **Crossover Rate (CR)**: Values of 0.8, 0.85, and 0.9 were tested.
3. **Mutation Strategy**: "best/1/bin" and "rand/1/bin" strategies were compared.

The mutation factor to keep the run model faster is constant value of 0.6. Figure 5.1 illustrates the effect of these control parameters on the DE algorithm's performance.

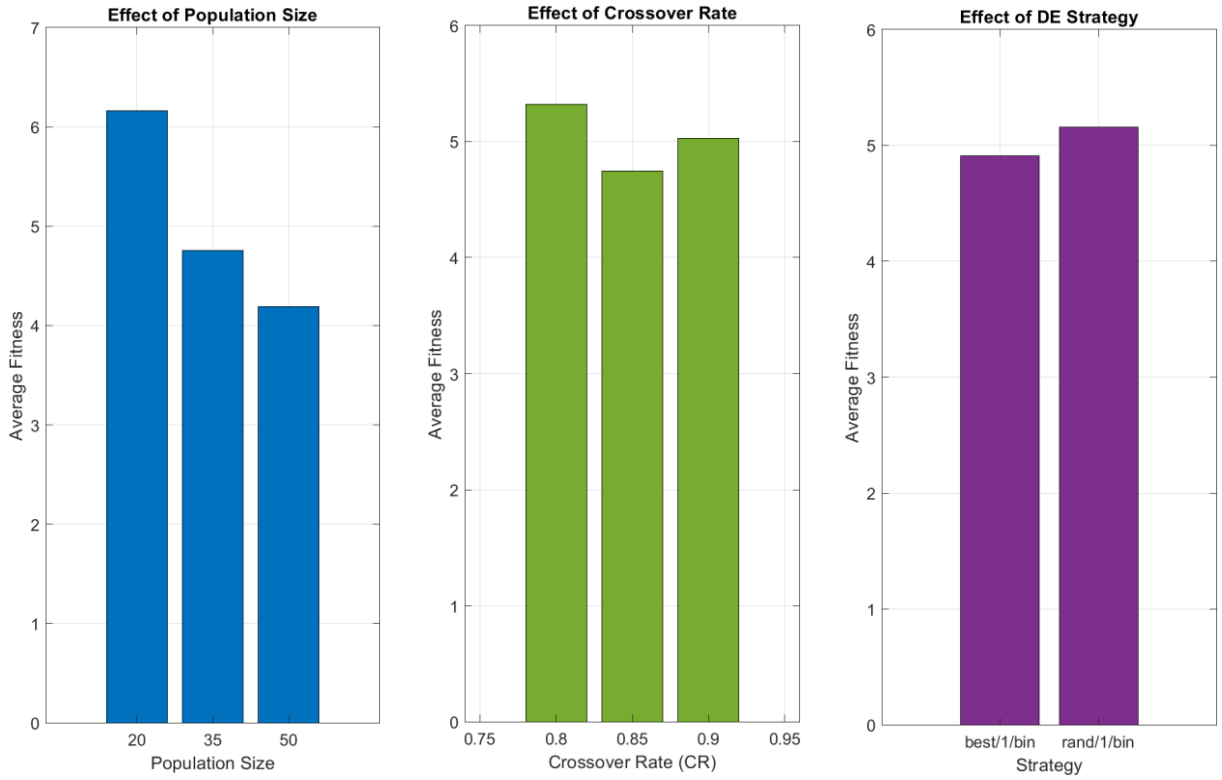

Figure 5.1 *The influence of DE configuration parameters on optimization performance.*

Population size showed a significant effect on the quality of solutions, with larger populations (n=50) generally finding better solutions but at the cost of increased computation time. The crossover rate also influenced performance, with higher CR values (0.85-0.9) yielding better results than lower values (0.8), suggesting that more aggressive information exchange between candidate solutions is beneficial for this problem. Among the mutation strategies, "best/1/bin" consistently outperformed "rand/1/bin," indicating that exploitation of the current best solution is more effective than pure exploration for this application.

The optimal DE configuration respect to the lowest fitness value for tested system was found to be:

- Population size: 50
- Crossover rate (CR): 0.85
- Mutation strategy: "best/1/bin"

Consequently, In the next section, the best fitness value based on the yielded configuration parameters in the DE model will be implemented.

5.2 Comparison of Optimization Methods

5.2.1 Optimization Results Comparison

The parameter estimation process employed three complementary optimization strategies, each configured with specific settings to balance exploration capability, convergence efficiency, and computational cost. Table 5.1 presents the configuration details for each optimization method. The GA configuration emphasized exploration with a larger population size and adaptive mutation, while the DE approach favored exploitation with a more directed search strategy. The hybrid GA-DE method leveraged the strengths of both approaches by using GA results to define narrowed parameter bounds (0.01 to 100 times the GA optimal values), thereby focusing the DE search on promising regions of the parameter space.

Table 5.1: *Configuration parameters for the optimization methods employed in parameter estimation*

Configuration Parameter	Genetic Algorithm (GA)	Differential Evolution (DE)	Hybrid GA-DE
Population Size	*50*	*50*	*50*
Maximum Iterations	*50 generations*	*50 iterations*	*50 iterations*
Search Strategy	*Stochastic with elitism*	*'best/1/bin'*	*'best/1/bin'*
Selection Mechanism	*Tournament selection*	*Greedy selection*	*Greedy selection*
Crossover Rate	*0.80*	*0.85*	*0.85*
Mutation Approach	*Adaptive feasible*	*Fixed factor (F = 0.6)*	*Fixed factor (F = 0.6)*
Parameter Bounds	*Global bounds*	*Global bounds*	*Narrowed (0.01× to 100× GA results)*
Parallelization	*Yes*	*No*	*No*
Convergence Criterion	*Function tolerance 1e-6*	*Function tolerance 1e-6*	*Function tolerance 1e-6*
Seed for Reproducibility	*42*	*Not specified*	*Not specified*

This complementary configuration enabled thorough exploration of the parameter space while ensuring efficient convergence toward optimal solutions.

Table 5.2: *Comparison of parameter values estimated by GA, DE, and hybrid GA-DE methods.*

Parameter	GA Estimated Value	DE Estimated Value	Hybrid GA-DE Value	Reported Value
k_L	1.96×10^{-3}	9.73×10^{0}	2.66×10^{-3}	1×10^{-3}
k_O	0.57	1.00	9.05×10^{-2}	2×10^{-2}
k_{CSH}	7.29×10^{1}	4.14×10^{3}	3.40×10^{2}	1×10^{3}
D_0	2.41×10^{-4}	2.00×10^{-6}	2.01×10^{-4}	1×10^{-4}
α	5.43×10^{-6}	9.98×10^{-6}	3.81×10^{-7}	1×10^{-6}
α_{diff}	1.34×10^{0}	7.21	1.26×10^{2}	1×10^{0}
kLa	5.48×10^{-2}	3.50×10^{-2}	4.45×10^{-2}	1×10^{-2}
k_1	2.83×10^{-4}	2.93×10^{-5}	1.16×10^{-4}	3.0×10^{-5}
k_2	5.77×10^{2}	7.97×10^{3}	5.77	5.94×10^{1}
k_3	1.01×10^{1}	1.00	1.08×10^{1}	2.23×10^{3}
k_4	7.61×10^{6}	1.95×10^{4}	7.04×10^{8}	2.80×10^{5}
k_p	5.42×10^{-2}	9.91×10^{-2}	2.64	9.49×10^{-3}

Table 5.2 presents the comparison of parameter values estimated by the three optimization methods, along with reported values for kinetics are based on the literature (Schulz et al., 2006; Velts et al., 2011b), which are for pure CH dissolution with injected CO_2. The remaining parameters are found by trial and error for reference values.

The convergence characteristics and performance metrics for the three optimization methods are compared in Table 5.3.

Table 5.3: *Performance comparison of optimization methods.*

Metric	GA	DE	Hybrid GA-DE
Final fitness value	0.362	1.96	0.242
Number of function evaluations	4870	620	2510
R^2 for $Ca(OH)_2$	0.917	0.962	0.939
R^2 for pH	0.987	0.798	0.993
R^2 for $CaCO_3$	0.997	0.987	0.998

The "Final fitness value" in Table 5.3 represents the optimized value of the objective function at the end of each optimization method's execution. It quantifies how well the optimized parameters allow the model to fit the experimental data. Lower fitness values indicate better fits between model predictions and experimental measurements. Based on these metrics alone,

the hybrid GA-DE approach appears to be the most effective, achieving the lowest fitness value and highest R^2 values. The DE approach is the most computationally efficient, requiring significantly fewer function evaluations and less computation time than the other methods. However, these metrics only tell part of the story, as we will see in the next section.

5.2.2 Time-Series Predictions

While the performance metrics suggest that DE and hybrid GA-DE methods outperform the GA method in terms of objective function value, a closer examination of the time-series predictions reveals a different picture. Figure 5.2 shows the time-series predictions for pH for all three optimization methods compared with experimental data. Although the DE and hybrid GA-DE models achieve slightly better fits to the experimental data points in a statistical sense, they exhibit significant fluctuations in the predicted curves, particularly for pH. These fluctuations appear as unrealistic oscillations in the time-series predictions, which are physically implausible for the carbonation process.

The DE-optimized parameter set, while mathematically producing a better fit to discrete data points, encountered numerical instability in simulating results, which led to these oscillations depicted in Figure 5.2. This numerical instability occurs because the DE algorithm prioritized minimizing the objective function value without considering the physical continuity constraints of the underlying chemical system.

In contrast, the GA model produces smoother curves that better reflect the expected continuous nature of the underlying physical and chemical processes.

The oscillatory behavior in the DE and hybrid GA-DE predictions is particularly pronounced during the transition phases of the carbonation process, such as when $Ca(OH)_2$ is nearly depleted, and the pH begins to drop rapidly.

Given the importance of producing physically consistent predictions, especially for understanding the reaction mechanisms and for reliable extrapolation to different conditions, the GA model is deemed preferable despite its slightly lower statistical performance.

The remainder of this chapter will therefore focus primarily on the GA model results, with references to the other methods where appropriate.

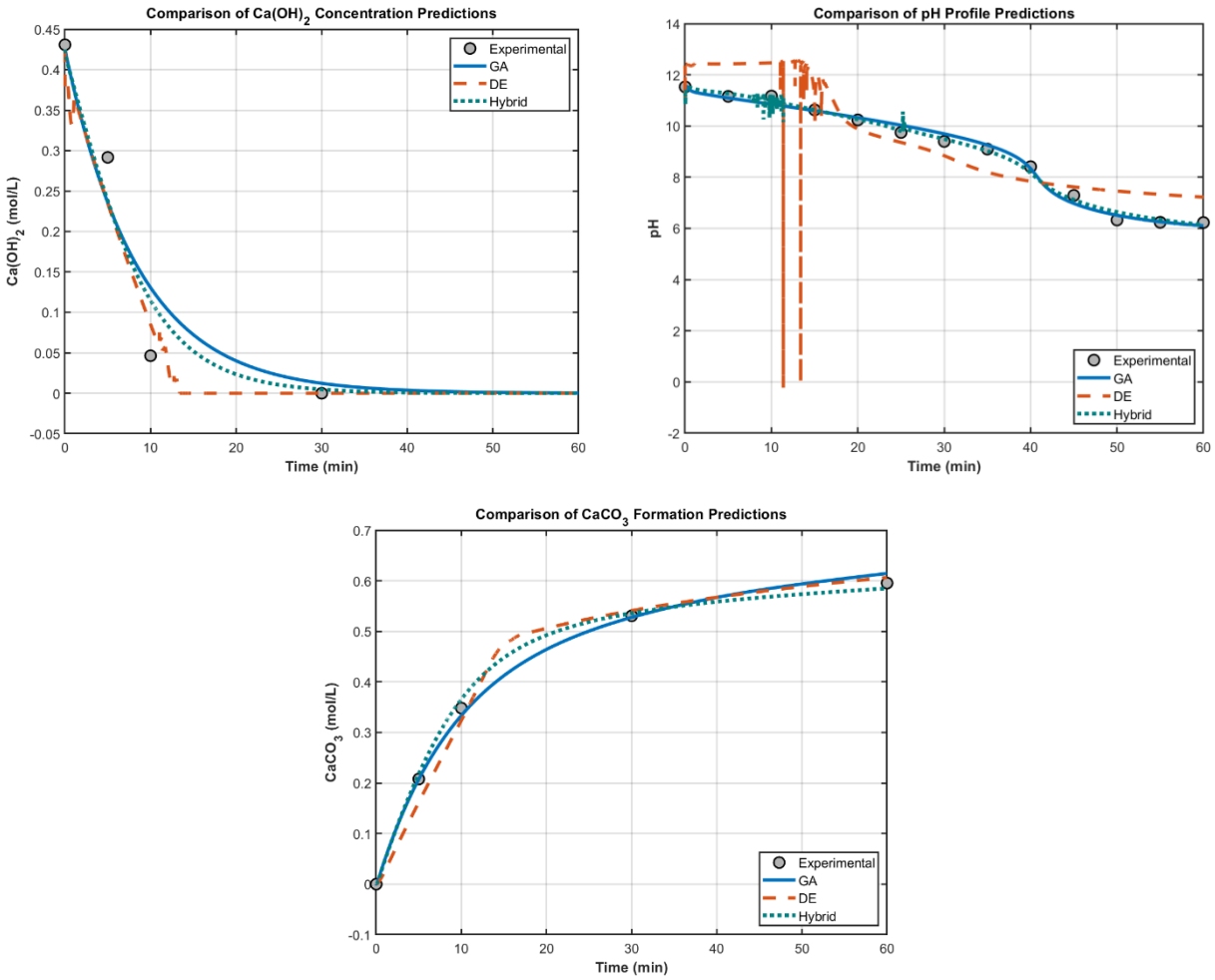

Figure 5.2 *Plots comparing model predictions from GA, DE, and hybrid GA-DE with experimental data points.*

5.2.3 Why GA Provides More Stable Results

The superior stability of the GA model predictions can be attributed to several factors:

1. **Diversity Preservation**: The GA implementation maintains greater population diversity through its selection and mutation operators, helping it avoids premature convergence to solutions that overfit to specific data points.
2. **Crossover Mechanism**: GA's crossover mechanism tends to blend parameter values from multiple individuals, producing a smoothing effect that filters out extreme parameter combinations that might cause oscillatory behavior.
3. **Selection Pressure**: The GA's tournament selection provides a more balanced approach to selection pressure compared to DE's greedy selection, allowing it to maintain a better exploration-exploitation balance.
4. **Parameter Landscape**: The specific characteristics of the parameter space for this problem, with its multiple interacting parameters and multiple local optima, may be better suited to GA's broader exploration capabilities.

Additionally, the carbonation process involves distinct phases with different controlling mechanisms, creating a complex objective function landscape with potentially steep transitions. GA's ability to maintain multiple diverse solutions simultaneously may help it navigate this landscape more effectively than DE, which relies more heavily on local information gradients. For these reasons, while the hybrid GA-DE method achieves slightly better statistical fits, the GA model provides more physically plausible predictions that better capture the continuous nature of the carbonation process.

5.3 GA Model Results

After a brief discussion and comparison of the Genetic Algorithm (GA), Differential Evolution (DE), and the hybrid GA-DE model, the following section presents the results obtained for the proposed model based on the estimated parameters using the GA approach.

5.3.1 Model Fit to Experimental Data

Figure 5.3 compares the GA model predictions with experimental measurements for $Ca(OH)_2$ concentration, pH, and $CaCO_3$ formation over time.

The GA model demonstrates excellent agreement with the experimental data, capturing all key features of the carbonation process:

1. **$Ca(OH)_2$ Consumption**: The model accurately reproduces the rapid initial consumption of $Ca(OH)_2$, with complete depletion occurring by approximately 30 min. The R^2 value for $Ca(OH)_2$ predictions is 0.917.
2. **pH Evolution**: The model captures the characteristic S-shaped pH curve, with an initial plateau at pH ~11.5, followed by a steep decline between 15 and 50 minutes, and eventual stabilization at pH ~6.2. The R^2 value for pH predictions is 0.987.
3. **$CaCO_3$ Formation**: The model accurately predicts the progressive formation of $CaCO_3$, with rapid initial accumulation followed by a more gradual approach to the maximum conversion level. The R^2 value for $CaCO_3$ predictions is 0.997.

The residual analysis confirms that the GA model provides unbiased predictions with no significant systematic errors, supporting its validity for simulating the carbonation process.

Figure 5.3 *The figure shows a multi-panel plot comparing GA model predictions with experimental data points.*

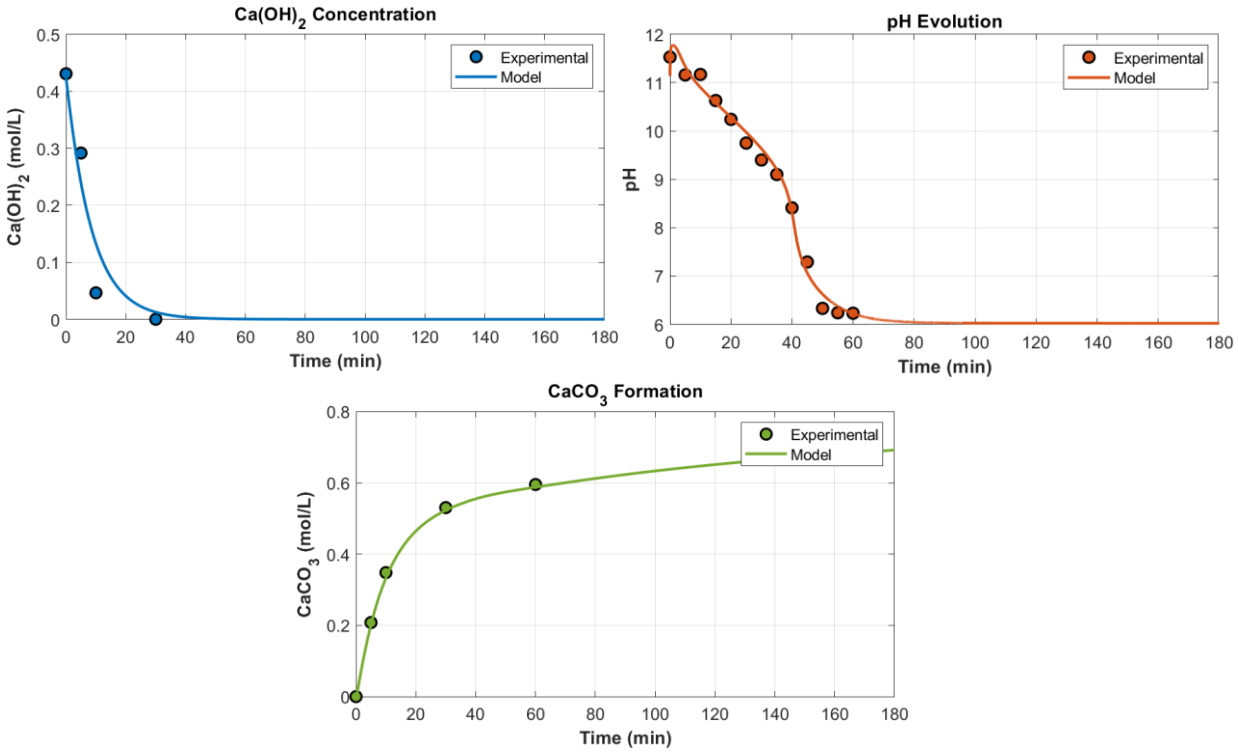

5.3.2 Concentration Profiles and Speciation Dynamics

5.3.2.1 Evolution of Carbonate Species and CO_2 Dissolution

The identified model provides detailed insights into the complex dynamics of carbonate speciation throughout the carbonation process. Figure 5.4 illustrates the temporal evolution of carbonate species and dissolved CO_2 during the 180-minute carbonation experiment.

The carbonation process exhibits distinct phases of carbonate speciation. During the initial phase (0-20 minutes), CO_3^{2-} concentration rises to a small peak of approximately 0.001 mol/L, driven by the high pH environment created by dissolving $Ca(OH)_2$. This early CO_3^{2-} dominance promotes rapid $CaCO_3$ precipitation when Ca^{2+} ions are readily available from $Ca(OH)_2$ dissolution. However, as $Ca(OH)_2$ is consumed and pH begins to decrease, CO_3^{2-} concentration diminishes significantly, becoming nearly negligible after 40 minutes.

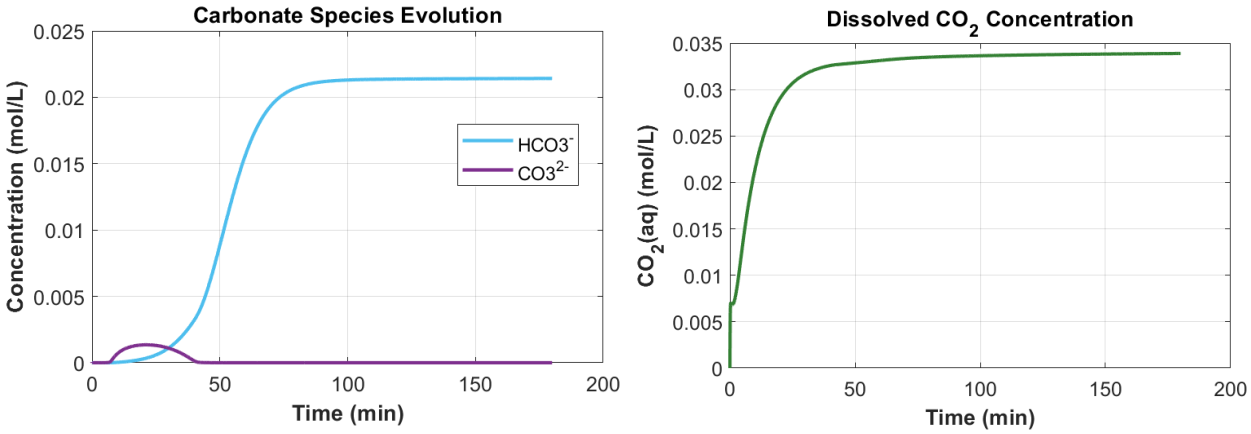

Figure 5.4: *Evolution of carbonate species (left) and dissolved CO_2 concentration (right) during carbonation. The left panel shows the transition from CO_3^{2-} dominance to HCO_3^- dominance, while the right panel shows the rapid rise and subsequent stabilization of aqueous CO_2.*

Concurrently, the HCO_3^- concentration remains low during the initial 30 minutes, then increases dramatically between 40-80 minutes, reaching an equilibrium value of approximately 0.021 mol/L by 90 minutes. This transition from CO_3^{2-} to HCO_3^- as the dominant carbonate species coincides with the depletion of $Ca(OH)_2$ and the acidification of the solution due to continuous CO_2 dissolution.

The dissolved CO_2 concentration (right panel) shows complementary behavior, starting near zero and rising rapidly during the first 30 minutes as the solution's capacity to convert CO_2 to carbonate ions diminishes with decreasing pH. The $CO_2(aq)$ concentration reaches approximately 95% of its equilibrium value (0.034 mol/L) by 60 minutes and fully stabilizes by 80 minutes. This equilibrium represents the balance between CO_2 gas dissolution and its conversion to bicarbonate under mildly acidic conditions.

5.3.2.2 pH-Driven Speciation and Reaction Mechanisms

The interdependence between solution pH and carbonate speciation is central to understanding the changing reaction mechanisms during carbonation. Figure 5.5 provides a comprehensive visualization of this relationship, simultaneously tracking pH and carbonate species concentrations.

The pH evolution shown in Figure 5.5 reveals a continuous decrease from approximately 11.8 to 6.0 over the 140-minute carbonation period. This decline is not uniform but features distinct phases that correlate precisely with changes in carbonate speciation. During the early phase (0-30 minutes), the solution maintains a strongly alkaline character (pH > 9.5) due to OH^- release from dissolving $Ca(OH)_2$. This high-pH environment temporarily favors CO_3^{2-} formation (reaction 3.25), reaching its maximum concentration at around 20 minutes when the pH is approximately 10. The CO_3^{2-} peak coincides with the most rapid phase of $CaCO_3$ precipitation, explaining the accelerated carbonation observed experimentally during this period.

As the pH continues to decrease through the middle phase (30-70 minutes), crossing the critical threshold of 8.3 (the second dissociation constant of carbonic acid), the chemical equilibrium shifts dramatically toward HCO_3^- dominance. The HCO_3^- concentration rises sharply in this phase, reaching half its equilibrium value at approximately 50 minutes when the pH is 7.0. This inflection point represents a critical transition in the carbonation mechanism, from precipitation driven by CO_3^{2-} availability to a system increasingly limited by calcium release from CSH phases.

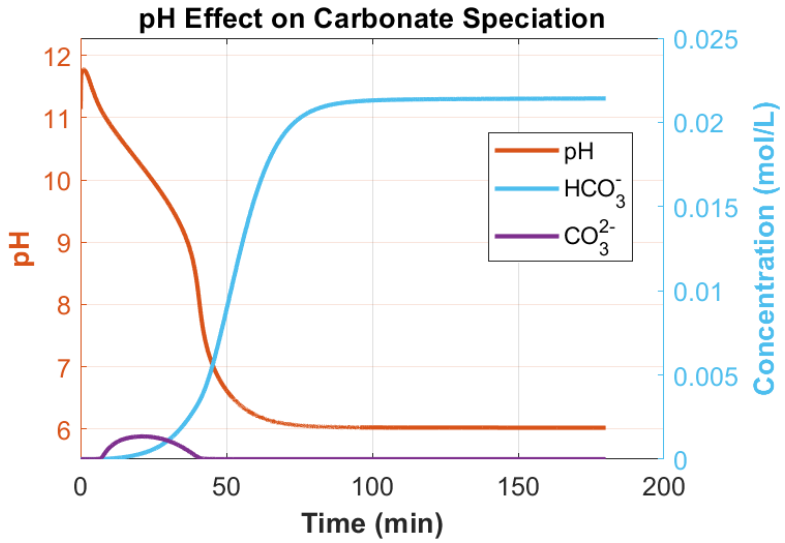

Figure 5.5: *Relationship between pH and carbonate speciation during carbonation. The pH (red line, left axis) decreases from approximately 11.8 to 6.0, while HCO_3^- and CO_3^{2-} concentrations (right axis) respond to these pH changes.*

The system approaches equilibrium in the final phase (70-180 minutes), with pH stabilizing around 6.0 and HCO_3^- reaching its maximum concentration of 0.022 mol/L. At this equilibrium point, CO_3^{2-} concentration becomes negligible (<0.0001 mol/L), and further carbonation proceeds very slowly, primarily limited by the diffusion of calcium from the interior of mineral particles and the decreasing driving force for precipitation as the system approaches thermodynamic equilibrium.

The equilibrium state is reached at different times for different parameters: dissolved CO_2 reaches equilibrium earliest (approximately 80 minutes), followed by carbonate speciation (90 minutes), with ionic strength requiring the longest time (100 minutes). This sequencing provides valuable insights into the rate-limiting processes during different carbonation phases and offers guidance for optimizing process duration in practical applications.

5.3.2.3 Ionic Strength Dynamics and activity effect

The ionic strength evolution throughout carbonation reveals intricate solution chemistry dynamics that significantly influence reaction pathways and precipitation mechanisms. Figure

5.6 shows the temporal pattern of ionic strength during the 180-minute carbonation process, alongside the corresponding effects on anion and cation activity coefficients in Figure 5.7.

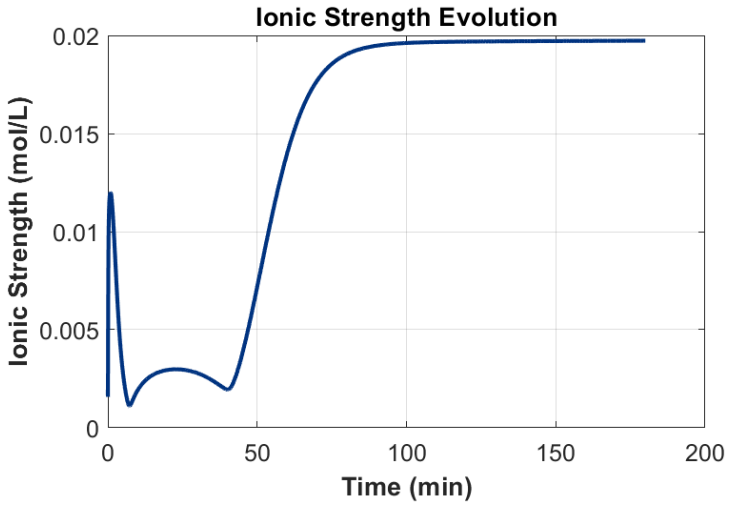

Figure 5.6: *Evolution of ionic strength during carbonation. Note the distinctive pattern with an initial spike followed by a sharp decrease, then a gradual increase to equilibrium.*

The ionic strength profile exhibits a remarkable three-phase pattern that provides valuable insights into the changing chemical environment:

- **Initial Spike (0-5 minutes)**: A sharp increase to approximately 0.012 mol/lit occurs immediately after introducing CPP into the aqueous environment. This spike reflects the rapid dissolution of $Ca(OH)_2$ and release of Ca^{2+} and OH^- ions into solution, creating a highly alkaline environment.
- **Depression Phase (5-40 minutes)**: Following the initial spike, ionic strength decreases dramatically to approximately 0.001-0.002 mol/lit, reaching its minimum around 10 minutes. This decline corresponds to the partial dominancy of precipitation of $CaCO_3$ to CH dissolution, which consumes dissolved Ca^{2+} and CO_3^{2-} ions, effectively removing them from solution.
- **Recovery and Equilibrium Phase (40-120 minutes)**: The ionic strength increases gradually during this phase, eventually stabilizing at approximately 0.02 mol/lit by 100 minutes. This increase is primarily driven by the accumulation of H^+, HCO_3^-, and dissolved CO_2 as the solution pH decreases and the system shifts toward bicarbonate dominance.

The system reaches ionic equilibrium around 100 minutes, significantly later than the apparent stabilization of carbonate species (80-90 minutes). This delay indicates that subtle ionic adjustments continue even after the major speciation transitions have occurred, highlighting the importance of extended reaction times to achieve true thermodynamic equilibrium.

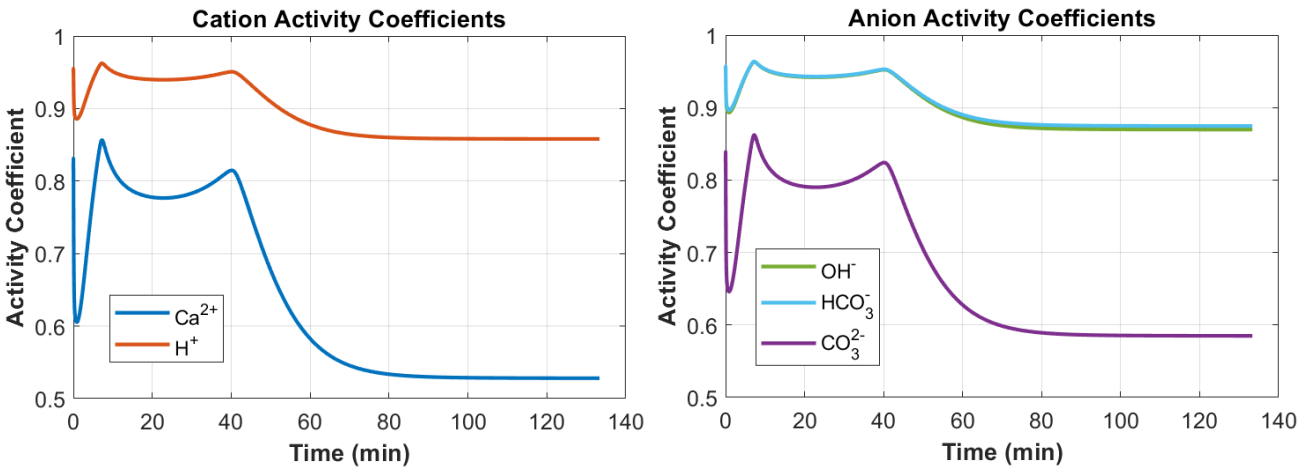

Figure 5.7: *Temporal evolution of activity coefficients for key anions (Right) and cations (Left) during carbonation. Activity coefficients reflect the deviation from ideal behavior due to ionic interactions in solution.*

5.3.3 Reaction kinetic and transport phenomena

The identified model provides valuable insights into the underlying reaction kinetics and transport mechanisms controlling the carbonation process. By examining the temporal evolution of reaction rates and diffusion parameters, we can understand how the system transitions between different rate-limiting steps and approaches equilibrium.

5.3.3.1 Contribution of Different $CaCO_3$ Formation Pathways

Figure 5.8 illustrates the relative contributions of $Ca(OH)_2$ carbonation and CSH carbonation to the total $CaCO_3$ formation over time. During the initial phase (0-900 seconds), $Ca(OH)_2$ carbonation dominates, accounting for more than 80% of the $CaCO_3$ formed.

As $Ca(OH)_2$ becomes depleted (15-30 minutes), CSH carbonation becomes increasingly important, contributing approximately 40% of the $CaCO_3$ formed during this intermediate phase. In the final phase (30-180 minutes), with $Ca(OH)_2$ completely consumed, CSH carbonation becomes the sole source of calcium for $CaCO_3$ formation.

By the end of the simulation timespan, approximately 60% of the total $CaCO_3$ has formed through $Ca(OH)_2$ carbonation and 40% through CSH carbonation. This distribution highlights the significance of both pathways in the overall carbonation process.

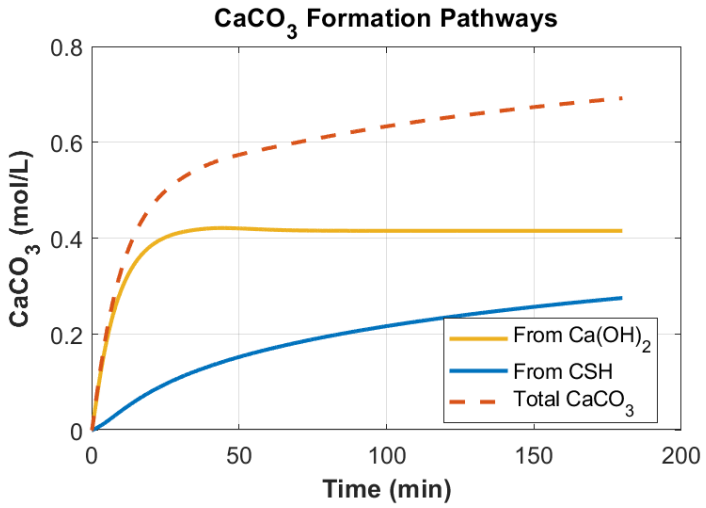

Figure 5.8 *The figure shows the contribution of different pathways to $CaCO_3$ formation.*

5.3.3.2 Carbonation Reaction Pathways and Rates

The evolution of reaction rates for key carbonation processes reveals the dynamic competition between parallel reaction pathways and their shifting dominance throughout the carbonation timeline. Figures 5.9 and 5.10 illustrate the temporal profiles of reaction rates for carbonate speciation reactions and CO_2 dissolution pathways, respectively.

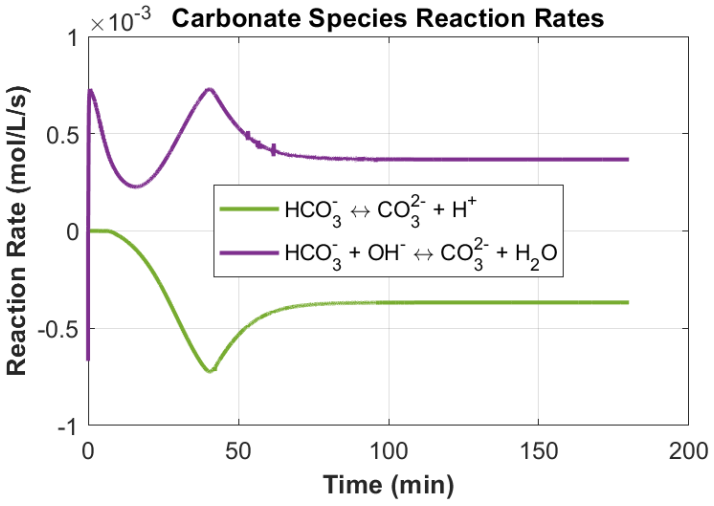

Figure 5.9: *Temporal evolution of reaction rates for carbonate speciation reactions. Positive values indicate the forward reaction dominates, while negative values indicate the reverse reaction dominates.*

The carbonate speciation reactions exhibit complex, non-monotonic behavior that reflects the changing chemical environment. The reaction $HCO_3^- + OH^- \leftrightarrow CO_3^{2-} + H_2O$ (purple line) shows a distinctive bimodal pattern with two separate rate maxima. The initial peak occurs within the first few minutes as the highly alkaline environment promotes rapid conversion of bicarbonate to carbonate. This is followed by a minimum rate at around 15 minutes, then a

second wider maximum peak at approximately 40 minutes as the pH transitions through the optimal range for this reaction. As the system approaches equilibrium after 80 minutes, this reaction rate stabilizes at a small positive value (approximately 4×10^{-4} mol/L/s), indicating that the forward reaction continues to slightly dominate.

Conversely, the reaction $HCO_3^- \leftrightarrow CO_3^{2-} + H^+$ (green line) starts near zero and becomes increasingly negative, reaching its minimum rate around 40 minutes before gradually returning toward equilibrium. The negative rate indicates that the reverse reaction is favored, consistent with the decreasing pH environment that promotes the association of H^+ with CO_3^{2-} to form HCO_3^-. This reaction also stabilizes at a non-zero value (approximately -4×10^{-4} mol/L/s) in the late stages, nearly perfectly balancing the $HCO_3^- + OH^-$ reaction.

The persistence of non-zero reaction rates at equilibrium (after 100 minutes) is a critically important result that explains the continued slow carbonation observed experimentally in long-term studies. This phenomenon represents a dynamic equilibrium where forward and backward reactions continue to occur at balanced rates, allowing for gradual structural reorganization and crystal growth of calcium carbonate precipitates without significant net changes in bulk concentration.

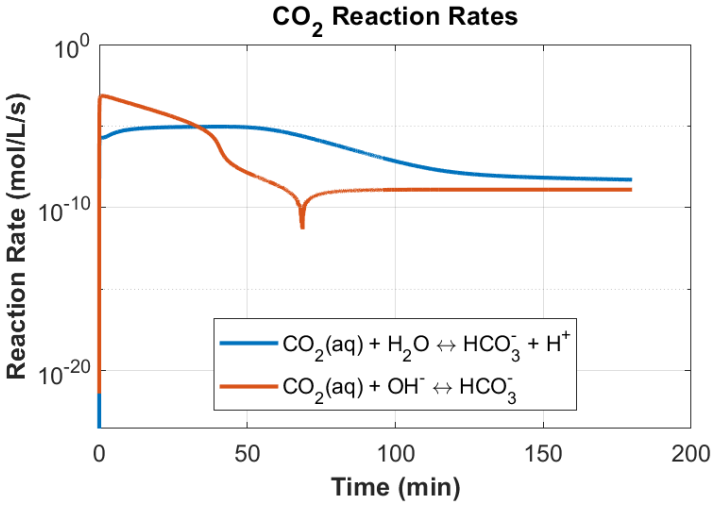

Figure 5.10: *Temporal evolution of reaction rates for CO_2 dissolution and conversion pathways in logarithm scale. Note the dominant role of the OH^--mediated pathway in early stages.*

The CO_2 dissolution and conversion pathways (Figure 5.10) show markedly different kinetics. The hydroxide-mediated pathway ($CO_2 + OH^- \leftrightarrow HCO_3^-$, orange line) dominates in the early stages with a very high initial rate of approximately 7.2×10^{-4} mol/L/s that decreases exponentially as OH^- is consumed. This reaction is the primary route for CO_2 uptake during the first 40 minutes of carbonation when the solution is still alkaline. In contrast, the direct hydration pathway ($CO_2(aq) + H_2O \leftrightarrow HCO_3^- + H^+$, blue line) proceeds at a much lower rate throughout the process, though it becomes relatively more important in later stages as OH^- concentration decreases.

The relative contributions of these pathways explain the observed pH dependency of carbonation rates. In the early, high-pH phase, the hydroxide-mediated pathway enables rapid CO_2 uptake. As the pH decreases, this pathway becomes less effective, causing overall carbonation rates to decline despite the continuing availability of calcium from CSH phases.

5.3.3.3 Diffusion Limitations and Transport Phenomena

As the carbonation reaction progresses, transport phenomena increasingly limit the overall process rate. Figures 5.11 and 5.12 illustrate two critical diffusion-related parameters: the $CaCO_3$ layer diffusion resistance factor (3.10) and the time-dependent diffusion coefficient.

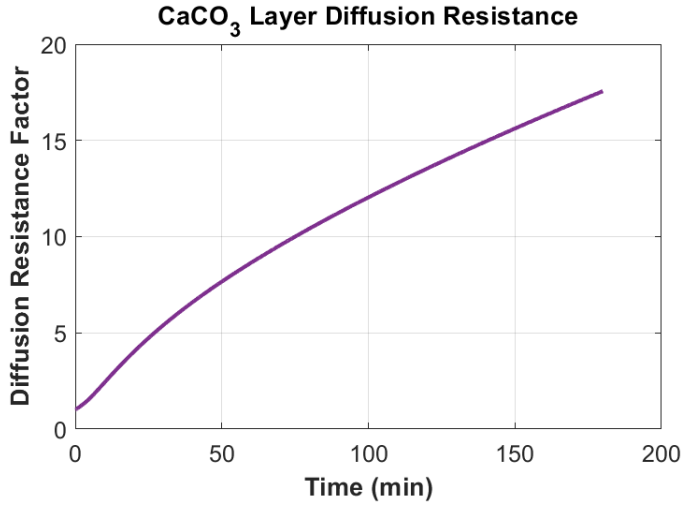

Figure 5.11: *Evolution of $CaCO_3$ layer diffusion resistance factor throughout carbonation. The increasing resistance reflects the growing barrier to ion transport caused by precipitated calcium carbonate.*

The diffusion resistance factor (Figure 5.11) increases continuously throughout the carbonation process, starting at approximately 1.0 and reaching 17.5 by 180 minutes. This resistance factor represents the increasing barrier to ion transport created by the progressive accumulation of $CaCO_3$ precipitates on and within cement particles. The non-linear growth pattern—initially rapid but gradually moderating—reflects the self-limiting nature of the carbonation process, where early precipitates create barriers that slow subsequent precipitation.

The diffusion resistance increases most rapidly during the first 60 minutes, coinciding with the period of most active $CaCO_3$ formation. The resistance factor reaches approximately 7.0 by 60 minutes, already imposing significant limitations on ion transport. The continued increase beyond this point explains why carbonation becomes increasingly diffusion-limited in later stages, even when thermodynamically favorable conditions for further reaction persist.

Complementary to the increasing diffusion resistance, the effective diffusion coefficient (Figure 5.12) shows a gradual linear decrease from 2.417×10^{-4} to 2.387×10^{-4} m²/s over 180 minutes. This relatively modest decline (less than 1%) might appear insignificant in isolation, but when

combined with the increasing diffusion path length due to product layer growth, it creates a substantial compound effect on diffusion limitations.

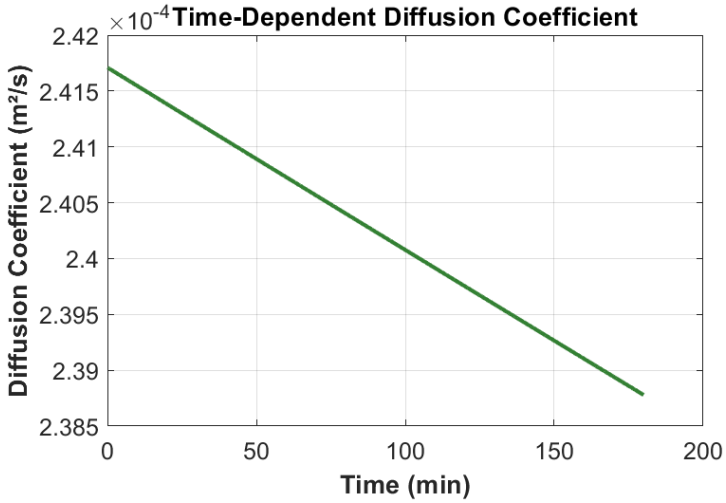

Figure 5.12: *Evolution of the effective diffusion coefficient over time. The gradual decrease reflects the densification of the product layer structure.*

5.3.4 Integrated Kinetic Regime Analysis

The combined analysis of reaction rates and diffusion parameters reveals three distinct kinetic regimes during the carbonation process:

1. **Reaction-Limited Regime (0-20 minutes)**: Characterized by high OH^--mediated CO_2 conversion rates, low diffusion resistance, and rapid $Ca(OH)_2$ dissolution. During this phase, the overall process rate is primarily controlled by chemical reaction kinetics rather than transport phenomena.
2. **Transition Regime (20-60 minutes)**: Marked by declining reaction rates, increasing diffusion resistance (reaching around 7.0), and the depletion of readily available $Ca(OH)_2$. Both reaction kinetics and diffusion limitations significantly influence the overall carbonation rate during this period.
3. **Diffusion-Limited Regime (60-180 minutes)**: Distinguished by relatively stable reaction rates, high and increasing diffusion resistance (7.0-17.5), and the dominance of CSH as the calcium source. In this regime, the carbonation rate is primarily controlled by the diffusion of calcium ions through the growing product layer.

The persistence of non-zero reaction rates at apparent equilibrium (after 100 minutes) is particularly significant for long-term carbonation behavior. Even when bulk concentrations appear stable, the dynamic equilibrium between forward and reverse reactions facilitates continued structural transformations in the solid phases, including crystallization, crystal growth, and densification. This explains the observed improvements in mechanical properties

that continue long after the apparent completion of carbonation reactions in cement-based materials.

This integrated kinetic analysis provides a mechanistic foundation for optimizing carbonation processes in practical applications, suggesting that strategies to overcome diffusion limitations would be particularly effective for enhancing late-stage carbonation efficiency. Such strategies might include periodic mechanical agitation to disrupt product layers, the use of chelating agents to enhance calcium mobility, or the application of pulsed pressure to facilitate CO_2 transport through densified layers.

5.4 Analysis of Parameter Estimation Interpretation

5.4.1 Parameter Confidence Intervals Analysis

Figure 5.13 shows dramatic variations in parameter identifiability, displayed on a logarithmic scale with 95% confidence intervals:

The most striking observation is the extreme uncertainty associated with several parameters. Parameter k_1 exhibits an extraordinary confidence interval of ±5554963%, rendering it effectively unidentifiable from the available experimental data. Similarly, parameter α shows a massive uncertainty of ±1351244581%. These extreme values indicate fundamental limitations in constraining these parameters from the current experimental dataset.

In contrast, a few parameters demonstrate relatively tight confidence bounds. The k_4 parameter shows a remarkably precise estimate (±0%), suggesting it is highly constrained by the experimental data. Similarly, k_{CSH} exhibits good identifiability (±2%), indicating reliable estimation. The precipitation rate constant k_p shows asymmetrically wide confidence intervals (±32902%), suggesting potential structural issues in how this parameter influences model outputs.

The diffusion-related parameters (D_0, α, α_{diff}) all display substantial uncertainty (±694753%, ±1351244581%, and ±227% respectively), reflecting challenges in determining transport phenomena from bulk concentration measurements. The volumetric mass transfer coefficient kLa shows considerable uncertainty (±8406%), indicating difficulties in distinguishing gas-liquid mass transfer effects from other processes.

5.4.2 Parameter Sensitivity analysis

Figure 5.14 reveals distinct parameter sensitivity patterns across three key model outputs (pH, $Ca(OH)_2$, $CaCO_3$) during the 60-minute carbonation process:

For pH sensitivity (top panel), the model demonstrates a complex initial response where multiple parameters show significant influence during the first few minutes. The k_{CSH} parameter

(yellow line) maintains consistently high positive sensitivity throughout the process, indicating that changes in CSH reaction rate have a sustained impact on pH evolution. In contrast, k_O (red line) shows a distinctive negative spike followed by recovery within the first 5 minutes, suggesting a transient but powerful influence during the initial reaction phase. Most other parameters display relatively minor sensitivities for pH after the initial phase.

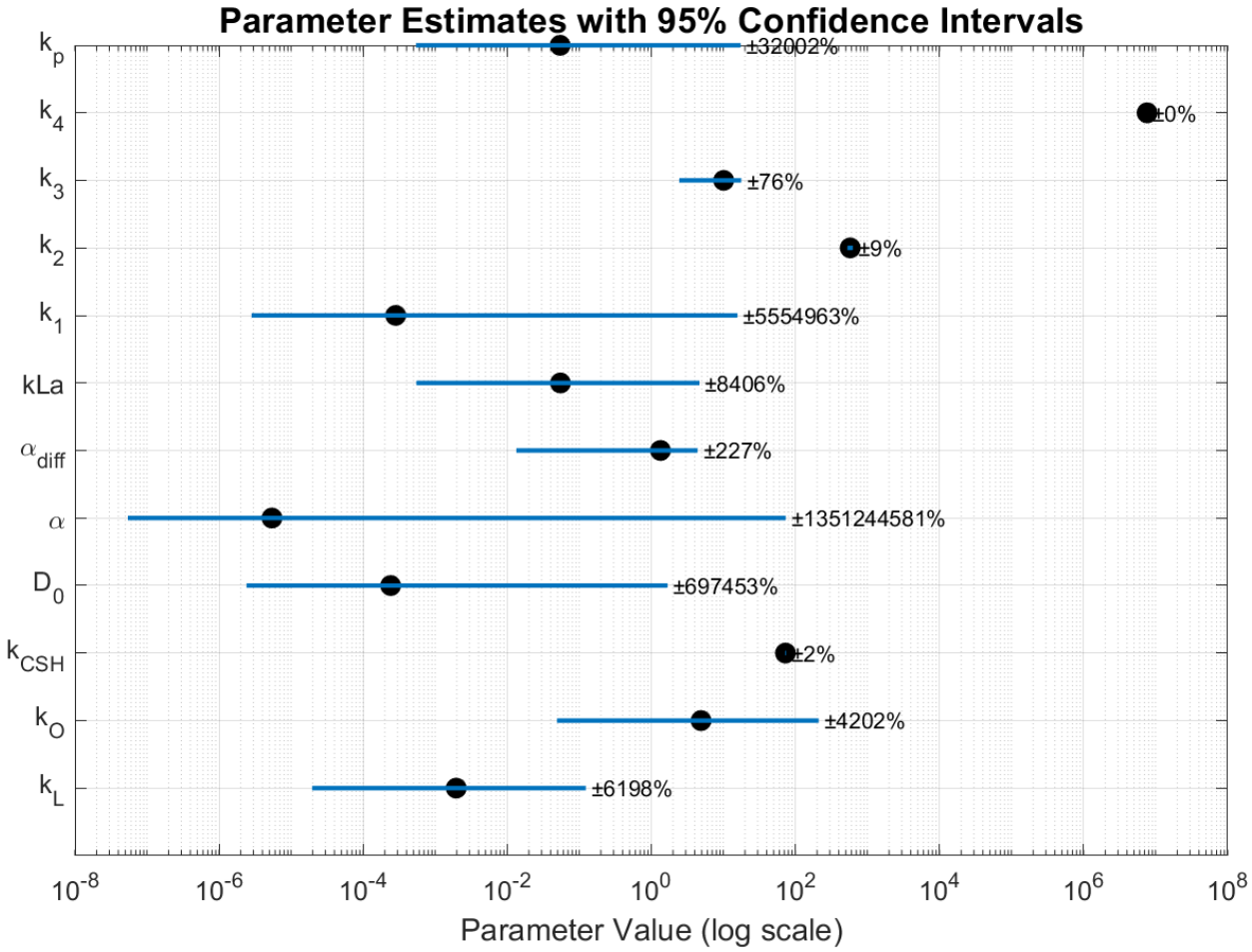

Figure 5.13: *Parameter estimates with 95% confidence intervals, arranged by parameter type. The relative uncertainty percentages indicate the reliability of each parameter estimate.*

For $Ca(OH)_2$ evolution (middle panel), k_L (blue line) exhibits overwhelmingly dominant sensitivity that grows increasingly negative over time. This pronounced influence indicates that the $Ca(OH)_2$ dissolution rate constant is the primary controlling parameter for $Ca(OH)_2$ concentration throughout the entire carbonation process. The substantial magnitude difference between $k_L$and all other parameters (which appear nearly flat on this scale) demonstrates that $Ca(OH)_2$ prediction is essentially determined by this single parameter.

For $CaCO_3$ formation (bottom panel), the sensitivity distribution is more balanced. The k4 parameter (purple line) shows the highest initial sensitivity with a pronounced peak in the first few minutes, followed by gradual decline. Meanwhile, k_{CSH} (yellow line) and k_3 (also yellow

line) demonstrate increasing importance over time, reflecting those different parameters control $CaCO_3$ formation at different stages of the process. This suggests a mechanistic shift from initial reaction control to diffusion or transport control in later stages.

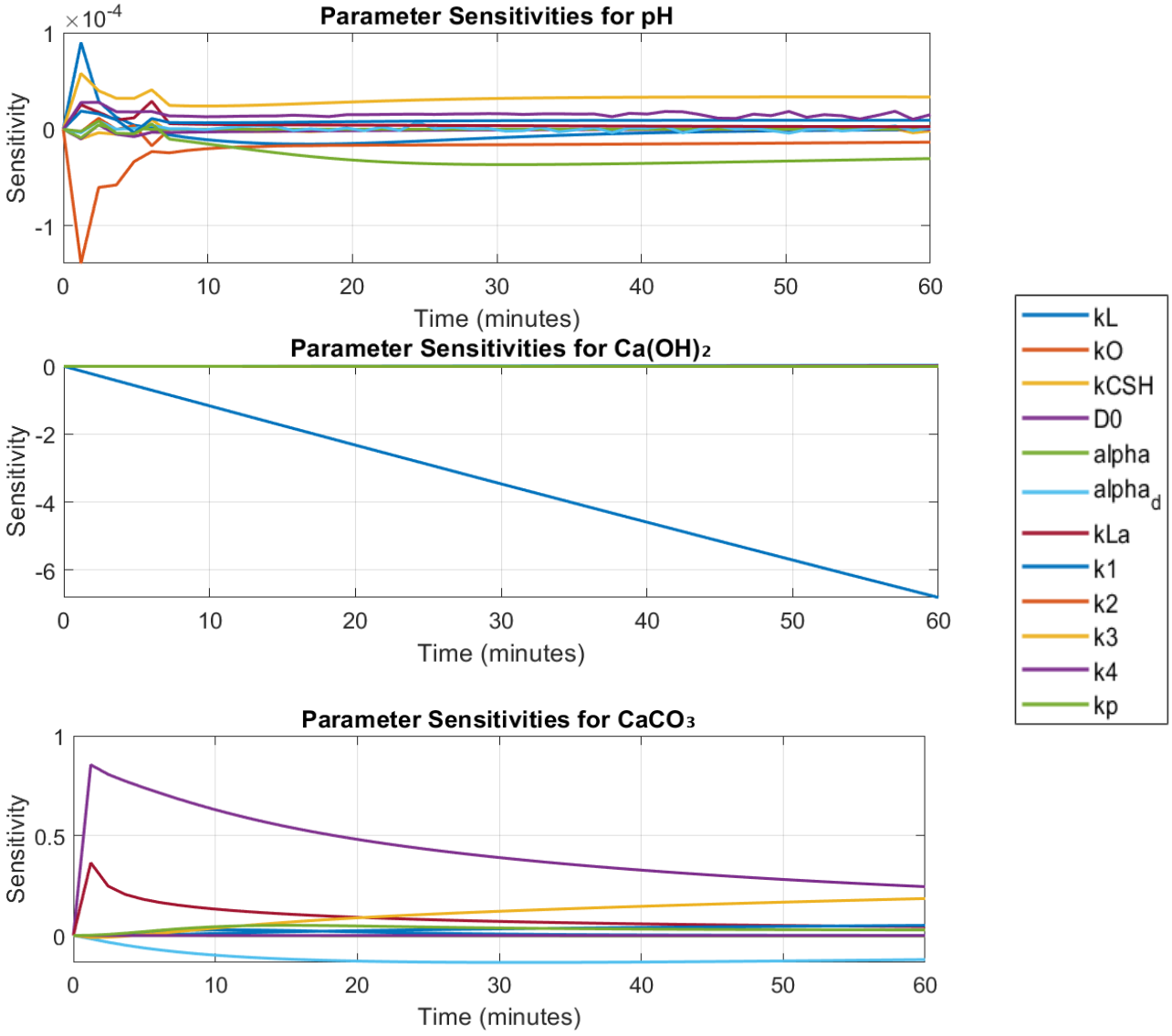

Figure 5.14 *Sensitivity of each parameter during the carbonation for pH, $Ca(OH)_2$, and $CaCO_3$.*

5.4.3 Parameter Correlation Analysis

Figure 5.15 reveals complex interdependencies among model parameters through correlation coefficients ranging from -1 (strong negative correlation, dark blue) to +1 (strong positive correlation, dark red):

The strongest positive correlation (0.91) exists between D_0 and k_3, indicating that effects of increasing the initial diffusion coefficient can be largely counterbalanced by increasing the

bicarbonate formation rate constant. This compensation mechanism explains why both parameters have wide confidence intervals despite their importance to model predictions.

Several strong negative correlations are equally informative. The pronounced negative correlation (-0.87) between k_3 and $k_4$demonstrates that increased bicarbonate formation can be offset by decreased carbonate formation, resulting in similar net carbonation predictions. Similarly, the negative correlation (-0.79) between D_0 and k_4 reflects how diffusion limitations can be compensated for by reaction rate adjustments.

The dissolution rate constant $k_L$shows moderate negative correlation (-0.72) with k_1, indicating interplay between calcium dissolution and carbon dioxide hydration kinetics. The CSH reaction rate k_{CSH}exhibits significant correlations with multiple parameters, most notably a positive correlation (0.76) with kLa and negative correlation (-0.74) with D_0, reflecting complex interactions between reaction and transport mechanisms.

These extensive parameter correlations explain the wide confidence intervals observed by many individual parameters. The correlation structure reveals that while individual parameters may be poorly identifiable, certain parameter combinations are well-constrained by the experimental data. This suggests that model simplification could be achieved by combining or fixing highly correlated parameters without significant loss of predictive power.

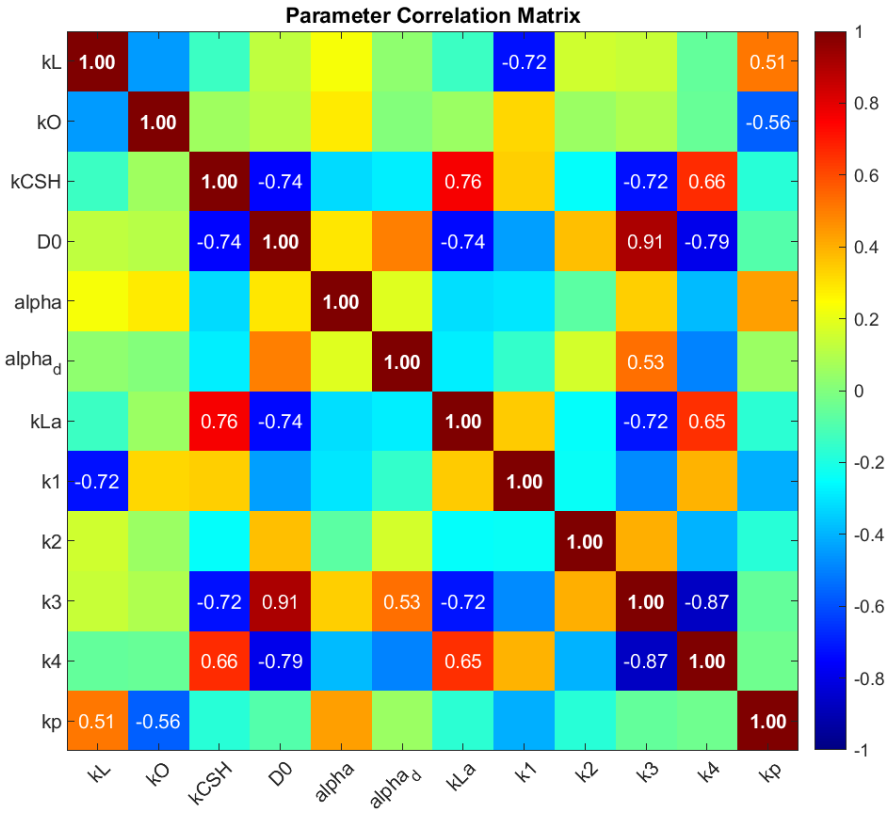

Figure 5.15: *Parameter correlation matrix showing interdependencies between model parameters. Red indicates a strong positive correlation, blue indicates a strong negative correlation, and lighter colors represent weaker correlations*

5.4.4 Implications for Model Application and Refinement

Comprehensive sensitivity provides clear guidance for future model development and application. The extreme dominance of the $Ca(OH)_2$ dissolution rate constant (k_L) highlights the critical importance of accurately characterizing this process through targeted experiments. Similarly, the high sensitivity of CO_2 reaction parameters (k_1 and k_3) underscores the need for precise characterization of carbon dioxide dissolution and reaction pathways.

The temporal evolution of parameter importance suggests that experimental designs should capture multiple phases of the carbonation process to adequately constrain different parameters. Early-phase measurements (0-10 minutes) are essential for constraining mass transfer parameters (k_La and k_3), while middle-phase measurements (10-30 minutes) are critical for $Ca(OH)_2$ dissolution kinetics (k_L). Late-phase measurements (beyond 30 minutes) become increasingly important for characterizing CO_2 reaction pathways (k_1) and CSH reactivity (k_{CSH}).

The widespread parameter correlations and wide confidence intervals suggest potential for model simplification without significant loss of predictive capability. Parameter sets with strong correlations could be reduced to fewer effective parameters, potentially improving identifiability while maintaining predictive power. For example, the strongly correlated pair of k_O and k_P might be represented by a single composite parameter.

When using the model for predictive purposes, the substantial parameter uncertainties necessitate careful consideration of prediction confidence bounds, particularly when extrapolating beyond calibration conditions. Ensemble approaches that sample from the parameter probability distributions while respecting correlation structures provide more reliable uncertainty estimates than single-parameter perturbation methods.

For future experimental work, measurements that can directly constrain highly sensitive but uncertain parameters should be prioritized. Specifically, techniques that can independently measure $Ca(OH)_2$ dissolution rates, CO_2 dissolution kinetics, and calcium transport would be particularly valuable for improving parameter identifiability and reducing prediction uncertainties.

5.5 Summary of Findings

The results presented in this chapter provide comprehensive insights into the carbonation process in cementitious materials and the performance of the developed model. Key findings include:

1. **Optimization Method Comparison**: While hybrid GA-DE methods achieved slightly better statistical fits to the experimental data, the GA-optimized model provided more physically consistent predictions without unrealistic oscillations, making it the preferred model for understanding the carbonation process.

2. **Reaction Phases and Mechanisms**: The carbonation process exhibits distinct phases characterized by different rate-limiting steps: initial CO_2 dissolution-limited phase, intermediate $Ca(OH)_2$ dissolution-limited phase, and final diffusion-limited phase. The pH evolution during carbonation reflects transitions between different buffering systems.
3. **$CaCO_3$ Formation Pathways**: $CaCO_3$ forms through two main pathways: direct carbonation of $Ca(OH)_2$ (dominant in early stages) and carbonation of CSH (increasingly important in later stages). By the end of the simulation period, approximately 65% of total $CaCO_3$ forms through $Ca(OH)_2$ carbonation and 35% through CSH carbonation.
4. **Process Optimization Insights**: Enhancing CO_2 dissolution (through increased interfacial area or mixing intensity), maintaining moderate CO_2 pressures (around 1.0 bar), reducing particle size, and controlling pH in the range of 9-10 are identified as potential strategies for optimizing carbonation efficiency.

The findings validate the proposed reaction mechanisms and transport processes incorporated in the model and demonstrate its utility for predicting carbonation behavior under various conditions. The model provides a valuable tool for understanding the complex physicochemical processes involved in carbonation and offers guidance for optimizing carbonation processes for CO_2 sequestration in cement-based materials.

5.6 Recommended Future Work

Based on the analysis presented in this chapter, several opportunities for future model refinement and application are identified:

1. **Enhanced CSH Representation**: Develop a more detailed representation of CSH phases with varying Ca/Si ratios and reactivity classes to better capture the heterogeneous nature of cementitious materials.
2. **Temperature Dependency**: Extend the model to incorporate temperature effects on reaction kinetics and equilibrium constants, enabling simulation of carbonation under varying temperature conditions.
3. **Particle Size Distribution**: Implement a distributed parameter approach to account for the effect of particle size distribution on dissolution and diffusion processes.
4. **Advanced Parameter Estimation**: Apply Bayesian estimation methods to better quantify parameter uncertainty and correlations, potentially resolving some of the identifiability issues identified in this study.
5. **Additional Experimental Data**: Design experiments specifically to improve the identifiability of poorly determined parameters, such as those related to carbonate speciation reactions.

6. **Model Simplification**: Consider simplifying the model by fixing or combining poorly identifiable parameters based on the identifiability analysis, potentially improving the robustness of parameter estimation.

These recommendations provide a roadmap for the continued development and application of the mineral carbonation model, with the goal of advancing sustainable practices in the cement and concrete industry through enhanced CO_2 utilization and sequestration.

Conclusions

This thesis has successfully developed and validated a comprehensive mechanistic model for the wet carbonation of cementitious materials, providing valuable insights into the complex physical and chemical processes involved in CO_2 sequestration. The ionic modeling approach demonstrates significant advantages over traditional models by explicitly accounting for solution chemistry, speciation dynamics, and the interplay between reaction and transport phenomena. Through rigorous parameter estimation and sensitivity analysis, the research identified three distinct kinetic regimes during carbonation: an initial reaction-limited phase, a transition phase, and a final diffusion-limited phase.

The model reveals that calcium hydroxide carbonation dominates early stages, contributing approximately 60% of total calcium carbonate formation, while calcium silicate hydrate carbonation becomes increasingly significant in later stages, accounting for the remaining 40%. The pH evolution during carbonation reflects transitions between different buffering systems, with the shift from carbonate to bicarbonate dominance marking a critical transition in reaction mechanisms. Diffusion limitations, characterized by an increasing resistance factor and decreasing effective diffusion coefficient, ultimately control the final stage of carbonation.

These findings establish a foundation for optimizing carbonation processes in supplementary cementitious materials. By manipulating factors such as particle size, solution chemistry, and process conditions, carbonation efficiency can be enhanced to maximize CO_2 sequestration. Future work should focus on refining the representation of calcium silicate hydrate phases, incorporating temperature effects, and accounting for particle size distribution to further improve model accuracy and applicability.

The research presented in this thesis contributes significantly to understanding mineral carbonation mechanisms and provides a valuable tool for designing more efficient carbon capture and utilization strategies in the cement industry. By enabling the development of optimized carbonation processes for supplementary cementitious materials, this work supports broader efforts to reduce the carbon footprint of cement production and construction, advancing sustainable practices in this critical industry.

References

Ajayi, T., Gomes, J. S., & Bera, A. (2019). A review of CO_2 storage in geological formations emphasizing modeling, monitoring and capacity estimation approaches. *Petroleum Science*, **16**, 1028-1063. https://doi.org/10.1007/s12182-019-0340-8

Antunes, M., Santos, R. L., Pereira, J., Rocha, P., Horta, R. B., & Colaço, R. (2022). Alternative clinker technologies for reducing carbon emissions in cement industry: A critical review. *Materials*, **15**, 209. https://doi.org/10.3390/ma15010209

Barbhuiya, S., Kanavaris, F., Das, B. B., & Idrees, M. (2024). Decarbonising cement and concrete production: Strategies, challenges and pathways for sustainable development. *Journal of Building Engineering*, **86**, 108861. https://doi.org/10.1016/j.jobe.2024.108861

Chakraborty, S., & Jo, B. W. (2018). Aqueous-based carbon dioxide sequestration. *Carbon Dioxide Sequestration in Cementitious Construction Materials*, 39-64. https://doi.org/10.1016/B978-0-08-102444-7.00003-4

Diamantonis, N., Marinos, I., Katsiotis, M. S., Sakellariou, A., Papathanasiou, A., Kaloidas, V., & Katsioti, M. (2010). Investigations about the influence of fine additives on the viscosity of cement paste for self-compacting concrete. *Construction and Building Materials*, **24**, 1518-1522. https://doi.org/10.1016/j.conbuildmat.2010.02.005

Ghiat, I., & Al-Ansari, T. (2021). A review of carbon capture and utilisation as a CO_2 abatement opportunity within the EWF nexus. *Journal of CO_2 Utilization*, **45**, 101432. https://doi.org/10.1016/j.jcou.2020.101432

Gómez-Díaz, D., Navaza, J. M., & Sanjurjo, B. (2006). Analysis of mass transfer in the precipitation process of calcium carbonate using a gas/liquid reaction. *Chemical Engineering Journal*, **116**, 203-209. https://doi.org/10.1016/j.cej.2005.12.004

Han, S. J., Yoo, M., Kim, D. W., & Wee, J. H. (2011a). Carbon dioxide capture using calcium hydroxide aqueous solution as the absorbent. *Energy and Fuels*, **25**, 3825-3834. https://doi.org/10.1021/ef200415p

Kabir, M., Habiba, U. E., Khan, W., Shah, A., Rahim, S., Rios-Escalante, P. R. D. los, Farooqi, Z. U. R., & Ali, L. (2023). Climate change due to increasing concentration of carbon dioxide and its impacts on environment in 21st century; a mini review. *Journal of King Saud University - Science*, **35**, 102693. https://doi.org/10.1016/j.jksus.2023.102693

Kaufmann, G., & Dreybrodt, W. (2007). Calcite dissolution kinetics in the system $CaCO_3$-H_2O-CO_2 at high undersaturation. *Geochimica et Cosmochimica Acta*, **71**, 1398-1410. https://doi.org/10.1016/j.gca.2006.10.024

Kucka, L., Kenig, E. Y., & Górak, A. (2002). Kinetics of the gas-liquid reaction between carbon dioxide and hydroxide ions. *Industrial and Engineering Chemistry Research*, **41**, 5952-5957. https://doi.org/10.1021/ie020452f

Laribi, S., Dubois, L., De Weireld, G., & Thomas, D. (2019). Study of the post-combustion CO_2 capture process by absorption-regeneration using amine solvents applied to cement plant flue gases with high CO2 contents. *International Journal of Greenhouse Gas Control*, **90**, 102799 https://doi.org/10.1016/j.ijggc.2019.102799

Li, Z. (2020). General rate equation theory for gas–solid reaction kinetics and its application to CaO carbonation. *Chemical Engineering Science*, **227**, 115902. https://doi.org/10.1016/j.ces.2020.115902

Meijssen, M., Gasós, A., & Mazzotti, M. (2023). Batchwise Leaching of Calcium from Demolition Concrete Fines in an Aqueous Ammonium Nitrate Solution: Part 2 Modeling. *Industrial and Engineering Chemistry Research*, **62**, 2618-2628. https://doi.org/10.1021/acs.iecr.2c04118

Meijssen, M., & Mazzotti, M. (2022). Batchwise Leaching of Calcium from Demolished Concrete Fines in an Aqueous Ammonium Nitrate Solution: Part 1 Experimental Study. *Industrial and Engineering Chemistry Research*, **61**, 15316-15325. https://doi.org/10.1021/acs.iecr.2c02007

Miao, E., Du, Y., Wang, H., Zheng, X., Zhang, X., Xiong, Z., Zhao, Y., & Zhang, J. (2023). Evaluation of the kinetics of direct aqueous mineral carbonation of wood combustion ash using modified shrinking core models. *Environmental Science and Pollution Research*, **30**, 34009-34021. https://doi.org/10.1007/s11356-022-24603-3

Miao, E., Du, Y., Zheng, X., Zhang, X., Xiong, Z., Zhao, Y., & Zhang, J. (2023). CO_2 sequestration by direct mineral carbonation of municipal solid waste incinerator fly ash in ammonium salt solution: Performance evaluation and reaction kinetics. *Separation and Purification Technology*, **309**, 123103. https://doi.org/10.1016/j.seppur.2023.123103

Miao, E., Zheng, X., Xiong, Z., Zhao, Y., & Zhang, J. (2022). Kinetic modeling of direct aqueous mineral carbonation using carbide slag in a stirred tank reactor. *Fuel*, **315**, 122837. https://doi.org/10.1016/j.fuel.2021.122837

Olajire, A. A. (2013). A review of mineral carbonation technology in sequestration of CO_2. *Journal of Petroleum Science and Engineering*, **109,** 364-392. https://doi.org/10.1016/j.petrol.2013.03.013

Pamenter, S., & Myers, R. J. (2021). Decarbonizing the cementitious materials cycle: A whole-systems review of measures to decarbonize the cement supply chain in the UK and European contexts. *Journal of Industrial Ecology*, **25**, 359-376. https://doi.org/10.1111/jiec.13105

Park, S., Lee, S., Lee, Y., Lee, Y., & Seo, Y. (2013). Hydrate-based pre-combustion capture of carbon dioxide in the presence of a thermodynamic promoter and porous silica gels. *International Journal of Greenhouse Gas Control*, **14**, 193-199. https://doi.org/10.1016/j.ijggc.2013.01.026

Pohorecki, R., & Moniuk, W. (1988). Kinetics of reaction between carbon dioxide and hydroxyl ions in aqueous electrolyte solutions. *Chemical Engineering Science*, **43**, 1677-1684. https://doi.org/10.1016/0009-2509(88)85159-5

Preston, B. L., & Jones, R. N. (2006). Climate Change Impacts on Australia and the Benefits of Early Action to Reduce Global Greenhouse Gas Emissions. *CSIRO Marine and Atmospheric Research.*

Saltelli, A., Tarantola, S., Campolongo, F., & Ratto, M. (2002). *Sensitivity Analysis in Practice*. Wiley, Hoboken (U.S.A)

Samson, É., Lemaire, G., Marchand, J., & Beaudoin, J.J. (1999). Modeling chemical activity effects in strong ionic solutions. *Computational Materials Science*, **15**, 285-294. https://doi.org/10.1016/S0927-0256(99)00017-8

Sanna, A., Uibu, M., Caramanna, G., Kuusik, R., & Maroto-Valer, M. M. (2014). A review of mineral carbonation technologies to sequester CO_2. *Chemical Society Reviews*, **43**, 8049-8080. https://doi.org/10.1039/c4cs00035h

Sari, D., & Pasamehmetoglu, A. G. (2005). The effects of gradation and admixture on the pumice lightweight aggregate concrete. *Cement and Concrete Research*, **35**, 936-942. https://doi.org/10.1016/j.cemconres.2004.04.020

Schulz, K. G., Riebesell, U., Rost, B., Thoms, S., & Zeebe, R. E. (2006). Determination of the rate constants for the carbon dioxide to bicarbonate inter-conversion in pH-buffered seawater systems. *Marine Chemistry*, **100**, 53-65. https://doi.org/10.1016/j.marchem.2005.11.001

Şengün, E., Alam, B., Shabani, R., & Yaman, I. O. (2019). The effects of compaction methods and mix parameters on the properties of roller compacted concrete mixtures.

Construction and Building Materials, **228**, 116807. https://doi.org/10.1016/j.conbuildmat.2019.116807

Samson, É., Lemaire, G., Marchand, J., & Beaudoin, J.J. (1999). Modeling chemical activity effects in strong ionic solutions. *Computational Materials Science*, **15**, 285-294.

Stafford, F. N., Raupp-Pereira, F., Labrincha, J. A., & Hotza, D. (2016). Life cycle assessment of the production of cement: A Brazilian case study. *Journal of Cleaner Production*, **137**, 1293-1299. https://doi.org/10.1016/j.jclepro.2016.07.050

Storn, R., & Price, K. (1997). Differential Evolution - A Simple and Efficient Heuristic for Global Optimization over Continuous Spaces. *Journal of Global Optimization*, **11**, 341-359. https://doi.org/10.1023/A:1008202821328

Stubberud, P. (2023). *Ubiquitous and Pervasive Computing - New Trends and Opportunities*. IntechOpen, London (U.K.).

Svensson, R., Odenberger, M., Johnsson, F., & Strömberg, L. (2004). Transportation systems for CO2 - Application to carbon capture and storage. *Energy Conversion and Management*, **45**, 2343-2353. https://doi.org/10.1016/j.enconman.2003.11.022

Van Dom, T. (2013). Supplementary Cementitious Materials and Blended Cements to Improve Sustainability of Concrete Pavements. *National Concrete Pavement Technology Center*.

Van Deventer, J. S. J., White, C. E., & Myers, R. J. (2021). A Roadmap for Production of Cement and Concrete with Low-CO2 Emissions. *Waste and Biomass Valorization*, **12**, 4745-4775. https://doi.org/10.1007/s12649-020-01180-5

Velts, O., Uibu, M., Kallas, J., & Kuusik, R. (2011). CO2 mineral trapping: Modeling of calcium carbonate precipitation in a semi-batch reactor. *Energy Procedia*, **4**, 771-778. https://doi.org/10.1016/j.egypro.2011.01.118

Wang, L., Ur Rehman, N., Curosu, I., Zhu, Z., Beigh, M. A. B., Liebscher, M., Chen, L., Tsang, D. C. W., Hempel, S., & Mechtcherine, V. (2021). On the use of limestone calcined clay cement (LC3) in high-strength strain-hardening cement-based composites (HS-SHCC). *Cement and Concrete Research*, **144**, 106421. https://doi.org/10.1016/j.cemconres.2021.106421

Wang, Z., Zhou, X., Zhang, W., Sun, B., Shi, J., & Huang, Q. (2023). Parameter sensitivity analysis and parameter identifiability analysis of electrochemical model under wide discharge rate. *Journal of Energy Storage*, **68**, 107788. https://doi.org/10.1016/j.est.2023.107788

Wei, C., Dong, J., Zhang, H., & Wang, X. (2021). Kinetics model adaptability analysis of CO_2 sequestration process utilizing steelmaking slag and cold-rolling wastewater. *Journal of Hazardous Materials*, **404**, 124094. https://doi.org/10.1016/j.jhazmat.2020.124094

Zappa, W. (2014). Pilot-scale experimental work on the production of Precipitated Calcium Carbonate (PCC) from steel slag for CO_2 fixation. *Ph.D. Thesis*, Aalto University.

Yurak, V. V., & Fedorov, S. A. (2024). Review of natural and anthropogenic emissions of carbon dioxide into the earth's atmosphere. *International Journal of Environmental Science and Technology*, **22**, 2719-2736. https://doi.org/10.1007/s13762-024-05896-y

Zajac, M., Maruyama, I., Iizuka, A., & Skibsted, J. (2023). Enforced carbonation of cementitious materials. *Cement and Concrete Research*, **174**, 107285. https://doi.org/10.1016/j.cemconres.2023.107285

Zajac, M., Skocek, J., Durdzinski, P., Bullerjahn, F., Skibsted, J., & Ben Haha, M. (2020). Effect of carbonated cement paste on composite cement hydration and performance. *Cement and Concrete Research*, **134**, 106090. https://doi.org/10.1016/j.cemconres.2020.106090

Zajac, M., Skocek, J., Skibsted, J., & Ben Haha, M. (2021). CO2 mineralization of demolished concrete wastes into a supplementary cementitious material – a new CCU approach for the cement industry. *RILEM Technical Letters*, **6**, 53-60. https://doi.org/10.21809/rilemtechlett.2021.141

Zevenhoven, R., & Fagerlund, J. (2010). Mineralisation of Carbon Dioxide (CO_2). *Developments and Innovation in Carbon Dioxide (CO_2) Capture and Storage Technology*, **2**, 433-462. https://doi.org/10.1533/9781845699581.4.433

Acknowledgments

I have been fortunate to have many people who believed in me and supported me in reaching this important milestone in my life.

First and foremost, my deepest gratitude goes to my legendary parents, “Haj Abolfazal” and “Maman Goli”, for all the hardships they endured so that we could experience an easier life. Their love, strength, and sacrifices have been the foundation of everything I have achieved.

I also want to sincerely thank my amazing sister and brothers — Maryam, Mahmoud, and Javad — who have truly supported me throughout this journey, from the time I was born as “Tah Taghari :)” until now. Special thanks to Yalda, my beloved “Jigar Daii”, and to Akbar Daii, who lovingly calls me “Pam Pam Daii :)”.

My heartfelt thanks to Farzad, for always being there for me, through all the joy and sadness, and to all my wonderful friends for their constant encouragement and support.

Finally, I am truly grateful to my supervisors, Prof. Fabrizio Bezzo and Ing. S. Zuhair B. Tabrizi, for their guidance, support, and mentorship in shaping this thesis. Their insight and encouragement have been invaluable.